Seismic behaviour of unreinforced masonry buildings with reinforced concrete slabs: Assessment of in-plane and out-of-plane response

Prepared for the Swiss Federal Office of the Environment

Katrin Beyer
Marco Tondelli
Francesco Vanin
Sarah Petry
Alessandro Paparo

Earthquake Engineering & Structural Dynamics Laboratory (EESD)
École Polytechnique Fédérale de Lausanne (EPFL)

April 2015

ÉCOLE POLYTECHNIQUE
FÉDÉRALE DE LAUSANNE

TABLE OF CONTENT

1 INTRODUCTION

Unreinforced masonry (URM) buildings are cost effective and offer excellent environmental features: sustainability, energy efficiency, good indoor climate and fire resistance [1]. As a result, residential buildings are often constructed with URM walls. Their main drawback results from the vulnerability when subjected to seismic loading. Before the introduction of modern seismic design guidelines in Switzerland in 1989 [2] and in particular their revised version in 2003 [3], such URM buildings passed in general the force-based seismic design check without any difficulties. The Swiss loading standard of 2003 introduced higher seismic design forces for non-ductile structures. As a result most URM buildings did no longer satisfy the force-based seismic design check and in new construction projects a number of URM walls—though typically the minority of them—was replaced by RC walls (Figure 1.1 and Figure 1.2). A large part of the existing residential buildings are hence either URM buildings with RC slabs or buildings with both RC and URM walls and RC slabs.

Figure 1.1: Residential buildings in Switzerland with RC and URM walls (Photos: T. Wenk)

Figure 1.2: Residential building in Switzerland with RC and URM walls (Photo: T. Wenk)

Today the seismic safety of a larger number of URM buildings or mixed RC-URM wall buildings needs to be assessed. The global behaviour of these buildings is controlled by the in-plane failure of the URM walls. While force-based design approaches are well adopted by practising engineers, displacement-based approaches are known to lead to less conservative, and therefore, more realistic designs and assessment. However, currently available displacement-based design approaches for URM structures (e.g. [4]–[7]) offer methodologies, which require some additional information before becoming universally applicable to URM structures. Additional information is in particular required with respect to the deformation capacity of URM piers and by the coupling effect by slabs and URM spandrels.

The displacement-based assessment approach for URM buildings that is commonly used in Swiss engineering practice is documented in SIA D0237 "Beurteilung von Mauerwerksgebäuden bezüglich Erdbeben (Seismic assessment of masonry buildings)" [7]. In this approach, the coupling effect is currently included on a global level by choosing the height of zero moment of the URM wall [7], which is typically set to one storey height. Equivalent frame models of URM buildings (e.g. [8]–[10]) model the framing effect explicitely by including horizontal elements in the numerical model that represent stiffness and strength of slabs and spandrels. Several projects of engineering consulting offices in Switzerland showed that the pushover curves obtained with these two methods varied greatly. In particular it was found that the pushover curves obtained by means of the hand-calculation method proposed in SIA D0237 yielded typically much more conservative results that the results of the program 3muri.

The second failure mode of URM buildings relates to the out-of-plane response of URM walls. Typically out-of-plane failure does not trigger the entire collapse of a building as mostly only top storey walls are affected. However, the out-of-plane vulnerability of URM piers could prove to be the Achilles' heel of typical Swiss URM structures. Dazio [11] showed that most Swiss walls do not fulfil the slenderness criteria in Eurocode 8 [12]. He also showed that the current slenderness criteria in all international design codes fail to capture the boundary conditions of the walls, which have an important influence on the out-of-plane behaviour of URM walls. Premature out-of-plane failure might prevent the structure from reaching its full in-plane strength.

1.1 The OFEV-project and its report

Over the last five years, several research projects that were carried out at the Earthquake Engineering and Structural Dynamics laboratory (EESD) of EPFL treated the seismic performance of modern URM buildings in Switzerland. The type of masonry that was addressed used modern hollow core clay bricks and standard cement mortar. The mortar joints were of normal thickness (~1cm) and the vertical joints were fully filled ("Doppelspatz"). The RC slabs of the addressed buildings were stiff and had thicknesses between 20-30 cm. As reference buildings served buildings with four storeys since most of the residential buildings constructed with URM walls have 3-5 storeys.

Next to the OFEV-project, the following EESD-projects addressed the behaviour of modern URM buildings and buildings with URM and RC walls:

- The PhD project by Sarah Petry: This project addressed the in-plane drift capacity of modern storey-high URM walls. Full-scale tests on clay brick masonry walls were conducted and empirical and mechanical drift capacity models developed.
- The PhD project by Alessandro Paparo: This project addressed the behaviour of buildings with URM and RC walls. Tests on subassemblies of such buildings were performed, different numerical models validated against these tests and a displacement-based assessment approach for such mixed structures developed.
- The CoMa-WallS project with main contributions by Marco Tondelli, Sarah Petry, Simone Peloso (EUCENTRE): Within the framework of an FP7-project a shake table test on a four-storey structure built at half scale was conducted. The four-storey structure had URM and RC walls and RC slabs and was therefore representative for the typology of modern residential buildings in Switzerland. More information on this project is given below.

The objective of the shake table test conducted within the FP7-Series project "Seismic behaviour of mixed reinforced concrete – unreinforced masonry wall structures" was to investigate the seismic behaviour of

mixed RC-URM wall structures, which have not been tested in the past. In a mixed structure with RC and URM walls, the stiffnesses of the two parallel systems are comparable. For this reason the system stiffness and behaviour will strongly depend on both types of structural elements. At the same time, the mixed structure will allow evaluating the out-of-plane behaviour of URM walls under different boundary conditions in buildings with RC slabs.

The objective of the OFEV-funded project was to develop synergies with the CoMa-WallS project and to address aspects that are of particular interest to the Swiss engineering community. The OFEV-project had the following objectives:

- To post-process and curate the data in such a way that it can be easily used by third parties to validate design approaches and numerical models. The data has been made publically available and can be accessed through the webpage http://eesd.epfl.ch/data_sets. In addition, a publication with information on the test setup, instrumentation, and the data structure of the test has been prepared [13].
- To analyse the out-of-plane response of the URM walls during the shake table test. The results of this part of the work are presented in two chapters of this report. The first chapter (Chapter 3) presents the experimental results from the shake table test and the validation of a numerical model. The second chapter (Chapter 4) uses the numerical model for a parametric study and compares code provisions for maximum slenderness ratios to these numerical results.
- To compare the results of the displacement-based assessment approach in SIA D0237 "Beurteilung von Mauerwerksgebäuden bezüglich Erdbeben (Seismic assessment of masonry buildings)" [7] to results obtained from numerical models and there in particular to analyses conducted with the software 3muri [14]. Several projects of engineering consulting offices in Switzerland showed that the pushover curves obtained with these two methods varied greatly. In particular it was found that the pushover curves obtained by means of the hand-calculation method proposed in SIA D0237 yielded typically much more conservative results that the results of the program 3muri. Chapter 2 of this report compares the different methods by analysing a reference building, discusses the reasons for the discrepancies and makes recommendations for the refinement of the method in SIA D0237. This part of the work was completed by Francesco Vanin.

To set the OFEV-project into the context of the other EESD-research projects on URM This first chapter summarises briefly the experimental campaigns and the models and design approaches that were derived within the scope of these different research projects. A list of all related scientific articles, data sets, PhD theses and Master projects that were published by members of the EESD-laboratory can be found in Chapter 6.

1.2 Summary of PhD project by Sarah Petry

A major impediment in the application of displacement-based assessment procedures to URM structures are the weaknesses of current displacement capacity models for URM piers (for a review of these models see [15]). With her thesis, Sarah Petry contributes to the improvement of these models [16]:

- The performance of two test series on URM walls, one full-scale and one half-scale, which tested for the first time boundary conditions other than cantilever or fixed-fixed (Section 1.2.1).
- The development of new empirical drift capacity models (Section 1.2.2).
- The development of a mechanical model for predicting the force-displacement response including the 1.2.3).

1.2.1 Quasi-static cyclic tests on URM walls

Six quasi-static cyclic tests on storey-high full-scale URM walls were performed [15]. The objective of these tests was to investigate the influence of the boundary conditions on the force-displacement response of in-plane loaded URM walls. The boundary conditions were characterized in terms of:

- Applied axial stress ratio;

- Shear span.

The tests complemented existing tests on URM walls in the literature which have all been tested as cantilever or with fixed-fixed boundary conditions. The continuous measurements of the coordinates of four LEDs per brick allowed to derive also local and deformation measurements (average strains, crack widths). The test setup consisted of three servo- hydraulic actuators which were controlled in a fully-coupled mode. The three actuators applied an axial force, an in-plane bending moment and an in-plane shear force at the top of the wall (Figure 1.3). For the construction of the masonry a hollow core clay brick (Figure 1.5a) and a standard cement mortar was used. Figure 1.4 shows the failure modes of the six walls. The data of these tests is publically available (http://eesd.epfl.ch/data_sets) and all information on the test and the post-processing of the data documented in [17].

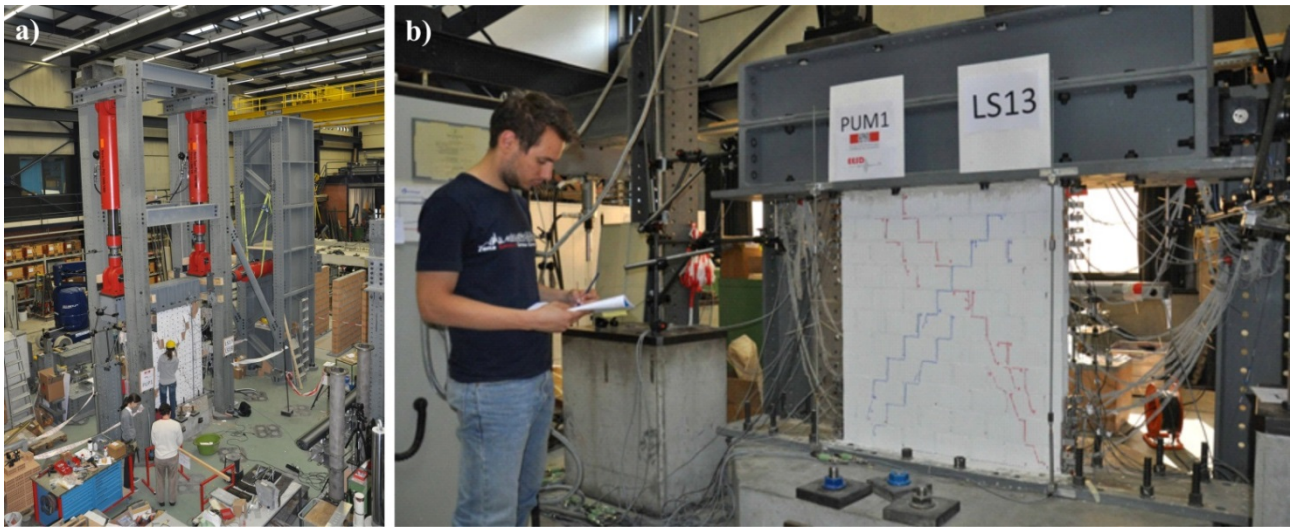

Figure 1.3: Setup for quasi-static cyclic tests on URM walls: Setup for full-scale tests [17] (a) and setup for half-scale tests [18] (b).

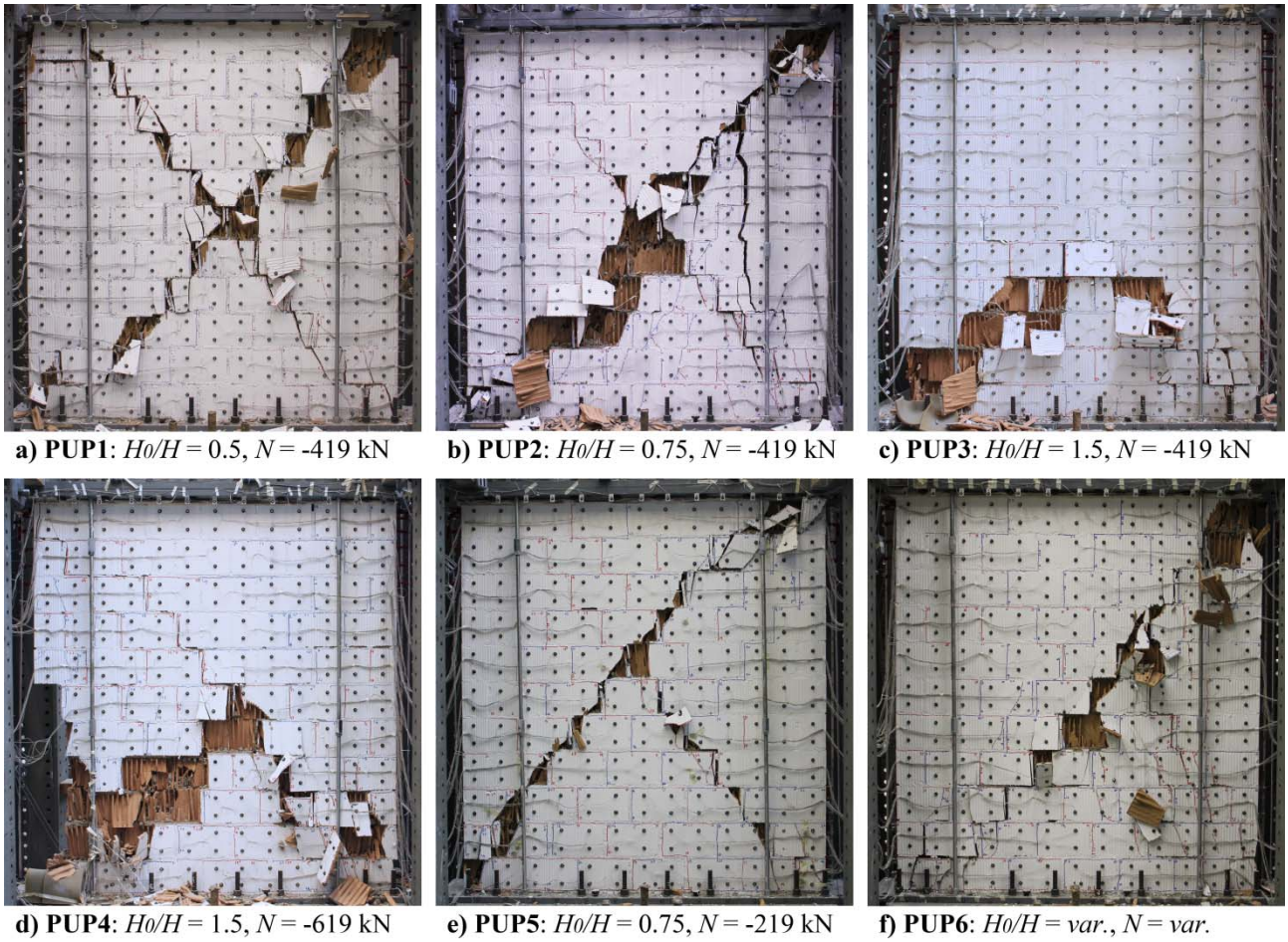

a) PUP1: $H0/H$ = 0.5, N = -419 kN **b) PUP2**: $H0/H$ = 0.75, N = -419 kN **c) PUP3**: $H0/H$ = 1.5, N = -419 kN

d) PUP4: $H0/H$ = 1.5, N = -619 kN **e) PUP5**: $H0/H$ = 0.75, N = -219 kN **f) PUP6**: $H0/H$ = *var.*, N = *var.*

Figure 1.4: Full-scale tests on URM walls: Crack patterns at failure [15], [17].

Due to limitations in size and weight, the building to be tested on the shake table (Section 1.4) had to be constructed at half-scale (Section 3.1). Purpose-manufactured bricks at half-scale were used. To develop these bricks, numerous tests on clay bricks with different hole patterns were conducted. The objective was to develop a brick which had very similar properties as the full-scale brick used for the wall tests presented in the previous section (Figure 1.6). Figure 1.5b shows next to the full-scale brick the half-scale brick which was finally selected and produced by Morandi Frères SA.

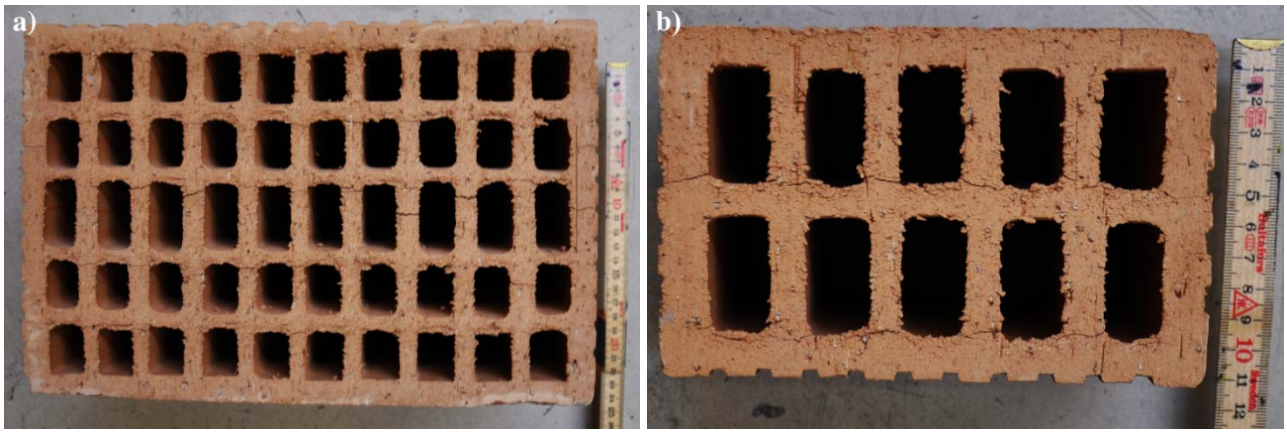

Figure 1.5: Hollow core clay bricks for URM walls: (a) Brick for full-scale tests [17] and (b) brick for half-scale tests [18].

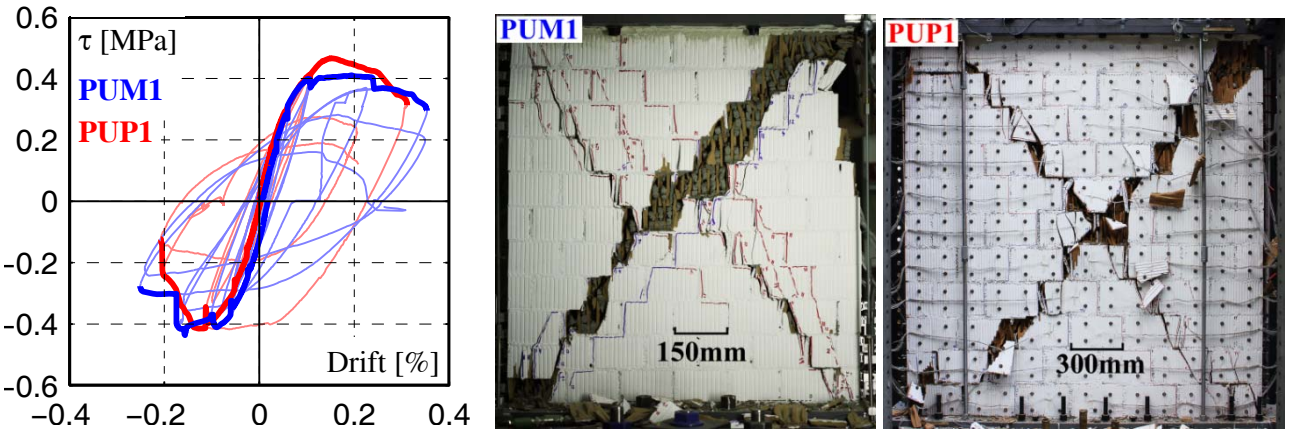

Figure 1.6: Half-scale tests: Comparison of hysteresis and crack pattern at failure of half-scale test (PUM1) to full-scale test (PUP1) [18].

1.2.2 Empirical drift capacity models

Current drift capacity models in the Eurocode and other codes around the world assign a drift capacity to the shear failure mode and a drift capacity to the flexural failure mode. EC8 – Part 3 [19], for example, assigns the following drift capacities at the Significant Damage limit state:

$$\text{Cantilever}: \delta_{SD} = 0.4\ \% \tag{1.1}$$

$$\text{Flexural failure}: \delta_{SD} = 0.8\ \% \cdot \frac{H}{l_w} \tag{1.2}$$

Lang [5] and later Lang et al. [7] in SIA D0237 propose drift capacity models that are dependent on the axial stress ratio and in [7] also on the shear span:

$$\text{Cantilever}: \delta_{SD} = 0.8\ \% \cdot (1 - \frac{\sigma_0}{f_d}) \tag{1.3}$$

$$\text{Fixed-fixed}: \delta_{SD} = 0.4\ \% \cdot (1 - \frac{\sigma_0}{f_d}) \tag{1.4}$$

where σ_0 is the applied axial stress and f_d the design value of the compressive strength. Using a homogenised and larger database on clay brick masonry walls and generalizing the form to a larger range of shear spans, we obtained [15]:

$$\delta = 0.64\ \% \cdot (1 - 0.94\frac{\sigma_0}{f_d}) \cdot \frac{H_0}{H} \tag{1.5}$$

which is valid for $0.1 \leq \sigma_0/f_d \leq 0.7$ and $0.5 \leq H_0/H \leq 1.5$. H_0 is the height of zero moment measured from the base and H the wall height.

When analysing the wall data base further, it was found that [15]:

(i) Drift capacities are sensitive to the loading history that is applied. The displacement capacities from monotonic tests are approximately twice as large as those from quasi-static cyclic tests (Figure 1.7). From statistical analysis it is known that the loading histories that are used at present are often too demanding compared to the demand that results from earthquakes in low to moderate regions [20]. Also the comparison of walls where one was subjected to symmetric cycles and the other one to asymmetric cycles showed that symmetric cycles lead to the smallest drift capacity.

(ii) Drift capacities of smaller walls are larger than drift capacities of larger walls ("size effect"). A size effect for clay brick masonry walls had so far only been considered with regard to the ultimate strength but not with regard to the displacement capacity [21].

Based on these findings a new model was proposed, which accounts for the first time also for the height of a wall. In addition a 5% fractile value was determined [15]:

$$\delta_{SD,5\%} = (0.7 - 1.0)\ \% \cdot (1 - 0.9\frac{\sigma_0}{f_d}) \cdot \frac{H_0}{H} \cdot \left(\frac{2.4\,m}{H}\right)^{0.5} \tag{1.6}$$

Figure 1.8 shows the displacement capacities obtained from the quasi-static cyclic tests in comparison to the lower bound value of Eq. (1.6).

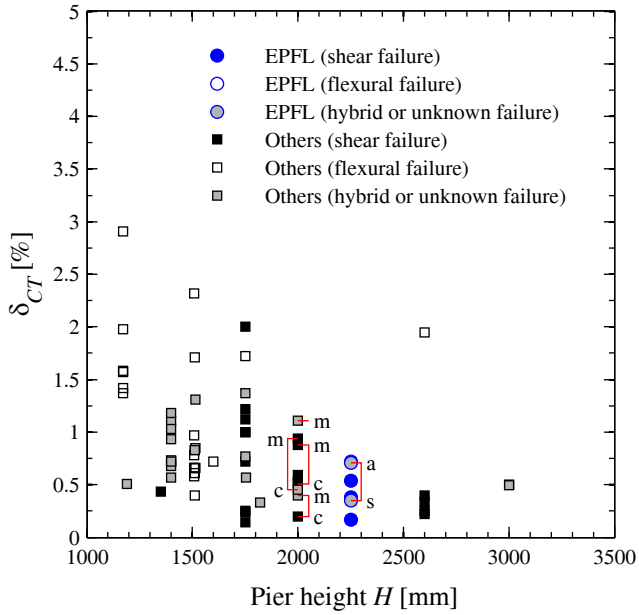

Figure 1.7: Drift capacity of clay brick masonry walls as a function of wall height H [15]. Drift capacities where determined by means of quasi-static cyclic tests. The letters "m" and "c" annotate pairs of walls for which one was subjected to monotonic and the other to symmetric cyclic loading. The letters "s" and "a" annotate pairs of walls for which one was subjected to symmetric and the other to asymmetric cycles.

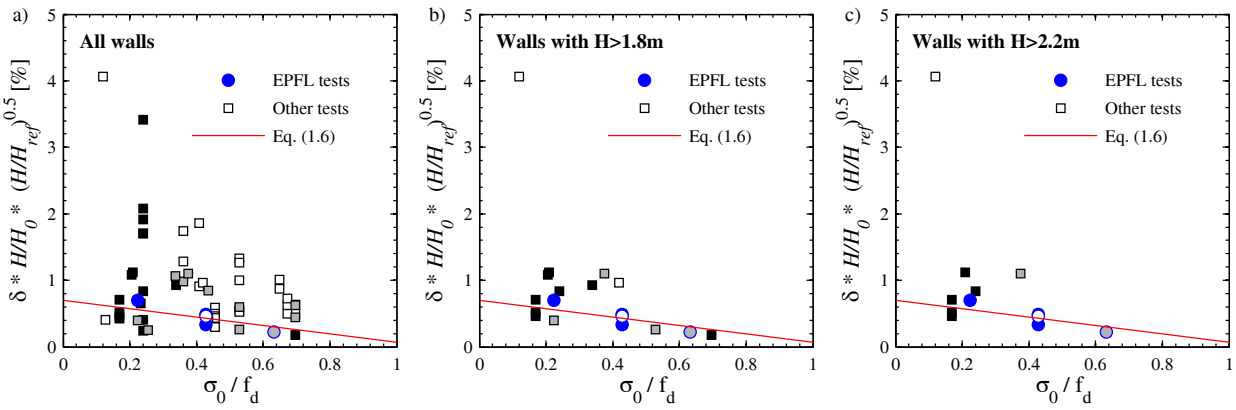

Figure 1.8: Drift capacity as a function of wall height H. Comparison of best-fit drift capacities to drift capacities obtained from quasi-static cyclic tests on piers.

1.2.3 Mechanical drift capacity model for URM walls failing in flexure

Present drift capacity models in codes, including those that are presented in the previous section, are based on empirical approaches. Drift capacity models that are based on sound mechanical principles have the potential (i) to predict more accurately the experimental data than current empirical models, (ii) to account for the wide variety of masonry typologies through standard material tests, (iii) to provide insights into the parameters controlling drift capacities, (iv) to predict drift capacities at several limit states up to axial load failure.

For URM walls failing in flexure, a drift capacity model was developed that is based on an analytical formulation of the force-displacement response [22] (Figure 1.9) and limit state criteria on the local level that have

been validated against experimental results [23]. The model builds on previous analytical formulations of the force-displacement response by Benedetti and Steli [24] and Penna et al. [25]. The proposed model shares with these models the two principal hypotheses, i.e., plane sections remaining plane and a constitutive relationship of the masonry with zero tensile strength and a linear behaviour in compression. The model comprises the following new features [22]:

(i) The shear and flexural flexibility are coupled by basing both on the compressed part of the wall. Hence, the shear stiffness reduces with increasing lateral load. The nonlinear elastic response is estimated based on a Timoshenko beam with variable cross-section along its length. Comparison with displacement components determined from the experimental tests described in Section 1.2.1 showed that the model is capable of predicting not only the shape of the global force-displacement response but also the contributions of shear and flexural deformations to the total displacement and the compressive strains at the wall toe.

(ii) New limit state criteria are proposed that allow estimating the displacement capacity of masonry walls failing in flexure. They characterise the onset of splitting and crushing at the wall toe. The limit states are described by means of stress limits at the base joint and the mortar joint above the base. At the height of the base joint, the mortar is confined by the foundation and cannot expand, increasing therefore the strength of the masonry. At the second joint this confinement effect is assumed to have vanished and the compression strength is reduced to that obtained from standard compression tests on masonry wallettes. The second failure criterion leads to a size effect with regard to the deformation capacity, i.e., the larger the test unit the smaller its drift capacity. This effect was also observed from the analysis of a database of URM walls (Section 1.2.2). The inelastic displacement component due to crushing of the base is accounted for by means of a plastic hinge approach similar to the one by Benedetti and Steli [24].

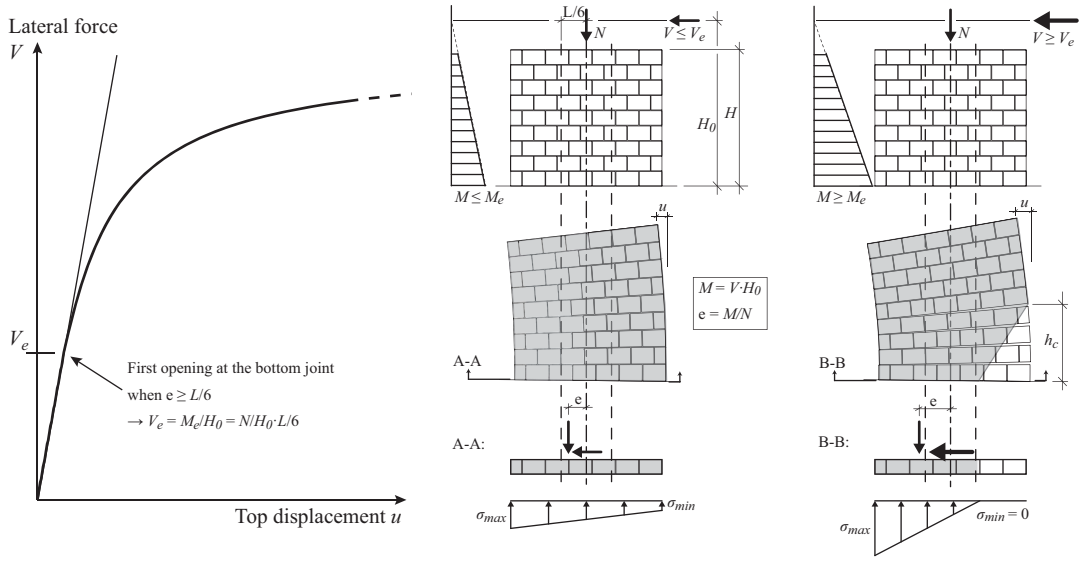

Figure 1.9: Force-displacement response of an URM wall assuming a material with zero tensile strength and linear-elastic behaviour in compression [22].

1.3 Summary of the PhD project by Alessandro Paparo

Although structures with RC and URM walls are rather common in Switzerland and other counties of moderate seismicity, their seismic behaviour is not well understood and often oversimplifying design assumptions such as neglecting the contribution of the URM walls are applied. The PhD thesis by Alessandro Paparo [26] contributed to the understanding of the seismic behaviour and the design of modern 3-5 storey structures with RC and URM walls and RC slabs through performing the following research tasks:

- Performance of quasi-static cyclic tests on subassemblies of such mixed structures;
- Validation of numerical models for these structures and the analyses of case studies which highlighted the parameters that control the seismic performance;
- Develoment of a displacement-based design approach for mixed RC-URM wall structures, which combines the established direct displacement-based design procedure [6] with novel components derived from shear-flexure cantilever models and continuous beam element models to account for the particularities of the mixed structural system and the coupling by the RC slabs.

1.3.1 Quasi-static cyclic tests on structures with an RC and an URM wall

To understand the interaction of URM and RC walls when subjected to seismic loading, large-scale experimental tests on two wall systems were conducted, which consisted each of a URM wall and a RC wall that were coupled by two RC beams [27]. A test stand was conceived that allowed measuring the reaction forces at the base of the URM walls (Figure 1.10b)—a true challenge considering the size of the forces and moments. The models, which were developed in the following, could therefore not only be validated with regard to the global response but also with regard to the force distribution between the walls and the evolution of this distribution with increasing displacement demand.

The RC walls of the test units have been designed to reach medium ductility levels ("DCM" class in Eurocode 8 [28]). With this design, the displacement capacity of the mixed structure was always controlled by the URM walls. The test units behaved differently for the two loading directions: For loading in the negative direction (towards left in Figure 1.10a), the axial load increased in the URM walls and therefore its deformation capacity reduced (see also Section 1.2.2). The displacement capacity in the negative loading direction was therefore always considerably smaller than for the positive loading direction. The variation in axial force results from the shear forces that are transferred by the RC beams (in Figure 1.10a these are covered by the horizontal steel beams). The tests showed further that the softening of the URM walls was somewhat compensated by the slender RC walls, which remained elastic over a large range of drifts. The most important result relates to the damage distribution within the structural system: Unlike in buildings with URM walls only, in which the damage in the walls tends to concentrate in the lowest storey, the inelastic deformations in mixed buildings tend to distribute over the height of the structure (Figure 1.11). This leads for the same interstorey drift capacity to an increase in global displacement capacity, which is beneficial for the seismic safety of such structures. The design approach presented in Section 1.3.3 builds on this finding.

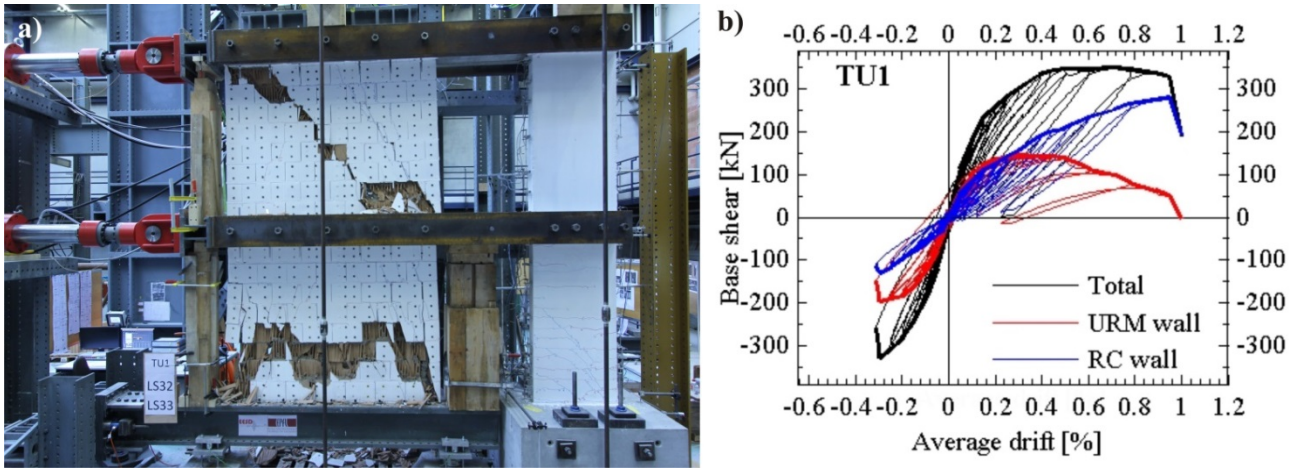

Figure 1.10: Static tests on mixed structural system: Test setup for quasi-static cyclic tests (a) and hysteresis curves for URM wall, RC wall and entire system (b) [27].

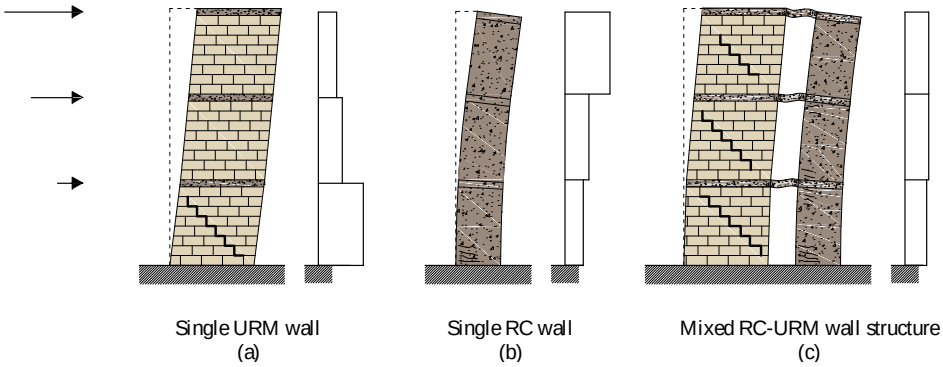

Figure 1.11: Deformation pattern and inter-storey drift profile due to lateral forces of a single URM wall with dominant shear behaviour (a), a single RC wall with dominant flexure behaviour (b) and a mixed RC-URM structure (c) [29].

1.3.2 Validation of numerical models for structures with RC and URM walls

Two numerical models of different complexity were used to analyse the experimental results presented in the previous chapter. The first model is a shell element model, which is analysed using the software ATENA [30]. In this model, the RC members are modelled by the nonlinear constitutive model SBETA, which is implemented in ATENA and the URM walls are modelled using a simplified micro-model, in which the bricks are modelled by elastic elements and the joints by interface elements of zero thickness. The interface elements were assigned a Mohr-Coulomb law. The material parameters of concrete, reinforcement and masonry are derived from material test results, which are summarised in [27].

The second model is an equivalent frame model, which was analysed using the program TREMURI [10]. In this model, the masonry elements were represented by the macro-element by Penna et al. [25] and the RC members by Timoshenko beams with plastic hinges [10] to which bilinear moment-rotation relationships were assigned. Based on the comparison to the experimental results and the results of the more advanced shell element model, recommendations for the computation of the macro-model parameters from material properties, the choice of the effective stiffness of the RC members and the effective length of the beam elements were formulated [29].

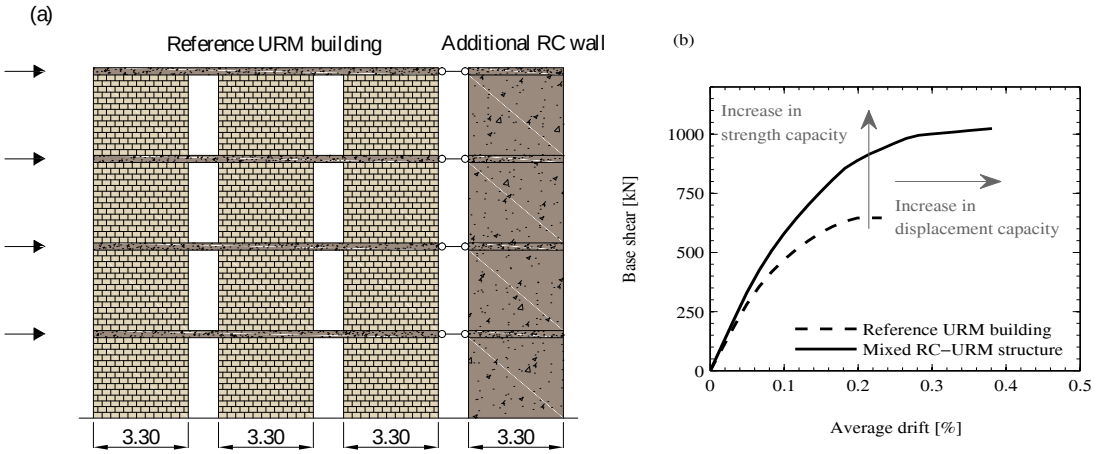

Figure 1.12: Reference URM structure and case study where one RC wall is added to the URM structure. Force-displacement relations of reference URM structure and case study. The ultimate displacement corresponds to the displacement for which the first wall reaches its drift capacity [26].

Both models were able to reproduce the experimental results rather well. The equivalent frame model was then used to analyse several case studies. An example of such a case study is illustrated in Figure 1.12. It shows that adding one RC wall to the reference URM building does not only increase the force capacity of the structure but also the displacement capacity. This results from the coupling of a shear dominant system (URM walls) to a flexure dominant system (RC wall), which was illustrated in Figure 1.11.

1.3.3 Displacement-based design approach for structures with RC and URM walls

To obtain the increase in displacement capacity that results from the coupling of a shear dominant system to a flexural dominant system, the stiffness and strengths of the two systems have to respect certain ratios. Based on a shear-flexure cantilever model, which has been developed in the past to analyse dual frame-wall systems, rules were developed to compute the required stiffness and strength ratio of the two systems which allowed to obtain an approximately linear displacement profile over the height [31]. To simplify the matter, it was assumed that the flexural flexibility of the URM walls and the shear flexibility of the RC walls can be neglected. The boundary conditions required to solve the differential equation describing the shear-flexure cantilever model were adapted to represent a RC wall that forms a plastic hinge at the base (Figure 1.13). In addition, a continuous beam element model was developed for estimating the moment transferred by the slabs and the equivalent viscous damping of URM walls failing in shear evaluated. These models were used to assess the seismic performance of buildings with URM and RC walls in the framework of the Direct Displacement Based Design approach, which was developed by Priestley, Calvi and Kowalsky [6]. The usage of these models in conjunction with force-based design is currently evaluated.

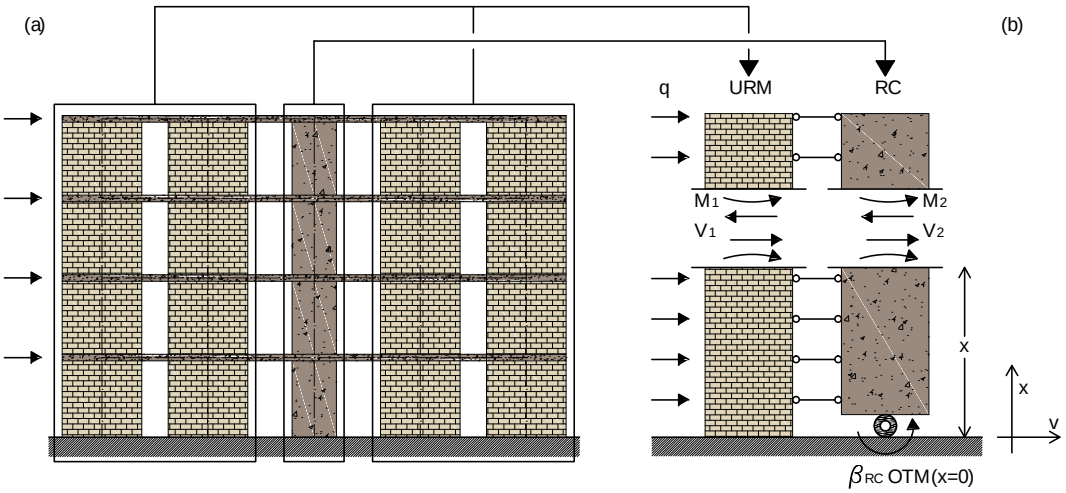

Figure 1.13: Mechanical model: identification of shear (URM) and flexural (RC) walls (a); definition of the reference system and of the internal forces (b)

1.4 Summary of the CoMa-WallS Project

Within the framework of a European FP7 research project, which was led by the EESD laboratory, a four-storey building with reinforced concrete and unreinforced masonry walls was tested on the shake table at the TREES laboratory of the EUCENTRE in Pavia (Italy, Figure 1.14). The building was subjected to uni-directional shaking and was conducted at half-scale. The main objective of the test was to gain new insights into the dynamic, non-linear in-plane behaviour of such mixed structures and to collect data for the validation of numerical models. In addition, the boundary conditions of the out-of-plane response of URM walls was investigated. To achieve this, a test unit with six in-plane loaded walls and two out-of-plane loaded walls was designed. The out-of-plane loaded walls were URM walls; of the six in-plane loaded walls four were URM and two RC walls. The RC walls were grouped at one end of the structure in order to investigate the effect on the two in-plane loading directions (positive vs negative loading direction) and on the boundary conditions of the adjacent out-of-plane loaded URM walls.

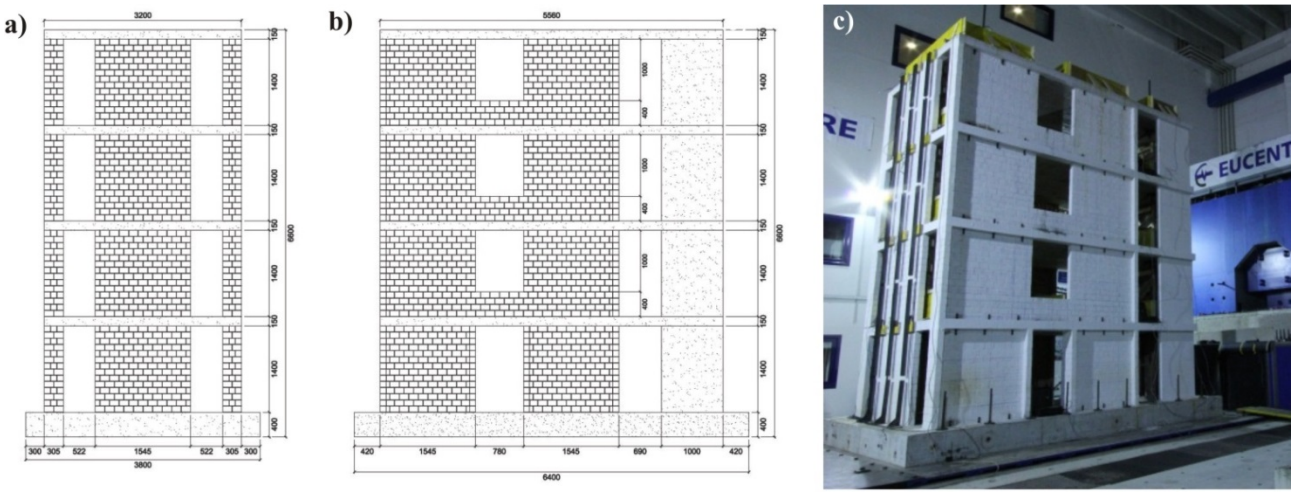

Figure 1.14: Dynamic test on building with RC and URM walls: Drawings of two North and West face of the buildings (a, b) and photo of the building before testing (c).

The test unit was subjected to nine runs with increasing intensity. During the last test, the building nearly collapsed (Figure 1.15). Collapse was prevented by the RC walls and the out-of-plane URM walls; the first two storeys of the in-plane loaded URM walls had lost their horizontal and axial load bearing capacity (Figure 1.16). As had been expected based on the results of the quasi-static tests on mixed systems (Section 1.3.1), the building failed for loading in the negative direction, i.e., when for the direction for which the axial force in the URM walls had increased.

During the last test, one of the out-of-plane loaded URM walls touched the support structure, which had been put in place to avoid that the wall fell onto the shake table, and two other showed significant out-of-plane deformations. More information on the performance of the out-of-plane loaded URM walls, observations on the boundary conditions of these walls in buildings with stiff RC slabs and the validation of a numerical model are presented in Chapter 3. A description of the planning of the test, the observations during the test, the comparison to the predicted response and the structure of the raw and post-processed data, which is publically available, are available [13]. Videos of the test as well as links to the data and the corresponding papers can be accessed through the following webpage: http://eesd.epfl.ch/data_sets.

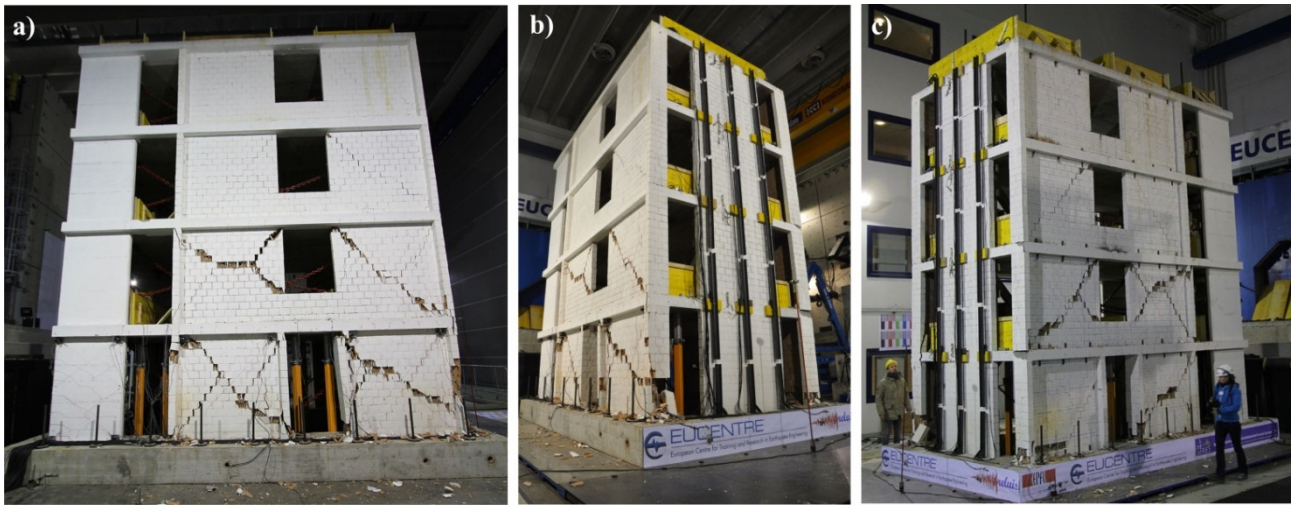

Figure 1.15: Dynamic test on building with RC and URM walls: Crack pattern after the last test.

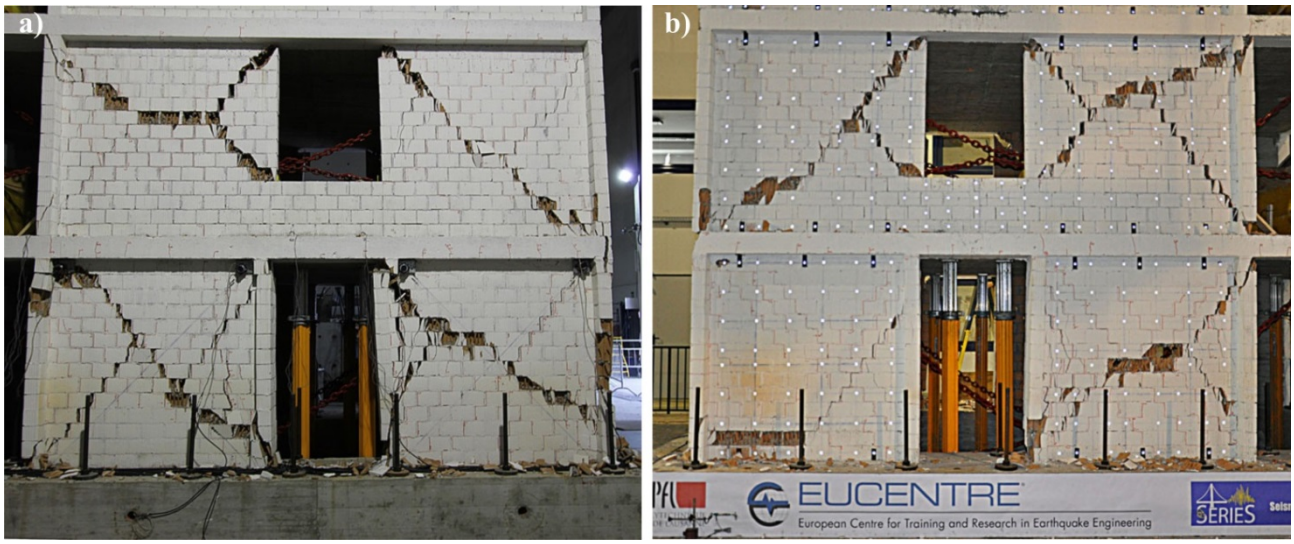

Figure 1.16: Dynamic test on building with RC and URM walls: Crack pattern of the in-plane loaded URM walls of the two lower storeys after the last test.

1.5 Acknowledgments

The work by Marco Tondelli was supported by the Federal Office of the Environment. The shake table test was financed through a grant of the European Community's Seventh Framework Programme [FP7/2007-2013] for access to TREES laboratory of EUCENTRE under the grant agreement n° 227887. The reduced scale bricks were fabricated and donated by Morandi Frères SA, Switzerland. Philippe Piguet, Claude Caillot, Raimond Girardier (Morandi Frères SA) and Rudi Räss (Association of the Swiss Clay Brick and Roofing Tile Industry) for the donation of the special half-scale bricks for the construction of the test unit and the transportation of the bricks to EPFL. The authors appreciate and gratefully acknowledge all contributions.

The authors would like to thank also all members of the CoMa-WallS project team namely Prof. B. Binici, Dr. C. Butenweg, Prof. M.A. Eberik, Dr. T. Wenk, Dr. P. Lestuzzi, Dr. J. Varga. The authors are indebted to all members of the TREES laboratory and in particular the head of the laboratory, Prof. A. Pavese, and to Dr. Simone Peloso for their invaluable support during the entire duration of the project.

2 DISPLACEMENT-BASED ASSESSMENT OF URM BUILDINGS WITH RC SLABS

Due to lack of time, the seismic assessment of unreinforced masonry (URM) buildings is often a task that needs to be performed without sophisticated numerical models. If sufficient resources are available, which allow that advanced numerical simulations are performed, it is desirable to check the results by means of simple spreadsheet calculations. In both cases, simple calculations serve only their purpose if they are sufficiently accurate to permit conclusions on the expected seismic performance of the building and therefore also on the validity of the advanced numerical simulations. The objective of this chapter is to analyse the seismic performance of a case study building with URM walls and reinforced concrete (RC) slabs by approaches of different complexity, to compare the results obtained and to discuss the origin of the discrepancies.

In the analysed example, the URM walls are constructed with hollow clay bricks and normal cement mortar and the RC slabs are 0.2 m thick. The RC slabs have several important effects on the seismic response of the URM building: (i) The RC slabs ensure that the shear forces can redistribute between the walls and that the walls in one plane are subjected to the same displacement demand. (ii) Since the free span of the slab between walls is often relatively small, the bending moments that are transferred by the slabs are not negligible. These bending moments and the resulting shear forces introduce a coupling moment into the walls and vary the axial force in the walls. This action is in the following referred to as "coupling effect by the slabs". (iii) The RC slabs define also the boundary conditions of the URM walls for out-of-plane failure. This is discussed in detail in Chapter 3.

The example building is analysed by three different models. The first model is a macro-element model which is analysed using the software Tremuri by Lagomarsino et al. [10]. Nonlinear static and dynamic analyses are performed; the latter serve as benchmark for all other types of models. The second model uses the same software but the masonry walls are modelled by bilinear rather than macro-elements; this element is also available in the professional version of the software, i.e., the program 3muri [14]. The final model is the approach presented in SIA D0237 by Lang et al. [7]. This approach does not involve finite element calculations but it is based on simple mechanical models that can be carried out with a spreadsheet. The models are compared in terms of the underlying assumptions with regard to the stiffness, force and displacement capacity of the URM wall elements. The analysis results are compared in terms of the predicted maximum PGA that the building can sustain.

The chapter concludes with recommendations for analysing URM buildings by means of simple methods that include spreadsheet or elastic frame models.

2.1 Case study

The case study is a four-storey residential building, which has been introduced as example by Lestuzzi and Badoux [29]. It is regular over the height and symmetric in plan. Figure 2.1 and Figure 2.2 show a plan view and 3D view of the building respectively. The storey height is 2.5 m, the storey mass of storey 1-3 (including mass of walls, slabs and permanent loads) is 240 t and the storey mass of storey 4 222 t. The expected material properties are summarised in Table 2.1. The building is assessed for a peak ground acceleration of 1.0 m/s^2 and spectrum Type I of EC 8 [12] for soil class C. No safety factors are applied—neither on the material properties nor on the force or displacement capacities.

Table 2.1: Example building: Expected material properties

Unreinforced Clay Brick Masonry	
Compression strength	f_m= 7.0 MPa
E-modulus	E_m= 7.0 GPa
G-modulus	G_m= 2.8 GPa
Cohesion of joints	f_{mvo}= 0.25 MPa
Friction coefficient of joints	μ= 0.4
Reinforced concrete	
E-modulus of concrete C30/37	E_c= *32 GPa*
E-modulus of reinforcing steel B500B	E_s= *200 GPa*

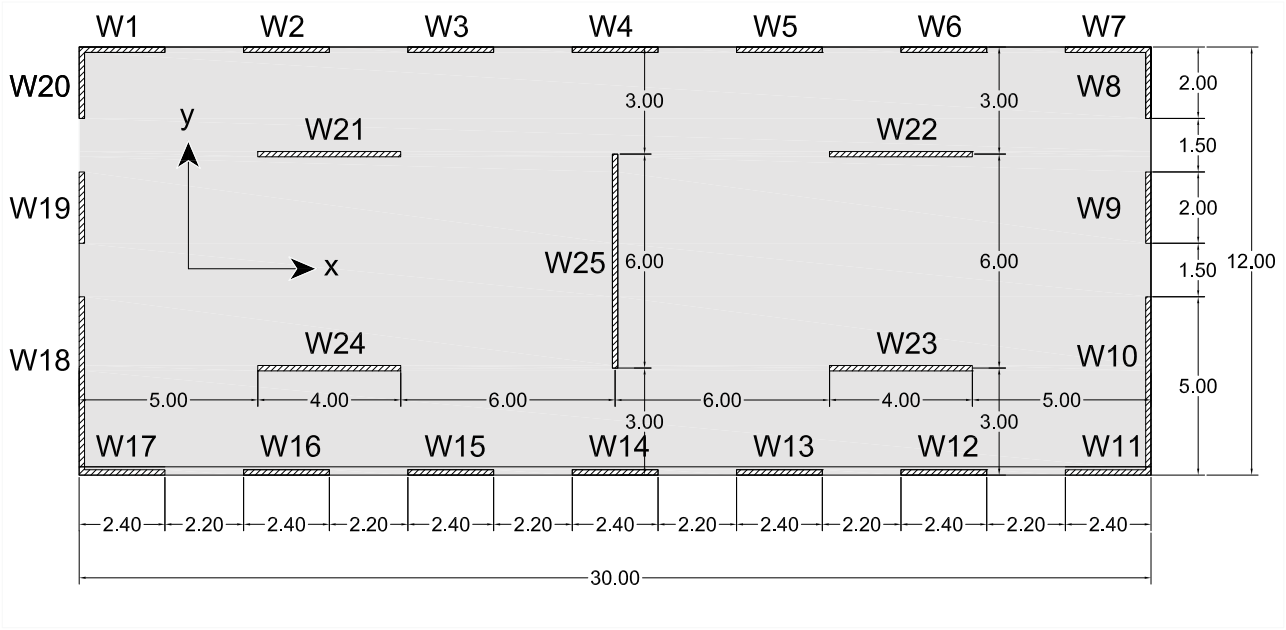

Figure 2.1 : Example building: Plan view, all dimensions in m. Thickness of all walls: 0.15 m (adapted from [32])

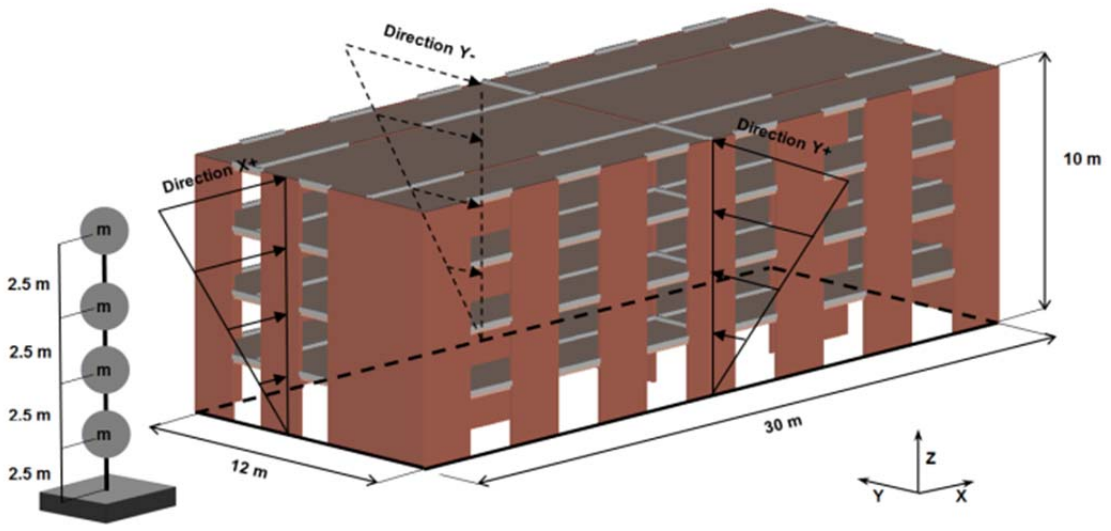

Figure 2.2 : Example building: 3D view from 3muri and corresponding stick model with four masses [33].

2.2 General modelling assumptions

2.2.1 Stiffness, strength and drift capacity of URM walls

The effective stiffness of URM walls is computed from the macro-element model that accounts for the effect of cracking on the stiffness reduction (see Section 2.3.1). The strength of the URM walls are computed based on Eurocode 8, Part 3 [19]. The flexural strength is computed assuming a stress block with $\sigma=0.85f_m$:

$$V_{R,f} = \frac{N \cdot l_w}{2 \cdot h_0}\left(1 - \frac{N}{0.85 \cdot f_m \cdot t_w \cdot l_w}\right) \tag{2.7}$$

where N is the axial force, l_w the wall length, t_w the wall width, h_0 the shear span, f_m the masonry compression strength. The axial force is positive, if the wall is in compression. Note that in Eurocode 8, Part 3 [19] the factor 1/0.85=1.17 is written as 1.15. The formulation is here changed to 1/0.85 to make it fully compatible with the formulae implemented in the bilinear element in Tremuri.

The shear strength is computed using the Mohr-Coulomb criterion:

$$V_{R,s} = f_{vm0} \cdot t_w \cdot l_{c,S} + 0.4 \cdot N \leq 0.065\, f_m \cdot t_w \cdot l_{c,S} \tag{2.8}$$

Where f_{cm0} is the shear strength at zero axial stress (cohesion) and $l_{c,S}$ is the compression zone length. When the wall is failing in shear, the compression zone length can be computed assuming a material that is linear elastic in compression and has zero tensile strength:

$$l_c = 3 \cdot \left(\frac{l_w}{2} - e_u\right) = 3 \cdot \left(\frac{l_w}{2} - \frac{|M_u|}{N}\right) \tag{2.9}$$

where e_u is the eccentricity of the axial force at the base of the wall.

$$V_{R,s} = min\left\{\begin{matrix} f_{mv0} \cdot t_w \cdot 3 \cdot \left(\frac{l_w}{2} - \frac{|V_{R,s}| \cdot h_0}{N}\right) + 0.4 \cdot N \\ 0.065 \cdot f_m \cdot l_c \cdot t_w \end{matrix}\right\} \tag{2.10}$$

Solving for the shear resistance, one obtains:

$$V_{R,S} = min\left\{\begin{matrix} \frac{N}{2} \cdot \left[\frac{(3 \cdot f_{vm0} \cdot t_w \cdot l_w) + 0.8 \cdot N}{(3 \cdot f_{vm0} \cdot t_w \cdot h_0) + N}\right] \\ \frac{0.0975 \cdot f_m \cdot t_w \cdot l_w}{1 + 0.195 \cdot f_m \cdot t_w \cdot h_0/N} \end{matrix}\right\} \tag{2.11}$$

The smaller of the two values determines the capacity and the failure mode of the URM wall.

The drift capacity of walls failing in shear or flexure was assumed as 0.4%. A differentiation of the drift capacity with failure mode [19] or axial stress [7] was not included as this would complicate the comparison of the pushover curves obtained from different methods. Assigning the same drift capacity to all walls allows to focus on reasons for discrepancies which might not become obvious if walls are assigned drift capacities depending on failure mode or axial stress ratio. The discrepancies that are obtained in the following between the different methods can therefore be considered a lower bound estimate of the discrepancies.

2.2.2 Stiffness, strength and rotation capacity of RC slabs

The RC slabs will be modelled by means of equivalent beams. It is assumed that these beams remain elastic and that the effective stiffness of these beams corresponds to 50% of their gross sectional stiffness [34]. The effective width of these beams was assumed as six times the wall thickness for beams spanning between interior walls and 3.5 times the wall thickness for beams spanning between exterior walls [34]. The span of the beams was taken as the free span plus the slab thickness t_s on either side of the beam [6], [29].

The concrete and steel properties of the RC slab are those of C30/37 and B500B. The gross-sectional stiffness of the concrete beams is reduced to half to account for cracking of the slab. It is assumed that the slab remains elastic and does not reach its deformation capacity.

2.3 Benchmark model: Tremuri model

2.3.1 Description of the benchmark model

As benchmark, the building is modelled using the software Tremuri by Lagomarsino et al. [10]. The version 2.0 from 2012 has been used for all analyses (Tremuri Ricerca 2.0, 2012). The URM walls are modelled by means of the macro-element by Penna et al. [25] that is implemented in the program. The macro-element accounts for elastic flexural and shear deformations and axial elongation due to rocking by means of analytically derived relationships and uses phenomenological relationships to describe the pre-peak softening, the post-peak shear strength degradation and the hysteretic response.

The in-plane stiffness is modelled by membrane elements [10] and the out-of-plane stiffness by elastic beam elements that are assigned the properties described in Section 2.2.2. The model is shown in Figure 2.2. When setting up a Tremuri model where the URM walls are modelled with macro-elements, the following points need to be given some considerations:

Stiffness of the macro-element in the elastic range:

The macro-element model is based on the idea of separating the wall into a central part and two interfaces at the bottom and top of the wall. Shear deformations are allocated to the central part of the wall and the flexural deformations are lumped at the interfaces. The macro-element formulation assumes a constant curvature from the base to midheight of the wall and a constant curvature from midheight to the top. The curvatures are computed for the interfaces at the base and the top. As a result, the flexural stiffness of the macro-element is different to that of an elastic Timoshenko beam. For a wall of height h and a zero moment height h_0 (Figure 2.3a), the top displacement u_f and the top rotation θ_f due to flexure and the top displacement due to shear deformations u_s are the following:

Timoshenko beam element:

$$u_f = \frac{Vh^3}{3EI} + \frac{V(h_0 - h)h^2}{2EI} \tag{2.12}$$

$$\theta_f = \frac{Vh(2h_0 - h)}{2EI} \tag{2.13}$$

$$u_s = \frac{Vh}{GA_s} \tag{2.14}$$

Macro-element by [25]:

$$u_f = \frac{Vh_0h^2}{2EI} \tag{2.15}$$

$$\theta_f = \frac{Vh(2h_0 - h)}{2EI} \tag{2.16}$$

$$u_s = \frac{Vh}{GA_s} \tag{2.17}$$

where A_s is taken equal to the gross area.

The macro-element yields the same top rotation but a different top displacement than the Timoshenko beam. The flexural top displacement of the Macro element is for $h_0/h>0.5$ larger than the flexural top displacement of the Timoshenko beam element. The ratio of the flexural stiffnesses of the macro-element to the Timoshenko beam varies with h_0/h (Figure 2.3b). Since the difference in top displacement results from the simplifying assumption of the macro-element that the curvatures are constant over half the wall height, the E-modulus of the macro-element model should be adapted to correct for the resulting error in flexural stiffness. For the case study analysed here, the following approach was adopted:

- The uncracked stiffness of the building was determined by means of an elastic model where all elements were modelled by Timoshenko beam elements. The E-modulus and G-modulus of the masonry was 7.0 GPa and 2.8 GPa (Table 2.1).
- The E- and G-moduli of the masonry in the model with macro-elements was then tuned to reach for a horizontal load with triangular distribution over the height of the building the same uncracked

stiffness than the model with Timoshenko beam elements. To do this purpose, the E- modulus had to be multiplied with a correction factor R=1.075; the G-Modulus was multiplied with R and the factor 5/6 (to account for the fact that in Tremuri $A_s=A_{gross}$), i.e., with 0.90. Hence, the E- and G-modulus specified in Tremuri were 7.53 GPa and 2.51 GPa respectively.

As an alternative to the model with Timoshenko beam elements, the correction factor can be estimated using an iterative approach by analysing the macro-element model, identifying a representative shear span ratio and applying the correction factor from Figure 2.3b.

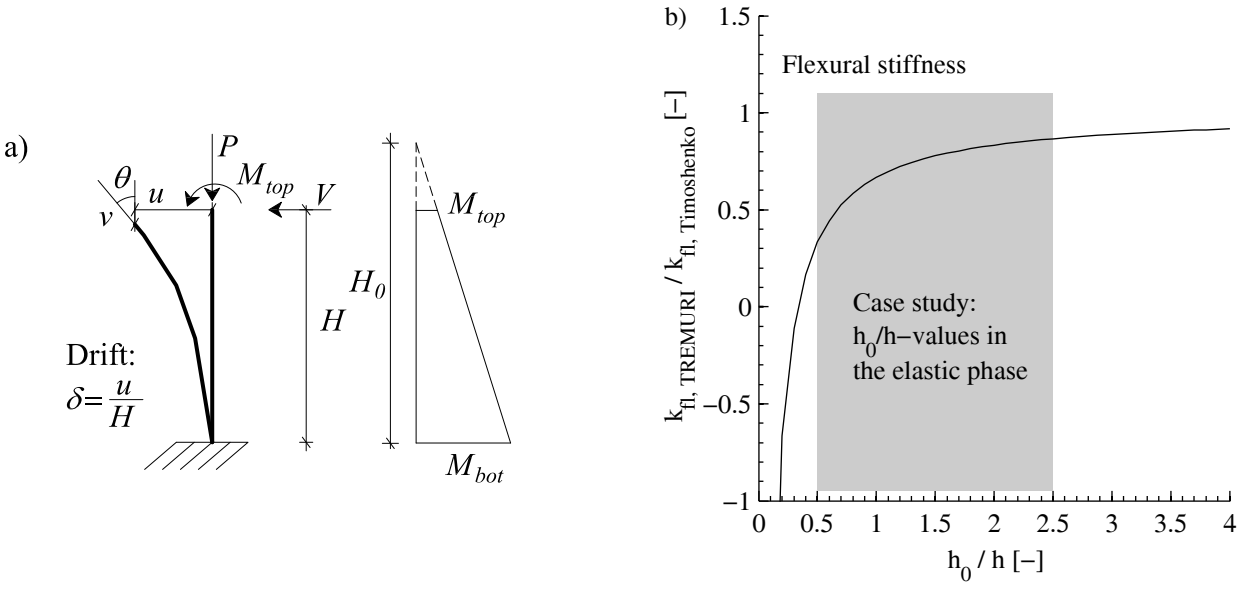

Figure 2.3 : Degrees of freedom of a URM wall (a). Ratio of flexural stiffnesses of macro-element to Timoshenko beam (b).

Shear and flexural strength of the macro element:

The flexural strength of the macro-element [25] is determined via the constitutive model assigned to the interfaces. To include the effects of toe-crushing phenomena, the interfaces are assigned a bilinear elastic-perfectly plastic constitutive model, with zero tensile strength, finite compressive strength, and stiffness degradation in the cyclic behaviour. This implies that the ultimate flexural strength of the macro-element tends to approach the limit value (where N is considered positive in compression):

$$V_{R,f} = \frac{N \cdot l_w}{2 \cdot h_0}\left(1 - \frac{N}{f_m \cdot t_w \cdot l_w}\right) \tag{2.18}$$

Because the Eurocode 8, Part 3 considers a stress block with $\sigma=0.85f_m$ to compute the ultimate flexural strength, in this case study, to make the two formulations consistent, a factor 0.85 was applied to the compressive strength of the macro-element.

The shear strength of the macro-element is based on a shear constitutive model which applies a Mohr-Coulomb type criterion to the gross section. The constitutive model considers elastic deformations up to the static frictional strength of the element, followed by sliding deformations that take place if the frictional strength is exceeded; the additional strength is provided by the cohesion of the material. As the maximum cohesive strength is evaluated referring to the entire cross section, the shear strength of the macro-element is given by:

$$V_{R,s} = cA_{gross} + \mu N \tag{2.19}$$

where μ is the friction coefficient and c represents the strength due to material cohesion. Such formulation of the shear behaviour of macro-element does not allow for a perfect agreement between this model and the

expressions given in the Eurocode 8, that account for the cohesion only over the length of the compressed zone.

Drift capacity:

The macro-element requires as input an ultimate drift capacity for flexural and shear failure [25]. Note, however, that the drift definitions for the macro-element differ from the commonly used drift definition; therefore, different drift limits should be applied. A comparison of the different drift definitions and their impact on the limit drifts is documented in [23]. The macro-element uses different drift definition for flexural and shear failure:

$$\delta_{fl} = \left|\frac{u_j - u_i}{h} + \varphi_e\right| \leq \delta_{fl,lim} \tag{2.20}$$

$$\delta_{sh} = \left|\frac{\varphi_j + \varphi_i}{2} - \varphi_e\right| \leq \delta_{sh,lim} \tag{2.21}$$[1]

where u_i and u_j are the horizontal displacements of the two nodes of the macroelement, φ_i and φ_j are the rotations of the two nodes of the macroelement, and φ_e is one of the internal degrees of freedom, representing the absolute rotation of the central part.

If this drift capacity is reached, the resistance of the element with regard to the corresponding failure mode is set to zero. The following points need to be kept in mind:

- The axial load bearing capacity is maintained. For shear failure of modern URM walls, horizontal load failure is, however, often immediately followed by axial load failure [15].
- If an element fails in shear, it maintains its flexural load bearing capacity and vice versa. Experimental tests have, however, shown that the occurrence of one failure mode influences the resistance associated with the other failure mode.
- Mixed failure modes that are very common in reality cannot occur.
- The drift definition of URM walls failing in shear is different to the drift definition implemented in common codes, such as EC8-3 [19]. The drift limits proposed in EC8-3 can therefore not be applied to the drift definition implemented in the macro-element as it was shown that in particular for $h_0/h_s>1$, the difference between the two drift definitions is considerable.

For this reason, the failure of the building was determined after the completion of the analysis as the minimum top displacement for which a maximum first storey drift of 0.4% was reached.

2.3.2 Modal analysis

The fundamental periods of the structure in x- and y-direction are 0.29 and 0.30 s respectively. These fundamental periods were determined on the basis of the gross sectional stiffness. The ratio of effective to gross sectional stiffness will be computed in Section 2.3.3. The first and second mode shapes are shown in Figure 2.4.

Table 2.2 : Example building: Results of modal analysis.

Mode	Frequency [Hz]	Period [s]	Part. mass x [%]	Part. mass y [%]
1	3.38	0.296	0.0	73.2
2	3.42	0.293	70.3	0.0
4	10.99	0.091	0.0	19.3
6	13.31	0.075	20.1	0.0

[1] Note that in [25] the drift definition for shear failure contains a $+\varphi_e$ instead of a $-\varphi_e$. However, we believe that it should be a minus sign and it seems also to be implemented in Tremuri with $-\varphi_e$.

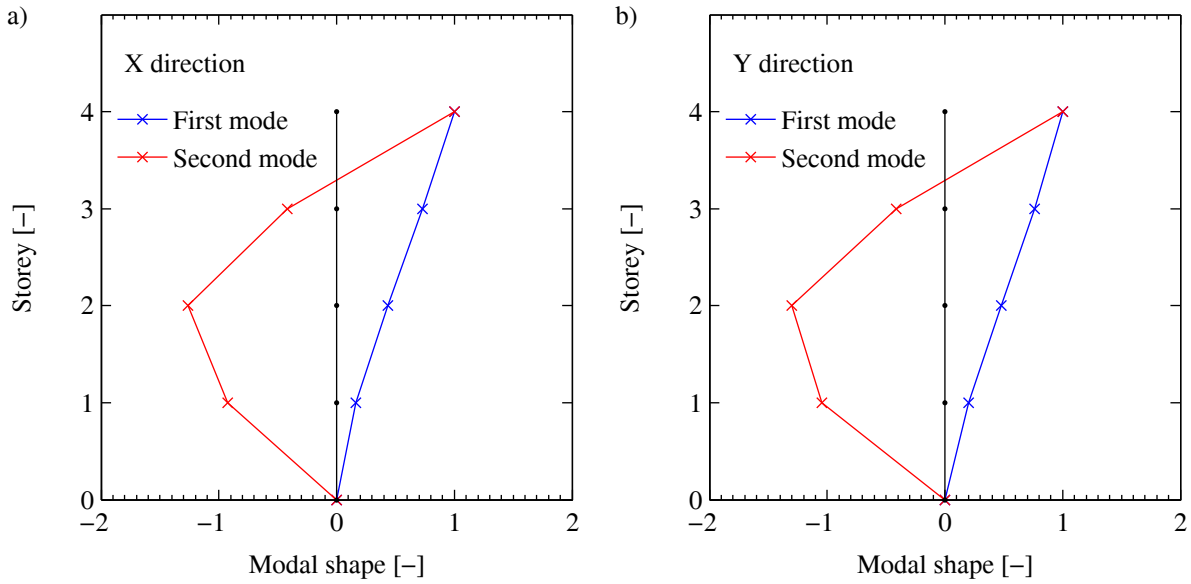

Figure 2.4 : Example building: Mode shapes of the first and second mode in the x-direction (a) and the y-direction (b).

2.3.3 Pushover analysis in the y-direction

As a first step, a pushover analysis with a triangular force pattern is carried out. The considered loading direction is the negative y-direction. The analysis results are shown in Figure 2.5 to Figure 2.7. The structure is symmetric for loading in the y-direction, i.e., all walls will be subjected to the same displacements. In total, there are seven walls. The two facades are identical, which consist of three walls each. For this reason, the pushover curves are only plotted once (Wall 8-10). The total resistance in y-direction corresponds therefore to two times the resistance of the Walls 8-10 and once the resistance of the central wall 25. The pushover analysis is stopped when an interstorey drift of 0.4% is reached in the first storey. Due to significant bending deformation, a drift of 0.4% is reached first in one of the top storeys; this point is indicated in all figures with a cross. A significant portion of this interstorey drift results, however, from rigid body deformations. The SIA D0237 method, to which the macro-element results will be compared in Section 2.4, can only account for first storey failures. Limiting the application of the failure criterion to the first storey only, eliminates therefore one possible reason for differences between the two models.

Figure 2.6 shows that the axial force and shear span vary with the displacement demand. This applies in particular to the shear span in the elastic range and to a lesser extent to the inelastic range. The variation of the shear span will be of consequence for the spreadsheet calculation method in Section 2.4. When adding up the axial force of all walls in y-direction (Figure 2.7a), one notices that it does not remain constant with increasing displacement demand: The slabs redistribute part of the axial force to walls in the x-direction. Figure 2.7b shows the pushover curve for loading in the negative y-direction and its bilinear approximation. The latter will be used in the following section for determining the seismic demand for which the building reaches a first storey drift of 0.4%. The bilinear approximation was obtained as follows [35]:

- The effective stiffness was defined as the secant stiffness which passes through the point that corresponds to 70% of the peak strength.
- The ultimate strength was computed by imposing that the areas underneath the actual and the bilinear curve are equal.
- The ultimate displacement of the bilinear approximation corresponds to the ultimate displacement of the actual capacity curve.

For loading in the negative y-direction the effective stiffness corresponds to 67% of the gross sectional stiffness. For loading in the positive y-direction, the effective stiffness is only 42% of the gross sectional stiffness (Section 2.3.4).

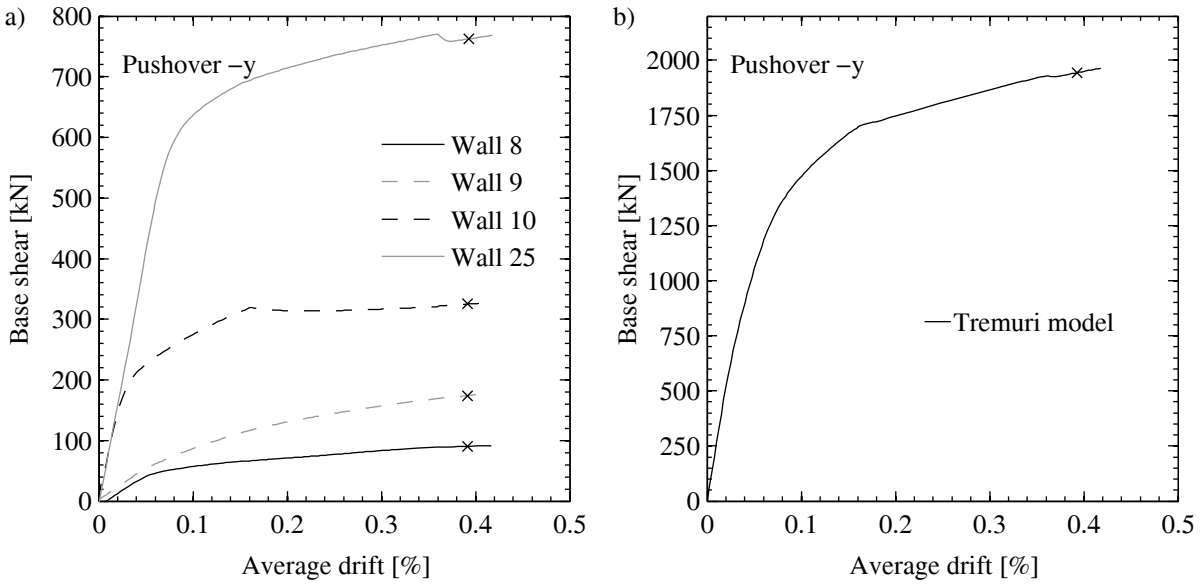

Figure 2.5 : TREMURI, pushover analysis in the negative y-direction: Pushover curves of individual walls (a) and pushover curve of system for loading. The ultimate displacement corresponds to 0.4% drift of the first storey. The cross marks the first attainment of 0.4% in one of the upper stories.

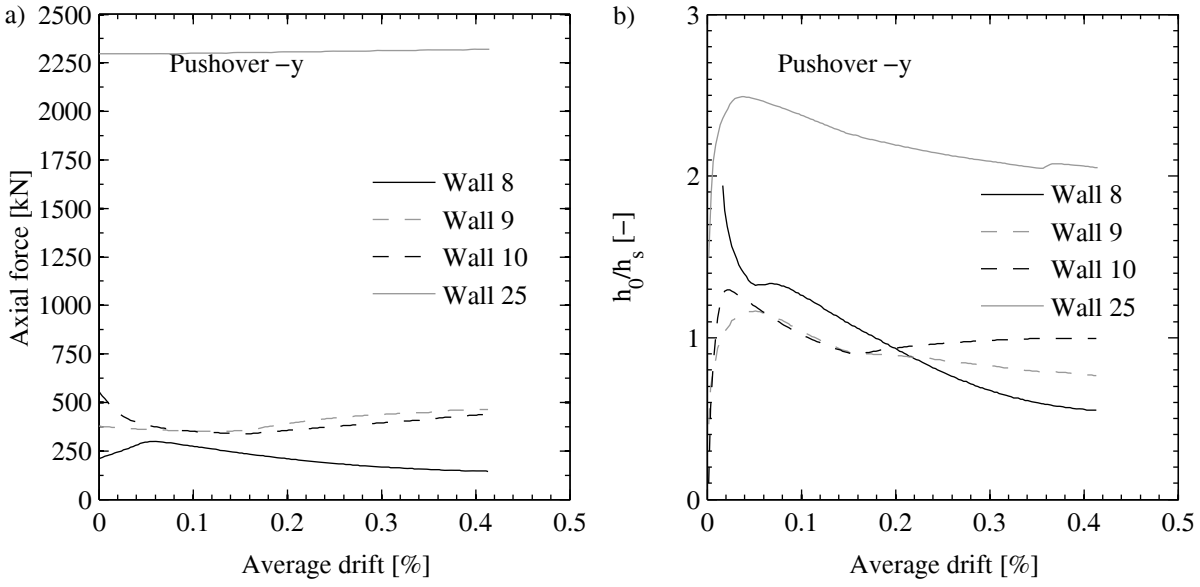

Figure 2.6 : TREMURI, pushover analysis in the negative y-direction: Variation of axial force (a) and height of zero moment (b) for the walls 8, 9, 10, 25.

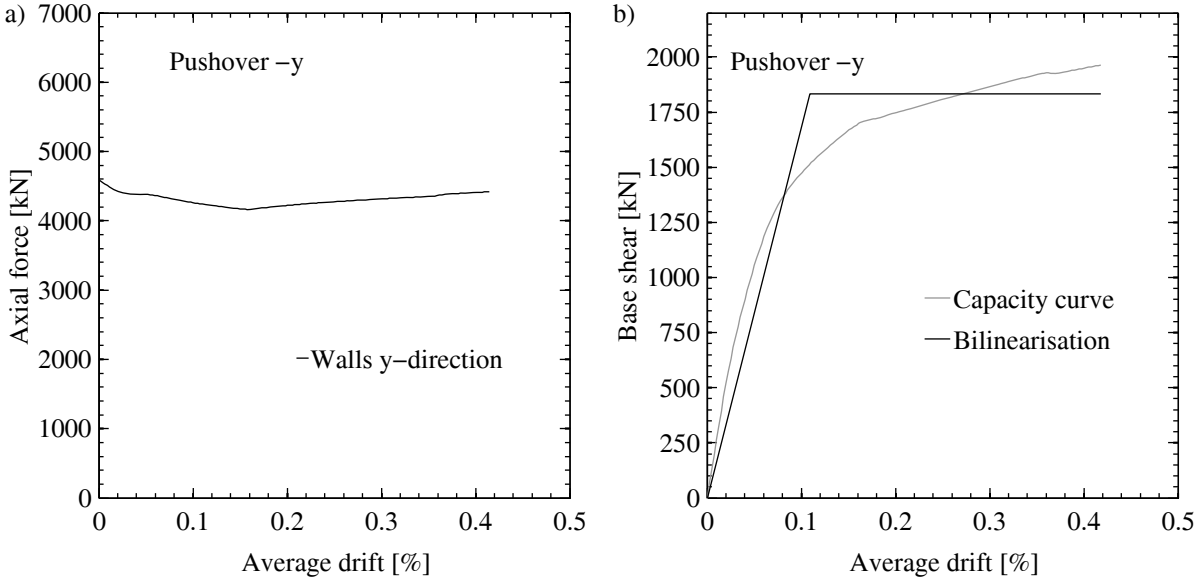

Figure 2.7 : TREMURI, pushover analysis in the negative y-direction: Variation of total axial force carried by the walls 8, 9, 10, 25 (a). Bilinearisation of the global pushover (b).

2.3.4 Capacity spectrum method

The structure is evaluated for a EC8-Type 2 spectrum of soil class C [12]. The corner periods of this spectrum are T_B=0.2 s, T_C=0.6 s, T_D=2.0 s and the soil factor is S=1.15. EC8 proposes as nonlinear static assessment method a capacity spectrum method [36]. The evaluation of seismic performance of the MDOF system according to this method comprises two steps: First, the pushover curve of the MDOF system is transformed into the pushover curve of an equivalent SDOF system, which yields the displacement capacity of this equivalent SDOF system. Second, the displacement demand on the equivalent SDOF system is determined and compared to the displacement capacity.

There are different ways of computing the mass and force of the equivalent SDOF system, which eventually all yield the same result. The one included here corresponds to the most physical representation: The period of the equivalent SDOF system is equal to the fundamental period of the MDOF, the mass of the equivalent SDOF corresponds to the effective modal mass of the first mode of the MDOF and the base shears of both systems are equal. The displacement of the SDOF is the top displacement of the MDOF system divided by the participation factor Γ:

$$m_{SDOF} = \frac{(\sum m_i \varphi_i)^2}{\sum m_i {\varphi_i}^2} \tag{2.22}$$

$$\Gamma = \frac{\sum m_i \varphi_i}{\sum m_i {\varphi_i}^2} \tag{2.23}$$

$$\Delta_{SDOF} = \frac{\Delta_{top}}{\Gamma} \tag{2.24}$$

$$V_{SDOF} = V_{base} \tag{2.25}$$

$$k_{SDOF} = \frac{V_{base}}{\Delta_{y,top}/\Gamma} \tag{2.26}$$

$$T_{SDOF} = 2\pi \sqrt{\frac{m_{SDOF}}{k_{SDOF}}} = T_1 \tag{2.27}$$

where ϕ_i is the vector of the first mode at storey i normalised to unity at the top floor; m_i is the mass of storey i. In this method, the target displacement demand is evaluated based on the spectral displacement at the effective first period T_1 of the structure. For short period structures ($T<T_C$) it is increased to account for

$T_1<T_C$:

$$q_u = \max(S_e(T_1) \cdot m_{SDOF}; 1) \tag{2.28}$$

$$S_u(T_1) = S_e(T_1) \cdot \left(\frac{T_1}{2\pi}\right)^2 \tag{2.29}$$

$$\Delta^* = \frac{S_u(T_1)}{q_u}\left(1 + (q_u - 1)\frac{T_C}{T_1}\right) > S_u(T_1) \tag{2.30}$$

$T_1>T_C$:

$$\Delta^* = S_u(T_1) \tag{2.31}$$

The displacement check is satisfied if the displacement capacity of the equivalent SDOF is larger than the displacement demand Δ*:

$$\Delta_{u,SDOF} \geq \Delta^* \tag{2.32}$$

In the following, different analysis methods are compared. These comprise next to the capacity spectrum method also dynamic analyses. To compare the different analysis methods, we determine for each analysis method that peak ground acceleration (PGA) for which the displacement capacity equals the displacement demand. The peak ground acceleration corresponds to the maximum absolute acceleration of the ground, i.e., to:

$$PGA = a_g \cdot S \tag{2.33}$$

where a_g is the peak ground acceleration for rock and S the site amplification factor.

Figure 2.8 shows for the negative and positive y-direction the maximum PGAs that the structure can sustain according to the capacity spectrum method. The PGAs in the two directions differ by 25% (2.71 m/s^2 and 2.16m/s^2) as the structure has slightly different force capacities and displacement capacities in the two directions.

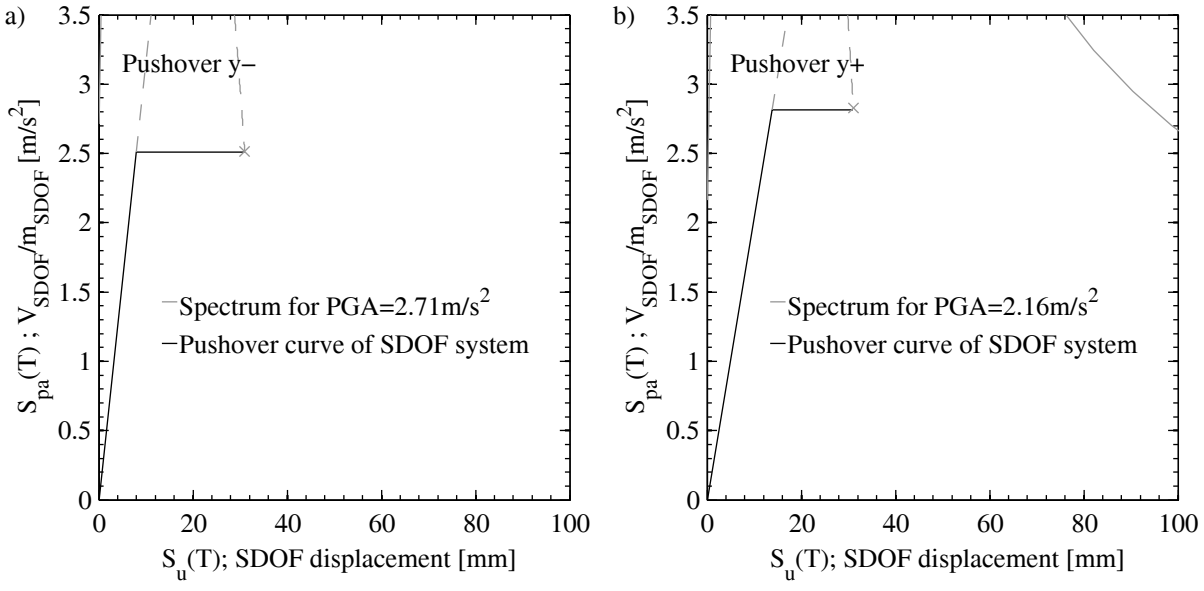

Figure 2.8 : TREMURI, capacity spectrum method: PGA that lead for the negative and positive direction to the attainment of 0.4% first storey drift.

Table 2.3: Tremuri model: Equivalent SDOF system for loading in the negative y-direction

Storey	m_i	φ_i	$m_i\varphi_i$	$m_i\varphi_i^2$
4	222	1.00	222	222
3	240	0.73	175	128
2	240	0.43	104	45
1	240	0.17	40	7
Sum	942		541	402

$$m_{SDOF} = \frac{(\sum m_i\varphi_i)^2}{\sum m_i{\varphi_i}^2} = \frac{541^2}{402} = 729\ t$$

$$\Gamma = \frac{\sum m_i\varphi_i}{\sum m_i{\varphi_i}^2} = \frac{582}{432} = 1.35$$

$$k_{SDOF} = \frac{V_{base}}{\Delta_{y,top}/\Gamma} = \frac{1830}{0.0107} \cdot 1.35 = 2.29 \cdot 10^5\ \frac{kN}{m}$$

$$T_{SDOF} = 2\pi\sqrt{\frac{m_{SDOF}}{k_{SDOF}}} = 2\pi\sqrt{\frac{729}{2.29 \cdot 10^5}} = 0.35s$$

2.3.5 Dynamic analyses

As benchmark analyses, nonlinear time history analyses with twelve spectrum compatible records are carried out. The records are twelve non-stationary records for soil class C [37]. Figure 2.9 shows the acceleration and displacement response spectra for a PGA of 1.15 m/s^2. The structure was analysed using an initial stiffness and mass proportional Rayleigh damping model. The damping coefficient was set to 5% of damping in the first and second mode.

For each record, the accelerations were scaled such that the maximum absolute value of the first storey drift corresponded to 0.4%±0.02%. The resulting PGA-values for each record are summarised in Table 2.4. The third column labelled with "PGA" corresponds to the actual peak acceleration of the record. The fourth column labelled with "PGA code spectrum" corresponds to the peak ground acceleration of the code spectrum, which fits the spectrum of the record best; it is this PGA value which the discussion will be based on. The average PGA-value, for which the structure reaches a peak first storey drift of 0.4%, is 2.18 m/s^2. The base shear – top displacement hysteresis curves for the 12 records are shown in Figure 2.10.

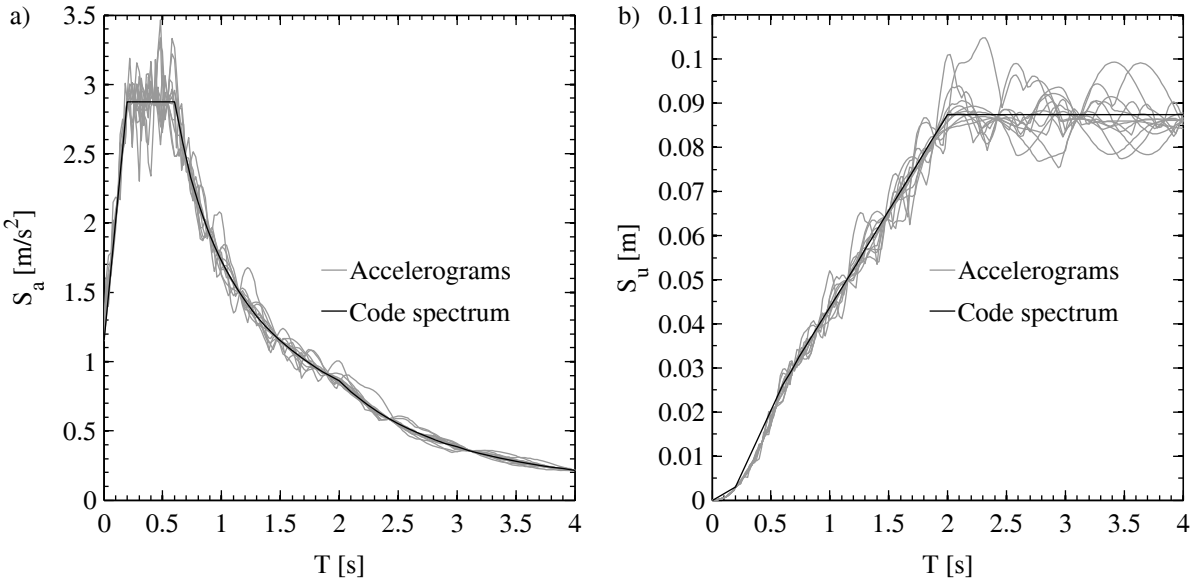

Figure 2.9 : Dynamic analyses: Acceleration (a) and displacement (b) spectra for the 12 records used for the dynamic analyses and comparison to the design spectra. The spectra are plotted for a PGA of 1.15m/s^2.

Table 2.4 : Dynamic analyses: PGA-values for each record that led to a maximum first storey drift of 0.4%.

Record	**PGA [m/s^2]**	**PGA [m/s^2] code spectrum**
1	2.22	2.11
2	2.13	1.98
3	2.01	1.79
4	2.47	2.48
5	2.32	2.27
6	2.12	2.07
7	2.12	1.96
8	2.98	2.69
9	2.58	2.29
10	2.11	1.98
11	2.85	2.64
12	1.95	1.85
average	**2.32**	**2.18**
min.	**1.95**	**1.79**

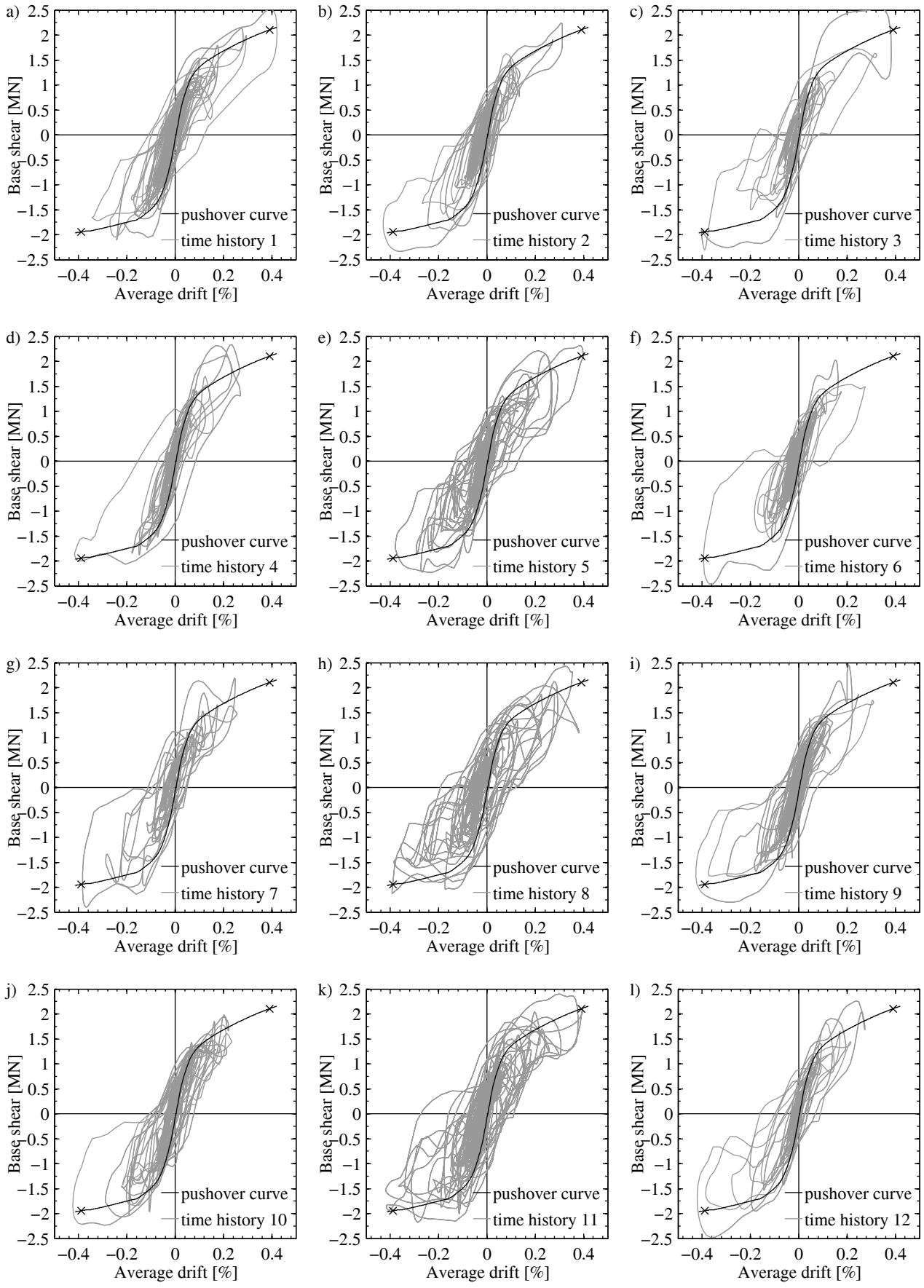

Figure 2.10 : TREMURI, dynamic analyses: Global-force displacement response and comparison to pushover curves.

2.3.6 Discussion

The nonlinear static and dynamic evaluations of the building that were presented in Sections 2.3.4 and 2.3.5 respectively were both based on the same Tremuri-model (Section 2.3.1). Differences in the predicted capacities, which were expressed in terms of the maximum PGA that the structure could sustain, result therefore from the analysis method and not the numerical model. The comparison shows, however, that the two analysis methods (capacity spectrum method, time history analyses) yield very similar PGA-values: according to the capacity spectrum method the maximum PGA is 2.16 m/s^2; according to the dynamic analyses the structure can sustain a PGA of 2.18 m/s^2.

2.4 Computing the pushover curve with spreadsheet calculations

For engineering practice, nonlinear static or even dynamic analyses might often not be practical and much simpler and faster analyses methods are required. One such method was developed by Lang in her thesis [5] and has also been included in the technical documentation SIA D0237 [7]. It is an extension of the storey-mechanism approach, which was introduced by [38] for computing the force capacity, to a method that allows computing the entire pushover curve of a building. The SIA D0237 method computes pushover curves for each wall and calculates the structure's pushover curve as sum of all individual wall curves that are oriented in one direction. To determine the displacement demand, the capacity spectrum method as implemented in EC8 [12] is applied (see Section 2.3.4).

2.4.1 Assumptions behind the SIA D0237 method

Computing the pushover curve of the building by means of simple spreadsheet calculations requires some simplifying assumptions. The assumptions behind the SIA D0237 method are discussed in the following as not all of these are outlined in [7].

Effective stiffness: A predefined ratio of the gross sectional stiffness is used as effective stiffness in order to account for the effect of cracking. The SIA D0237 method assumes that the stiffness reduces uniformly over the wall height.

Mode shape: No modal analysis is performed but it is assumed that the mode shape is linear over the height of the building. This assumption is often very reasonable and appropriate.

Coupling effect by spandrels and slabs: Spandrels and slabs (in particular RC slabs) transmit shear forces and change therefore the height of zero moment and the axial force of the walls, as well as the deformed shape at failure. The coupling effect is accounted for in an approximate manner by the following assumptions:

- The height of zero moment h_0 of each wall is set to a predefined value and assumed independent of the applied lateral displacement. If the building features continuous RC slabs, SIA D0237 recommends $h_0=h_s$ (if the slab features large openings, $h_0=2h_s$ is recommended).
- The variation in axial force due to the coupling effect is neglected and the resistance of the walls computed for the axial force resulting from gravity loads only.

Note also that this approach of treating the coupling effect does not satisfy the global moment equilibrium: For a building with n storeys and constant storey heights and masses, if one assumes, for example, a horizontal force distribution with equal forces at each storey level, the height of the resultant force is $h_{eff}=((n-1)/2+1)\ h_s$ and the overturning moment demand therefore $OTM=V_{base}\ h_{eff}$. For a building with four storeys this would correspond to 2.5 h_s. The overturning resistance of the structural model is, however, $OTM=V_{base}\ h_0=V_{base}\ h_s$. The difference results from the variation of the axial force variation in the walls due to the overturning moment, which is neglected in the SIA D0237 method.

Reduced height due to spandrels: Spandrels decrease the free wall height, i.e., the height of the wall that will be subjected to significant deformations. Neither for the displaced shape at yield nor at ultimate does the SIA D0237 method account for the reduced deformable storey height. Hence, in the case of spandrels the displacement at yield and ultimate is overestimated while the strength is underestimated. To eliminate the

effect of the spandrels when comparing the results of the different methods, the spandrels are also not in-included in the finite element models although the reference structure featured spandrels [32].

Failure mode: The SIA D0237 method considers only the possibility of first storey failures. Failure in higher storeys is not evaluated. To eliminate any differences that could result from failures at higher storeys, the macro-element model and the bilinear model also consider first storey failure only.

Deformed shape at failure: With regard to the deformed shape at failure, the SIA D0237 method assumes that inelastic deformations occur only in the first storey and that these inelastic deformations result only in a translation and not in a rotation at the height of the first storey slab. The latter is only applicable if $h_0=0.5h_s$ and therefore not compatible with the general recommendation in SIA D0237 of $h_0=h_s$.

Computation of the capacity curve of the system: To obtain the capacity curve of the system, the capacity curves of all walls are added up. To do so, one plots the force-top displacement curves of each wall and adds up the wall resistances as a function of the top displacement. With this approach the displacements of the individual walls are not compatible at the storey levels. This results from the difference in deformation profiles before and after yield and the fact that the yield displacements of the walls are in general not identical.

2.4.2 Force-displacement curves of individual walls

In this document the pushover curves of the walls are determined as described in SIA D0237 but applying the EC8 strength formulae instead of the stress-field approach of SIA 266 [39]. Using the assumptions with regard to axial force and height of zero moment that were outlined above, the strength of each wall can be readily determined (see equations in Section 2.2.1).

For the complete pushover curve of each individual wall, estimates of its yield displacement and displacement capacity are required. The yield displacement at the first floor is estimated as:

$$\mathrm{d_{y1}} = \frac{\mathrm{V_{Rd}} \cdot \mathrm{h_s^3}}{3 \cdot \mathrm{EI_{eff}}} + \frac{\mathrm{M_1} \cdot \mathrm{h_s^2}}{2 \cdot \mathrm{EI_{eff}}} + \frac{6}{5} \cdot \left(\frac{\mathrm{V_{Rd}} \cdot \mathrm{h_s}}{\mathrm{GA_{eff}}}\right) \tag{2.34}$$

where V_{Rd} is the shear resistance of the wall (min of Eq. (2.7) and (2.11)), M_1 is the moment at the top of the first storey wall ($h=h_s$), EI_{eff} and GA_{eff} are the effective stiffnesses. The moment at the top of the first storey wall is:

$$\mathrm{M_1} = \mathrm{V_{Rd}}(h_0 - h_s) \tag{2.35}$$

If $h_0 = h_s$, M_1 and therefore also the second term of Eq. (2.33) is zero. Note that in SIA D0237 the factor 6/5 was omitted. All attempts of computing the displacements of a squat URM wall based on beam theory must necessarily be rather crude. Hence, there is no need to "refine" the expression; the term was merrily included as it was also included in the Timoshenko beam model and therefore facilitates the comparison between the different approaches.

The objective of this study is to compare the different methods on the basis of assumptions that are as compatible as possible. For this reason, the values of E_{eff} and G_{eff} were determined from the ratio of the initial to the effective stiffness of the macro-element model:

$$\mathrm{E_{eff}} = \mathrm{E_m} \cdot \frac{k_{eff,Tremuri}}{k_{initial,Tremuri}} = 7.0\ GPa \cdot 0.67 = 4.69\ GPa \tag{2.36}$$

$$\mathrm{G_{eff}} = \mathrm{G_m} \cdot \frac{k_{eff,Tremuri}}{k_{initial,Tremuri}} = 2.8\ GPa \cdot 0.67 = 1.88\ GPa \tag{2.37}$$

It is assumed that the displacement profile over the height of the building is linear at yield. The top displacement is therefore:

$$\mathrm{d_{yn}} = \mathrm{n} \cdot \mathrm{d_{y1}} \tag{2.38}$$

where n is the number of storeys of the building.

To complete the pushover curve, an estimate of the displacement capacity is needed. It is assumed that all walls fail in the first storey where the shear force demand on the walls is largest. The ultimate displacement at the first storey is computed as:

$$d_{u1} = \delta_u \cdot h_{st} \tag{2.39}$$

where δ_u is the drift capacity of the wall (Section 2.2.1), which is here assumed as 0.4% for all walls and failure modes. The corresponding top displacement is estimated assuming that the inelastic deformations concentrate in the first storey only:

$$d_{un} = d_{u1} - d_{y1} + d_{yn} \tag{2.40}$$

Using this method, the pushover curves of all walls in the y-direction are determined and the corresponding values summarised in Figure 2.11a. To eliminate differences between models due to the gravity load case, the strength values of the SIA D0237 method were computed using the axial forces resulting from the gravity load case of the Tremuri model. Note that—due to the simplifying assumptions behind this method—the capacity curves for loading in the positive and negative y-direction are identical.

Table 2.5: SIA D0237: Force and displacement capacity of walls in the Y-direction

Wall	N[1)] [kN]	h_0 [m]	V_{Rf} [kN]	V_{Rs1} [kN]	V_{Rs2} [kN]	V_R [kN]	Δ_{y1} [mm]	Δ_{yn} [mm]	Δ_{u1} [mm]	Δ_{un} [mm]
1	205	2.50	73	82	75	73	3.6	14.4	10.0	20.8
2	379	2.50	120	152	129	120	5.9	23.7	10.0	27.8
3	574	2.50	502	343	455	343	2.9	11.7	10.0	18.8
7	2297	2.50	1601	1119	1346	1119	7.3	29.4	10.0	32.0

1) Axial force obtained from Tremuri calculations (gravity loads only)

2.4.3 Force-displacement curves of building and evaluation of seismic performance

The capacity curve of the building is computed as sum of the capacity curves of the walls that contribute to the resistance in the y-direction (Figure 2.11). In total, seven walls are aligned in y-direction and the building resistance in the y-direction is computed as two times the resistance of Walls 8-10 and once the resistance of Wall 25.

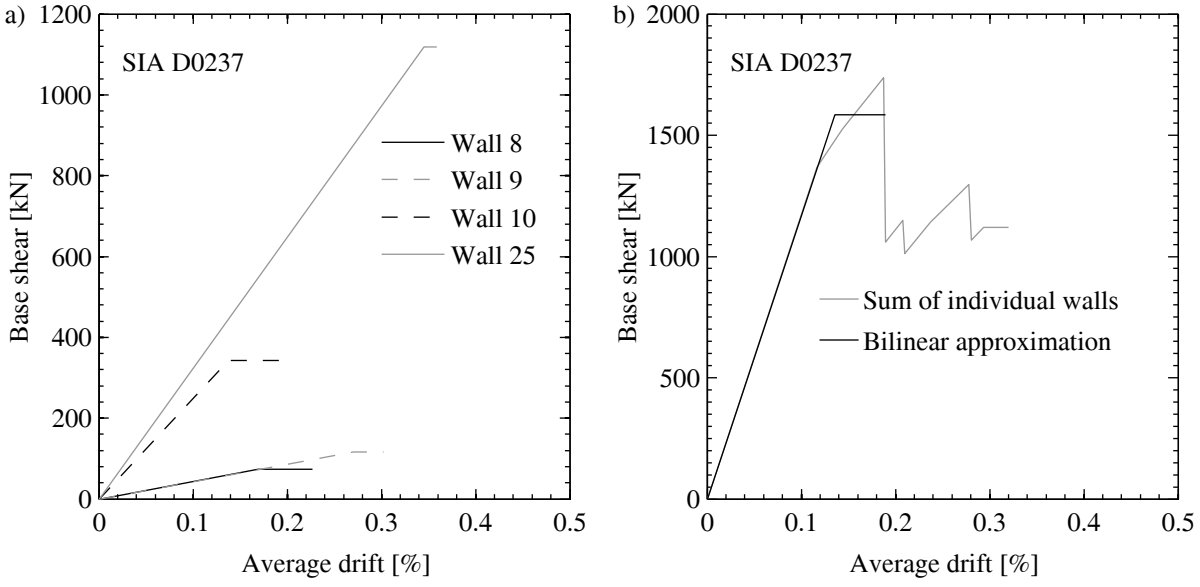

Figure 2.11 : SIA D0237: Pushover curves of individual walls (a) and pushover curve of system for loading in the y-direction (the results are the same for loading in the positive and negative direction).

The PGA, for which the structure would just reach its displacement capacity, is computed using the capacity spectrum method of EC8 (see Section 2.3.4). The effective period is 0.48 s (Table 2.6) and the PGA for which the displacement capacity is reached is 1.06 m/s^2 (Figure 2.12).

Table 2.6: SIA D0237: Equivalent SDOF system

Storey	m_i	φ_i	$m_i\varphi_i$	$m_i\varphi_i^2$
4	222	1.00	222	222
3	240	0.75	180	135
2	240	0.50	120	60
1	240	0.25	60	15
Sum	942		582	432

$$m_{SDOF} = \frac{(\sum m_i\varphi_i)^2}{\sum m_i\varphi_i^2} = \frac{582^2}{432} = 784\ t$$

$$\Gamma = \frac{\sum m_i\varphi_i}{\sum m_i\varphi_i^2} = \frac{582}{432} = 1.35$$

$$k_{SDOF} = \frac{V_{base}}{\Delta_{y,top}/\Gamma} = \frac{1580}{0.0135} \cdot 1.35 = 1.58 \cdot 10^5\ \frac{kN}{m}$$

$$T_{SDOF} = 2\pi\sqrt{\frac{m_{SDOF}}{k_{SDOF}}} = 2\pi\sqrt{\frac{784}{1.58 \cdot 10^5}} = 0.44s$$

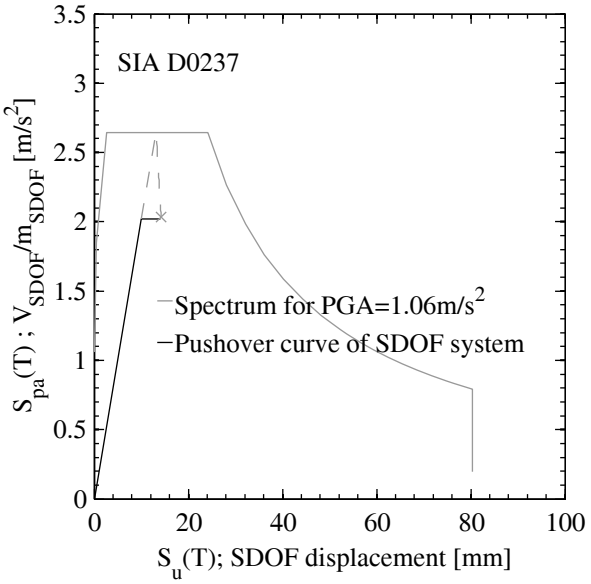

Figure 2.12 : SIA D0237: Performance point of building for loading in the y-direction (the results are the same for loading in the positive and negative direction).

2.4.4 Comparison to Tremuri model

The SIA D0237 method predicts that the capacity of the structure is only about 49% of the capacity of the structure predicted by the macro-element (SIA D0237: PGA = 1.06 m/s^2, Tremuri: PGA = 2.16m/s^2). This difference exists although several causes for possible differences have been eliminated artificially:

- Spandrels were not considered as the SIA D0237 does not account for the reduced effective height (Section 2.4.1).
- The ratio of effective to initial stiffness was set to be the same for both models.
- The SIA D0237 calculations were performed on the basis of the axial forces obtained from gravity load analysis with the macro-element model.

The differences must therefore be related to other assumptions on which the two models are based. Figure 2.13 shows the pushover curve of the building for loading in the negative y-direction. Taking the results

obtained with the macro-element model as benchmark, the comparison shows that the SIA D0237 method estimates the force capacity reasonably well (~-20%). The displacement capacity and the displacement ductility are, however, more strongly underestimated (-55% and 40% respectively). In the following the origin of these trends are discussed.

If one compares the pushover curves of the individual walls one notices that the differences between macro-element model and SIA D0237 model are larger than on the system level and also the force capacity is no longer well estimated (Figure 2.14). The differences result from the assumed shear span (h_0=h_s), the assumed axial forces and the assumed displaced shape at failure. Figure 2.16a shows that for macro-element model the shear span of the walls varies between 0.5-2.5 h_s while SIA D0237 assumes h_0=h_s. The figure suggests that for the shorter walls the preliminary estimate of 1h_s seems appropriate. However, for other locations of the wall (inner vs outer), other slab thicknesses, spacings of walls, and in particular other slab configurations (RC slabs, timber slabs, precast slabs, …), this finding might no longer hold. Figure 2.15 shows that the axial force in some of the walls of the macro-element varies with increasing lateral drift demand.

The largest influence on the performance of the SIA D0237 method seems to have the assumed displaced shape at ultimate displacement: Figure 2.16b highlights that in the SIA D0237 method the displaced shapes of the individual walls are not compatible (Section 2.4.1) and can vary rather widely if the system comprises walls of different length and / or different shear span. They also show that the assumption that all additional deformation beyond the yield point is concentrated in the first storey does not reflect reality. The reasons for this are twofold (see also Section 2.4.1):

- If the shear span is larger than 0.5h_s, inelastic deformation of the first storey will induce also a rotation at the first storey slab. This rotation causes a rigid body movement of the superior storey which is not captured by the SIA D0237 method.
- If walls that respond mainly in shear are coupled to walls that respond mainly in flexure, the deformed shape is often rather close to linear (depending on the relative strength and stiffnesses of the walls, [31]).

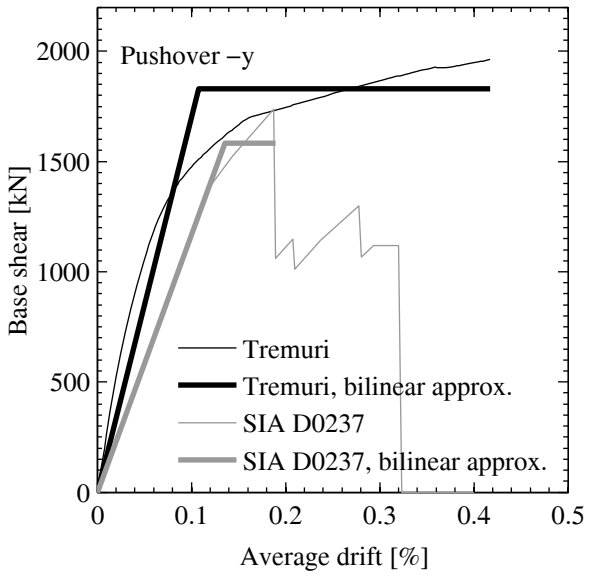

Figure 2.13 : Comparison of SIA D0237 and Tremuri model: Global pushover curves for loading in the negative y-direction.

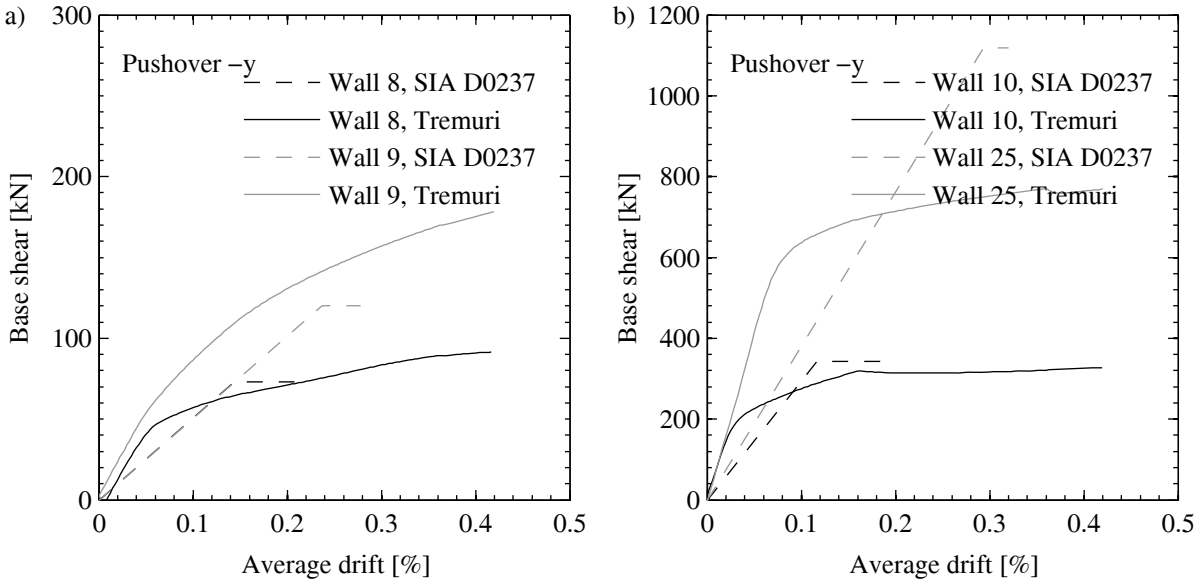

Figure 2.14 : Comparison of SIA D0237 and Tremuri model: Pushover curves of individual walls for the negative y-direction.

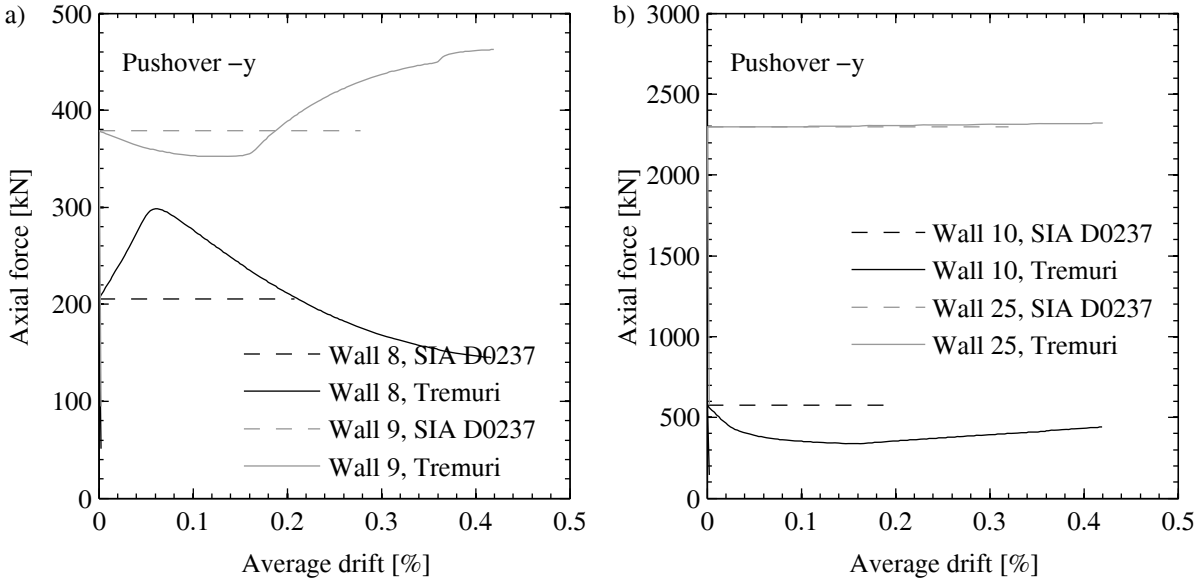

Figure 2.15 : Comparison of SIA D0237 and Tremuri model: Variation of axial force in individual walls for the pushover analyses in the negative y-direction.

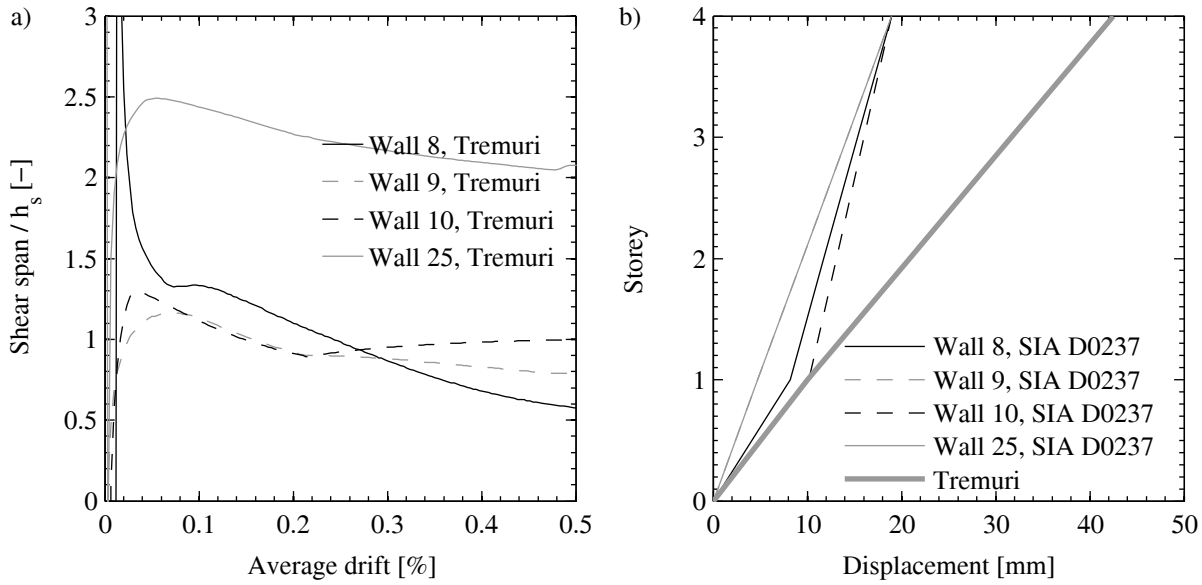

Figure 2.16 : Comparison of SIA D0237 and Tremuri model: Height of zero moment of walls in Tremuri model (a) and deformed shapes at ultimate displacement (b) for the pushover analyses in the negative y-direction.

2.5 Equivalent frame model with beam elements: 3muri

In Tremuri, the macro-element is not the only element type that can be used for modelling URM walls. As a second element a Timoshenko beam element with a beam element with plastic hinge is implemented. The hysteretic law of these plastic hinges is bilinear. In the professional version of Tremuri, which is called 3muri [14], only this bilinear element is available for modelling URM walls. For this reason, and to facilitate the reference to the two different models, the model of the example structure with beam elements is in the following labelled with "3muri" while the macro-element model is labelled with "Tremuri". The analyses are, however, carried out with Tremuri, but since both programs use the same solver the results with the beam element model are representative of the results 3muri would yield.

Important differences between the macro-element and the beam element relate to:

- The initial stiffness;
- The shear strength equations that are implemented;
- The definition of drift that is implemented;
- The fact that the beam element does not account for the vertical elongation of the wall due to rocking.

Section 2.5.1 outlines the modelling assumptions behind the beam element in 3muri. In Section 2.5.2 the capacity of the example structure when modelled with 3muri is assessed through the capacity spectrum method and in Section 2.5.3 the origins of the differences in the pushover curves obtained for the example structure with Tremuri and 3muri are analysed.

2.5.1 Nonlinear beam element model in 3muri

Stiffness of the nonlinear beam element in the elastic range:

The formulation of the nonlinear beam element applies in the elastic range the Timoshenko beam theory, resulting in the following expressions for the displacements (where a factor 5/6 is applied to the gross area to obtain A_s):

$$u_f = \frac{Vh^3}{3E_{eff}I} + \frac{V(h_0 - h)h^2}{2E_{eff}I} \tag{2.41}$$

$$\theta_f = \frac{Vh(h_0 - h)}{2E_{eff}I} \tag{2.42}$$

$$u_s = \frac{Vh}{G_{eff}A_s} \tag{2.43}$$

The E- and G-modulus represent effective properties. To allow for a fair comparison with the Tremuri model, these were derived—as for the SIA D0237 method—by multiplying the material values with the ratio of effective to initial stiffness that was obtained from the Tremuri analysis for loading in the negative direction:

$$E_{eff} = E_m \cdot \frac{k_{eff,Tremuri}}{k_{initial,Tremuri}} = 7.0\ GPa \cdot 0.67 = 4.69\ GPa \tag{2.44}$$

$$G_{eff} = G_m \cdot \frac{k_{eff,Tremuri}}{k_{initial,Tremuri}} = 2.8\ GPa \cdot 0.67 = 1.88\ GPa \tag{2.45}$$

Shear and flexural strength of the nonlinear beam element:

$$V_{fl} = \frac{N}{h_0}\left(\frac{L}{2} - \frac{N}{2 \cdot 0.85 \cdot f_m t}\right) \tag{2.46}$$

$$V_{R,s} = f_{vm0} \cdot t_w \cdot l_w + 0.4 \cdot N \leq 0.065\ f_m \cdot t_w \cdot l_w \tag{2.47}$$

Different criteria are available to define the shear strength of the bilinear element: in this case the Mohr-Coulomb criterion, applied on the gross area, was chosen in order to apply a similar formulation as to the macro-element. Other options, not considered in this case, are the Mohr Coulomb criterion applied on the compression area, and the Turnšek and Cačovic criterion.

Drift capacity of the nonlinear beam element:

The nonlinear beam element in 3muri, similarly to the macro-element in Tremuri, requires the definition of two ultimate interstorey drifts that define the failure drifts for shear and flexural failure. The drift definition differs, however, between the macro-element and the nonlinear beam element. For the nonlinear beam element the failure is determined on the basis of the common drift definition implemented in design codes:

$$\delta = \frac{u_j - u_i}{h} \tag{2.48}$$

Note, however, that the drift output of the nonlinear beam element is based on a further drift definition, which subtracts from the interstorey drift the rigid body rotation:

$$\delta = \frac{u_j - u_i}{h} + \frac{\varphi_j + \varphi_i}{2} \tag{2.49}$$

After the drift capacity is reached, the behaviour of the element is the same as the macro-element in Tremuri: the axial load bearing capacity is maintained, while the capacity to carry lateral loads is set to zero (no distinction between shear and flexural load bearing capacity is made).

To adopt the same failure criterion as for the Tremuri analysis and the SIA D0237 method, the failure of the building was assumed when the first storey reaches 0.4% drift.

2.5.2 Capacity spectrum method

The 3muri model yields fundamental periods of vibrations of 0.37 s and 0.36 s in the y- and x-direction respectively. The period T_y=0.36 s is very similar to the one obtained for the macro-element model on the basis of the effective stiffness, which is T_y=0.35 s (Section 2.3.4, in fact the differences result from rounding errors), since the E- and G-modulus of the 3muri model had been adapted to match the effective stiffness of the Tremuri model.

Using the pushover curve obtained with 3muri and applying the capacity spectrum method as outlined in Section 2.3.4, one obtains that the structure can sustain for loading in the negative y-direction a maximum PGA of 1.94 m/s^2 (Figure 2.17). For Tremuri, one had obtained for loading in the negative y-direction 2.71

m/s^2 (Section 2.3.4) and with the SIA D0237 method 1.06 m/s^2 (Section 2.4.3). 3muri leads therefore for the example structure to a capacity that is 25% lower than that of Tremuri and 100% higher than that of the SIA D0237 calculations. As outlined in Section 2.4.4, these differences are not representative but apply only to the example structure and the analysed direction of loading.

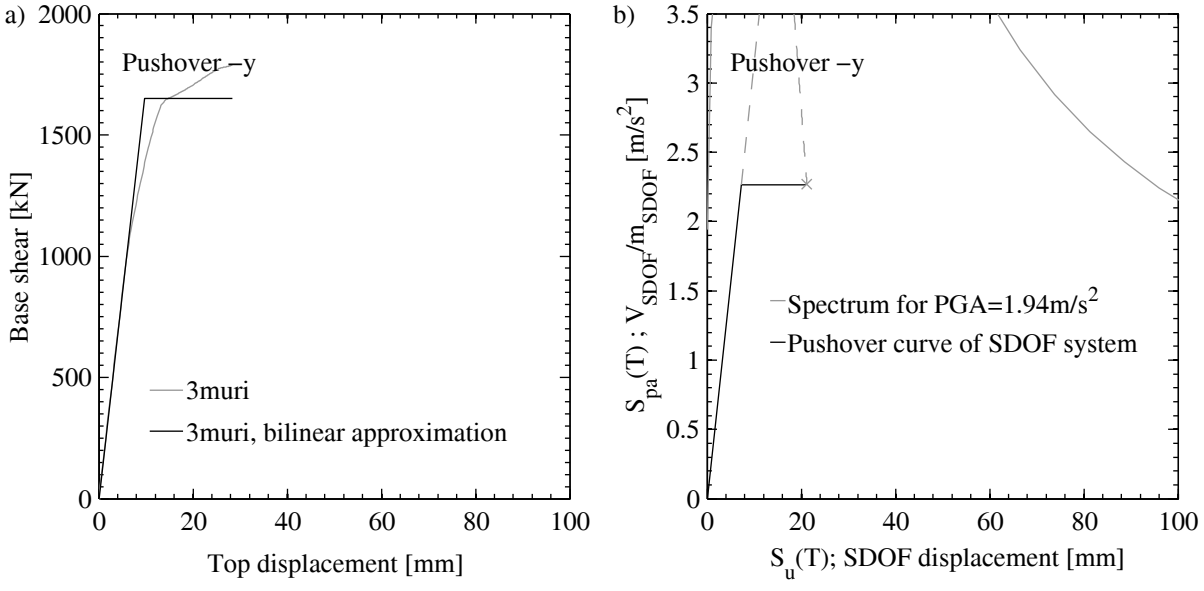

Figure 2.17 : 3muri: Pushover analysis in the negative y-direction and bilinear approximation (a) and capacity spectrum method which yields the PGA that leads to the attainment of 0.4% first storey drift.

2.5.3 Comparison to Tremuri model

In this section the results of the pushover analysis of the 3muri model are compared to the corresponding results obtained with the Tremuri model (Section 2.3.3). The comparison is carried out for loading in the negative y-direction.

Figure 2.18a shows the comparison of the pushover curves and their bilinear approximations. For the macro-element model, the elastic branch of the bilinear approximation corresponds to the secant stiffness at 70% peak strength. For the nonlinear beam element model, the elastic branch of the bilinear approximation corresponds to the initial stiffness of the nonlinear beam element model. Unlike the macro-element model, the nonlinear beam element model cannot capture the reduction in stiffness due to cracking. Any stiffness reduction in the beam element model results therefore from yielding of elements. For this reason, a different bilinear approximation was chosen. Since the effective stiffness values of the bilinear model were derived from the effective stiffness of the macro-element (see previous section), the two bilinear approximations have the same stiffness.

Figure 2.18b shows that the deformed shapes at 0.4% first storey drift are not identical, but the differences are significantly smaller than when compared to the SIA D0237 method. For all other quantities, i.e., shear forces and axial forces carried by the individual walls and the shear span, the two models yield somewhat different but in general comparable values (Figure 2.19 to Figure 2.21).

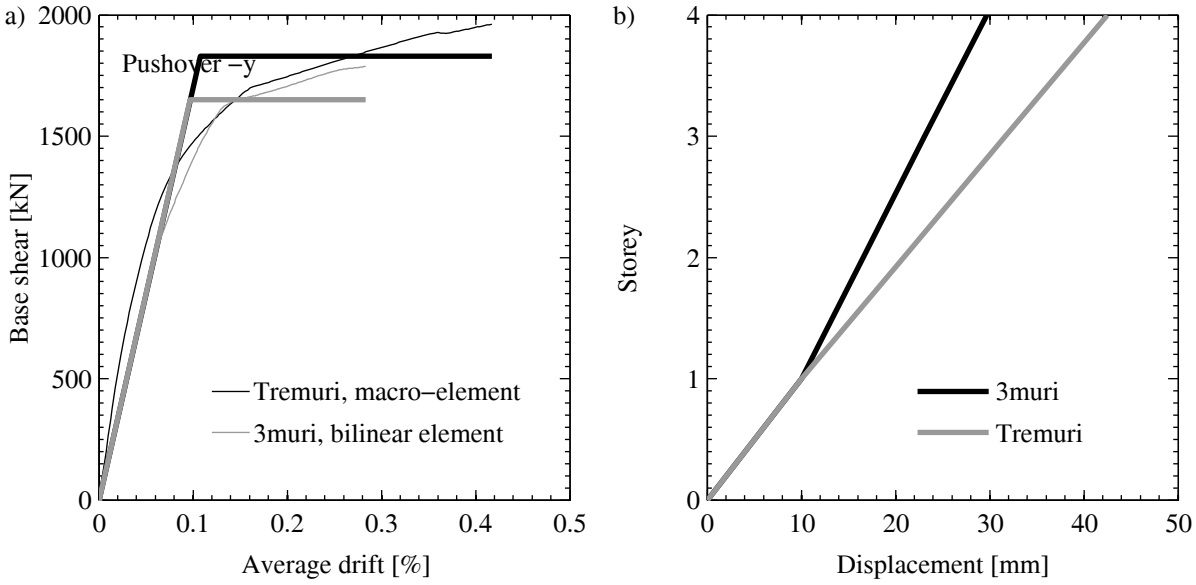

Figure 2.18 : Comparison of 3muri and Tremuri model: Pushover curves (a) and deformed shapes at ultimate displacement (b) for the pushover analyses in the negative y-direction.

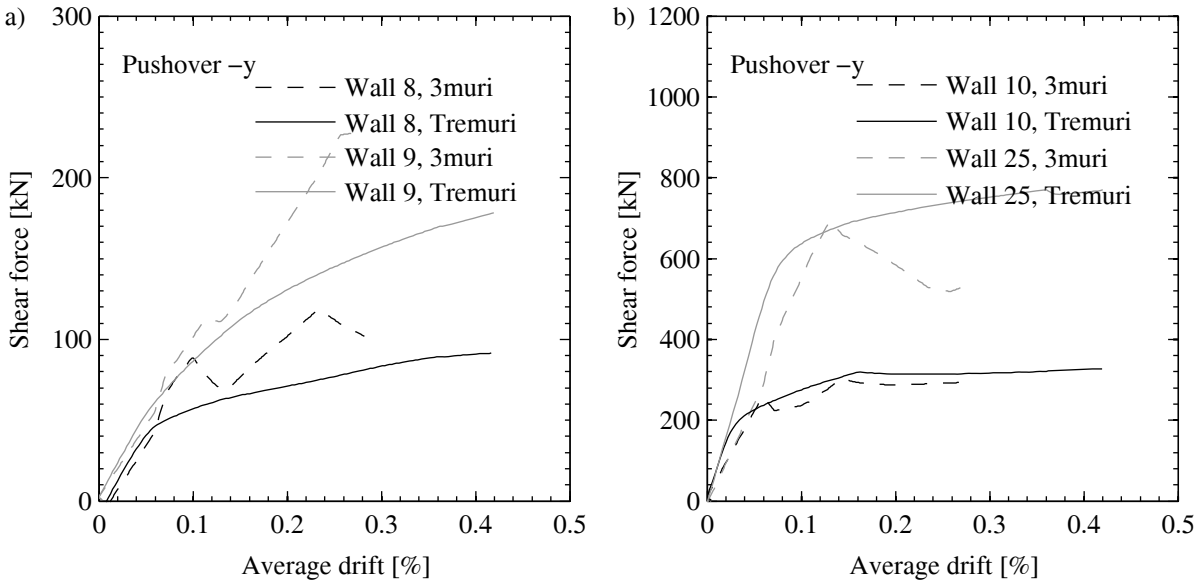

Figure 2.19 : Comparison of 3muri and Tremuri model: Pushover curves of individual walls for the negative y-direction.

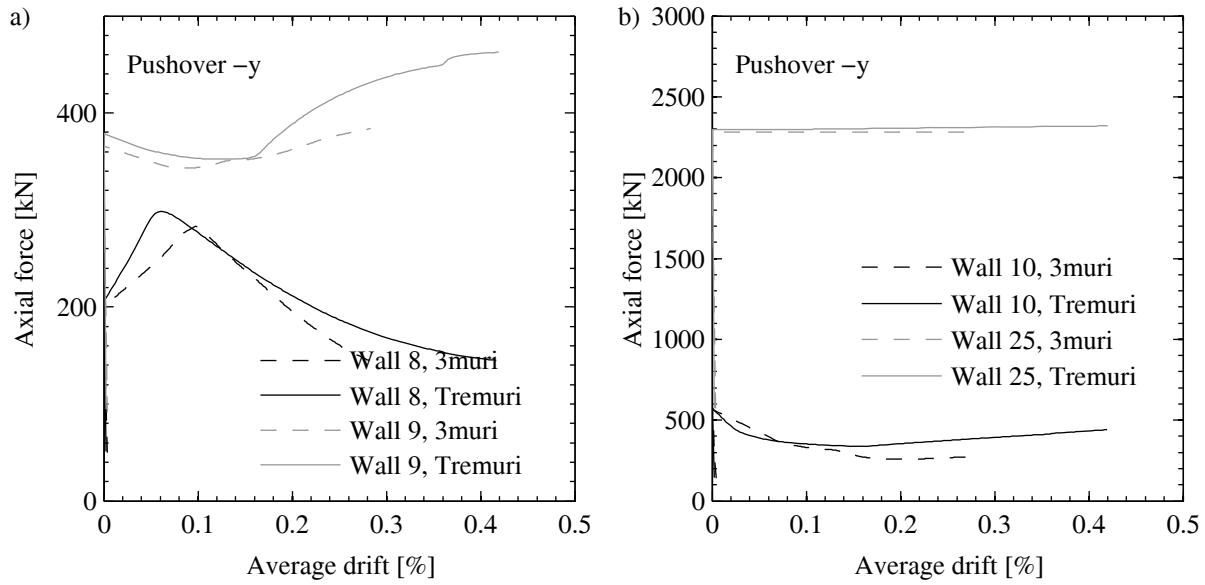

Figure 2.20 : Comparison of 3muri and Tremuri model: Variation of axial force in individual walls for the pushover analyses in the negative y-direction.

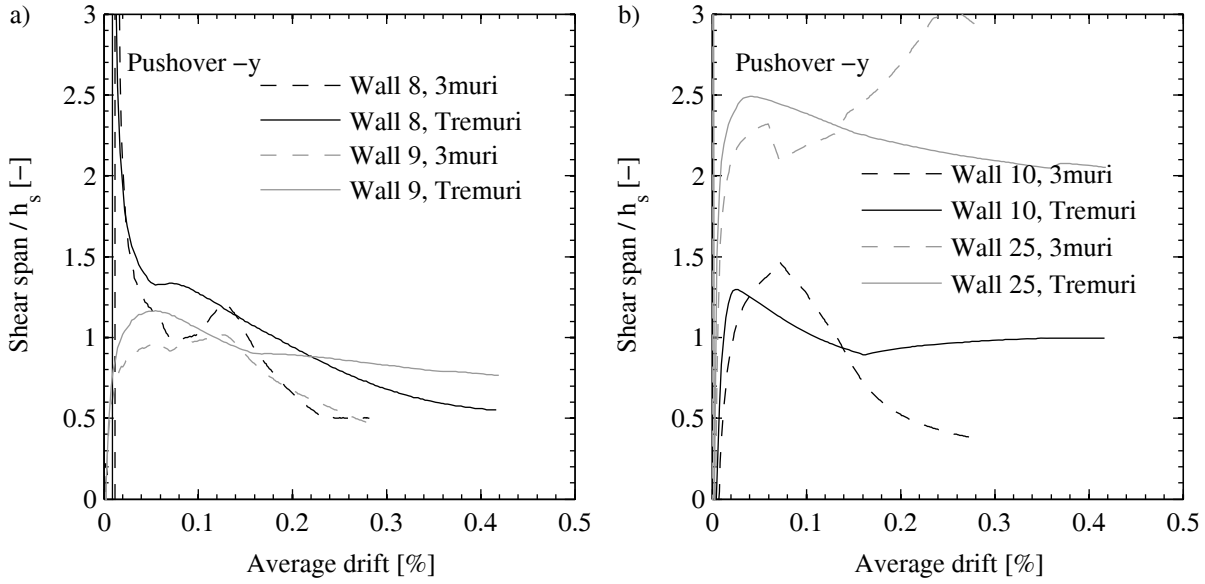

Figure 2.21 : Comparison of 3muri and Tremuri model: Variation of shear span in individual walls for the pushover analyses in the negative y-direction.

2.6 Conclusions and recommendations

The objectives of this chapter were the following:

- Identification of the assumptions underlying the assessment method in SIA D0237 [7].
- Comparison of the SIA D0237 method to the macro-element model, i.e., the Tremuri-model [10] which uses the macro-element by [25].
- Comparison of the 3muri-model [14] with the nonlinear beam element to the macro-element model.

The second and third objective was attained by analysing an example building with the three different models and comparing the results. This section summarises the results and formulates recommendations for the application of the SIA D0237.

Identification of the assumptions underlying the assessment method in SIA D0237

The spreadsheet calculations that are proposed in SIA D0237 are appealing because they are simple and finite element analyses not needed. However, as outlined in Section 2.4.1 they are based on several assumptions. These are:

1. A predefined ratio of the gross sectional stiffness is used as effective stiffness in order to account for the effect of cracking. The SIA D0237 method assumes that the stiffness reduces uniformly over the wall height. This is a common assumption that is also made in the context of other modelling approaches (e.g. for the nonlinear beam element model) although the extent of cracking and therefore the stiffness reduction might vary over the height of the wall.
2. The fundamental mode shape is assumed as a linear profile over the height of the building. This assumption is considered as very appropriate and does not need to be refined.
3. The height of zero moment h_0 of all walls is assumed as a preset value (typically $h_0=h_s$ where h_s is the first storey height). This choice of h_0 aims at considering the coupling effect by slabs and spandrels on the moment profile of the walls. The analysis of the example building has, however, shown that the actual h_0-values (i) differ between walls, (ii) differ from the assumed value (in the example, h_0-values between 0.5-2.5h_s were obtained), and (iii) vary with increasing displacement demand.
4. The change in axial forces in the walls due to the coupling effect by slabs and spandrels is neglected. As a result of assumptions 2 and 3, the global moment equilibrium of the structure is not satisfied.
5. Spandrels reduce the deformable height of the wall. This is at present not considered in the SIA D0237 method. The displacement capacity of a building with spandrels could therefore be overestimated.
6. Only failure modes that concern the first storey walls are considered by the SIA D0237 method. Although this is a common failure mode, failures of top storey walls are possible and would not be included in the assessment.
7. The rigid body rotation that results from inelastic rotations of the first storey walls are neglected. The latter would, however, only be applicable if $h_0=0.5h_s$ and therefore this assumption is not compatible with the general recommendation in SIA D0237 to set $h_0=h_s$. Neglecting the rigid body rotation leads to an underestimation of the displacement capacity. This seems to be in the case of the example building one of the main reasons why the SIA D0237 underestimates the capacity.
8. The capacity curve of the building is obtained by adding arithmetically the capacity curves of the individual walls. These curves are obtained without considering compatibility of displacements at the storey levels. The displaced shapes of the individual walls are therefore compatible at the top and at the base but not at the storey levels in between.

Analysis of the example building: Comparison of the results obtained with SIA D0237 method to the results obtained with the macro-element model

The SIA D0237 method was compared to the macro-element model by analysing an example building. For this building, the macro-element model predicted a 2.5 times higher capacity than the SIA D0237 method. The capacity was evaluated in terms of PGA that would lead to a first storey drift. This difference in PGA that was obtained for the example building analysed here is neither an upper bound nor a lower bound estimate of typical differences that can be expected between the two methods but the differences are strongly dependent on the actual building configuration. Moreover, two assumptions of the SIA D0237 method were compensated by making corresponding adjustments to the macro-element model. These were:

- Spandrels, despite being present in the original example building [32], were not included in the macro-element model.
- Failure modes other than first storey failures were not considered in the macro-element model.

Recommendation for the use of the SIA D0237 method

Evaluating whether the SIA D0237 method leads to conservative or non-conservative results is not straight forward as some assumptions tend to underestimate and some to overestimate the capacity of an URM building with RC slabs. The following recommendations are based on the results of this study and the authors' judgment.

It is felt that, due to assumption 6, the SIA D0237 method tends to produce conservative results for buildings without masonry spandrels, i.e., if the walls are only coupled by RC slabs. In this case, the results might, however, be rather conservative and therefore should be only used to verify the seismic performance of a structure. If the seismic performance check is not satisfied and retrofit measures are planned, it is recommended to use a more advanced assessment approach to avoid unnecessary interventions. If a larger set of buildings is analysed, it should be considered that assumption 6 might lead to an erroneous ranking of the structures that are most in need of interventions.

This study did not treat buildings with spandrels. For buildings with spandrels it is therefore at present not possible to state whether the SIA D0237 tends to over- or underestimate the capacity. The analysis of a larger set of example buildings would be necessary. In the meantime, it seems, however, possible to improve the SIA D0237 method by using elastic frame analysis.

- Improved shear span and axial force estimates could be obtained from an elastic equivalent frame model of the structure. The elastic model should be based on effective stiffness values. The nodes (intersections of walls and spandrels) should be modelled using rigid elements or assigning uncracked stiffness values.
- The same model could be used to determine the yield displacement.
- An elastic model where the stiffness of walls that are expected to undergo inelastic deformations could be used to estimate the ultimate displacement profile. First ideas in this regard were developed in [33].

The use of such elastic frame models could address the shortcomings related to the assumptions outlined at the beginning of this section.

Analysis of the example building: Comparison of the results obtained with the nonlinear beam element model to the results obtained with the macro-element model

The comparison showed that the Tremuri-model [10] which uses the macro-element by [25] and the 3muri-model [14] with the nonlinear beam element yield in many regards similar results. Nevertheless, the macro-element model predicts a 40% higher capacity than the nonlinear beam element model. Differences result from the different element formulation and in this regard in particular to the fact that the macro-model accounts for (i) an element elongation due to flexural deformations and (ii) a gradual reduction of the flexural stiffness due to decompression of the section and a reduction in shear stiffness due to shear cracking. The nonlinear beam element on the other hand is linear elastic up to the yield point. In the example analysed here, the ultimate drift capacities were set to large values and the ultimate displacement after the analysis evaluated as the top displacement for which a 0.4% first storey drift is reached. Note that the drift definitions that are implemented in the program differ between macro-element and bilinear element (see Sections 2.3.1 and 2.5.1).

3 OUT-OF-PLANE BEHAVIOUR OF URM WALLS - EXPERIMENTAL OBSERVATIONS AND VALIDATION OF A NUMERICAL MODEL[2]

Under earthquake loading modern unreinforced masonry (URM) buildings typically fail due to in-plane failure of the lower storey walls or due to out-of-plane failure of walls of the top storeys. In this paper, the out-of-plane failure of the top storey walls in modern URM buildings with stiff reinforced concrete (RC) floor slabs is investigated. The focus of this investigation lies on the boundary conditions that the RC slabs provide to the URM walls. More specifically, the paper investigates the influence of the in-plane deformations of flanking walls on these boundary conditions.

Hence, the paper treats the interaction of in-plane and out-of-plane URM wall response. The interaction of in-plane and out-of-plane response has also been recently studied for URM infills [40]–[44] and URM walls [45], [46]. However, these studies consider the coupling of the in-plane and out-of-plane response of the same wall element when subjected to bi-directional excitation. Here, a URM building subjected to only a uni-directional excitation is considered and the influence of the response of walls that are loaded in-plane on the boundary conditions of the walls that are loaded out-of-plane is investigated. The paper focuses on modern URM walls constructed with hollow core clay bricks and cement mortar joints of normal thickness (~1 cm).

The literature reports several experimental campaigns that investigate the dynamic out-of-plane behaviour of brick masonry walls under seismic excitation. An extensive study was carried out by the consortium ABK [47], in which twenty-two URM walls with different height-to-thickness ratios, were tested dynamically. The walls, which had rectangular cross sections, were built with different types of units (grouted clay bricks and grouted and ungrouted concrete blocks). The horizontal input motions applied at the top and bottom of the walls were obtained from nonlinear analyses of a one storey URM building using actual earthquake ground motions. The walls were pinned at the base while the top of the walls was free to rotate and displace vertically. An additional mass was placed on the top of the walls to simulate the weight of additional structural elements. The authors observed that after the formation of a mechanism the walls did not collapse immediately but developed a stable rocking mechanism with displacements significantly larger than before the onset of rocking.

Griffith et al. [48] performed both static and dynamic tests on half-scale clay brick walls characterized by rectangular cross section and two different values of thickness. The test apparatus was composed of a shake table with a braced steel frame that provided lateral support to the top of the walls. The same displacement was imposed at the base and the top of the walls with the objective of representing boundary conditions of stiff floor diaphragms and neglecting in-plane drifts. The top of the walls were free to rotate and displace vertically. An axial load could be applied at the top of the wall by using six pre-tensioned springs. The test results underlined the importance of displacement rather than acceleration demand when determining whether or not a wall loaded out-of-plane will collapse under seismic loading. Meisl et al. [49] performed shake table tests on four clay brick multi-wythe rectangular walls, and also concluded that the peak displacement demand has a greater influence on out-of-plane collapse than the peak acceleration demand.

[2] This chapter corresponds one to one to a manuscript that was submitted in February 2015 to the journal Earthquake Engineering & Structural Dynamics: Marco Tondelli, Katrin Beyer, Matthew DeJong "Influence of boundary conditions on the out-of-plane response of brick masonry walls in buildings with RC slabs".

The investigation of the seismic response of an out-of-plane loaded URM wall element as a component of a global building system was the focus of the experimental test performed by Simsir et al. [50]. The authors performed shake table tests on a half-scale building composed of two out-of-plane URM walls and two in-plane reinforced masonry walls connected by floor diaphragms of varying stiffness. All walls had rectangular cross sections and were built with lightweight hollow concrete blocks. The out-of-plane loaded walls were free to rotate at their base while the top of the walls was free to rotate and displace vertically. The tests showed that diaphragm flexibility increased the out-of-plane displacement of the walls since increased flexibility resulted in an increase of the period and of the spectral displacement demand. In addition, the axial load and the wall mass significantly affected the out-of-plane response; collapse was observed only for the specimen subjected to reduced axial load and increased wall mass.

Dazio [11] carried out shake table tests that aimed at investigating the influence of boundary conditions on the out-of-plane response of URM walls. Six test units, all with rectangular cross sections but different wall widths and slenderness ratios, were constructed with hollow core clay bricks and standard cement mortar. The test set-up was designed to provide five different boundary conditions at the top of the walls: a "simply supported" condition where the top of the wall was free to rotate and displace vertically, a "fixed" condition where rotation and vertical displacement at the top of the wall were fully restrained, and three intermediate conditions where the top support had varying values of axial and rotational stiffness and the axial load was applied with different eccentricities with regard to the wall axis. It was observed that the "Simply Supported" condition was not always the most critical but that an eccentric axial force can cause collapse for lower levels of shaking. Additionally, increased levels of axial load were found to favour a sudden transition from rocking to collapse.

Penner and Elwood [51] carried out a shake table test on five URM wall specimens to investigate the effect of flexible diaphragms. The test units were multi-wythe rectangular walls built with solid brick units. The shake table setup included top and bottom springs that could be varied to represent different levels of diaphragms stiffness. The experimental campaign underlined that walls connected to flexible diaphragms are more stable than walls connected to stiff diaphragms. Additionally it was observed that for some boundary conditions the transition from rocking to collapse can occur very suddenly.

The most recurrent parameters that were investigated by the experimental studies were the effect of wall slenderness [47], [48], [50], [51], axial load [48], [50], [51] and flexible diaphragms [49]–[51] on the out-of-plane response of URM walls. With the exception of Simsir et al. [50], who included in-plane loaded walls and the top slab in the test setup, all the afore-mentioned tests studied the out-of-plane behaviour analysing the walls as single elements, separated from the rest of the structure. At the base, all studies placed the walls onto a foundation, which allowed the walls to rock. The tests were designed to provide idealised boundary conditions at the top of the out-of-plane loaded walls. The idealised boundary conditions at the top reflected in most cases a roller condition [47]–[51]. Only Dazio [11] modified the pinned condition at the top to model a certain rotational restraint and an eccentric axial force. All studies applied the same motion at the top and the bottom support. Three studies [49]–[51] placed springs between wall and support in order to account for deformations of flexible diaphragms, which result from the inertia force of the supported wall. It is interesting to note that none of the existing studies applied different motions at the top and the bottom in order to account for acceleration amplification over the height of the building and higher mode effects due to in-plane deformation of walls that are orthogonal to the out-of-plane loaded walls.

Contrary to these previous studies, the aim of this paper is to investigate the influence of boundary conditions on the out-of-plane response of URM walls in buildings with stiff RC slabs, and the effect that in-plane response of orthogonal walls has on the horizontal and vertical boundary conditions. In addition, the effect of different input motions at the top and bottom of the wall is investigated. In Section 3.1 the results of a uni-directional shake-table test performed on a four-storey structure built at half-scale will be presented and the observations from the test will be discussed. The four-storey structure was designed to provide different types of boundary conditions to the out-of-plane load-bearing URM walls. The observations from this experimental campaign were the motivation to investigate these boundary conditions more systematically through a numerical study. Section 3.2 presents the validation of a discrete element model, which is analysed using the software UDEC [52]. The model is then used in Section 3.3 to investigate the relative influence of three key boundary conditions, i.e., the difference in horizontal and vertical movement of the top and bottom slab and the effect of a horizontal support at the top.

3.1 Experimental campaign

The shake table test presented in this section is part of a larger research initiative focused on the study of the seismic behaviour of structures with RC and URM walls, where the two structural systems are coupled by RC slabs [27]. The test was carried out at the TREES laboratory of the European Centre for Training and Research in Earthquake Engineering (EUCENTRE) in Pavia (Italy), within the scope of a SERIES grant of the FP7 programme.

3.1.1 Test unit

The test specimen was a four-storey structure built at half scale. The structure had a rectangular footprint and was symmetric along its longitudinal axis, i.e., the direction along which the uni-directional motion was applied. The test specimen was composed of two RC walls and six URM walls and these vertical elements were coupled by stiff RC slabs (Figure 3.1). Four out of the six URM walls were loaded in-plane and two out-of-plane (Figure 3.1). The plan distribution of the structural elements was conceived such as to provide different boundary conditions to the out-of-plane loaded URM walls of the North and the South face: at the North face, the out-of-plane loaded URM walls were flanked by two in-plane loaded URM walls, while at the South face the out-of-plane loaded URM walls were flanked by two in-plane loaded RC walls (Figure 3.1). The longitudinal reinforcement of the RC walls passed through the slabs and the RC walls could therefore not rock on the slabs. The flanking elements, URM walls on one side and RC walls on the other, were expected to provide different vertical constraints to the RC slabs and therefore induce different vertical boundary conditions to the out-of-plane loaded URM walls.

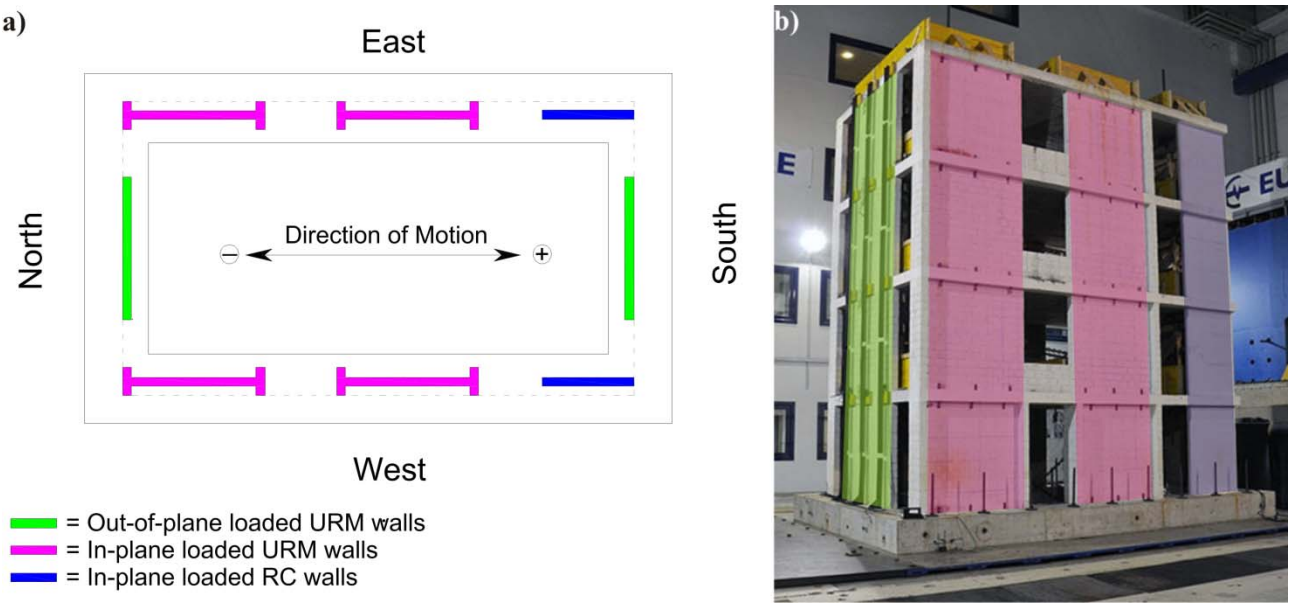

Figure 3.1. Test specimen: a) plan view and b) North-West view.

To perform the test at a reduced scale the *Artificial Mass Simulation* scaling law was applied [53]. This law requires that at reduced scale the stiffness, strength and deformation capacities of the construction materials are the same as at full-scale. For the applied scaling factor of two, the density of all materials should have been doubled. However, this is generally impossible to achieve and therefore additional masses were added in the form of concrete blocks, which were placed on the four RC slabs. Lumping the additional mass reproduces the in-plane behaviour of the structure relatively accurately. In order to correctly scale the seismic response of the out-of-plane URM walls it would have been necessary to "smear" the additional mass that relates to these walls over their height. Instead, the additional mass for the out-of-plane loaded walls was also included by placing additional concrete blocks on the slabs. This was done for ease of construction, while ensuring that the in-plane seismic loading obeyed scaling laws and to avoid out-of-plane collapse prior to realisation of the full in-plane capacity. The first out-of-plane collapse of a URM wall was

obtained in the final run, in which the in-plane loaded URM walls lost their axial load bearing capacity and the test was stopped.

The URM walls were constructed using half-scale hollow-core clay brick units that were specifically manufactured for this project. The units, with dimensions of 150 x 95 x 95 mm, were assembled using a standard mortar of class M15; both horizontal and vertical joints were 5 mm thick. The brick units were designed to reproduce the behaviour of full-scale bricks in masonry walls that were subjected to in-plane loading [54]. The out-of-plane loaded URM walls were 1.545 m long, 1.400 m high and 95 mm wide. A vertical section of these walls is shown in Figure 3.2.

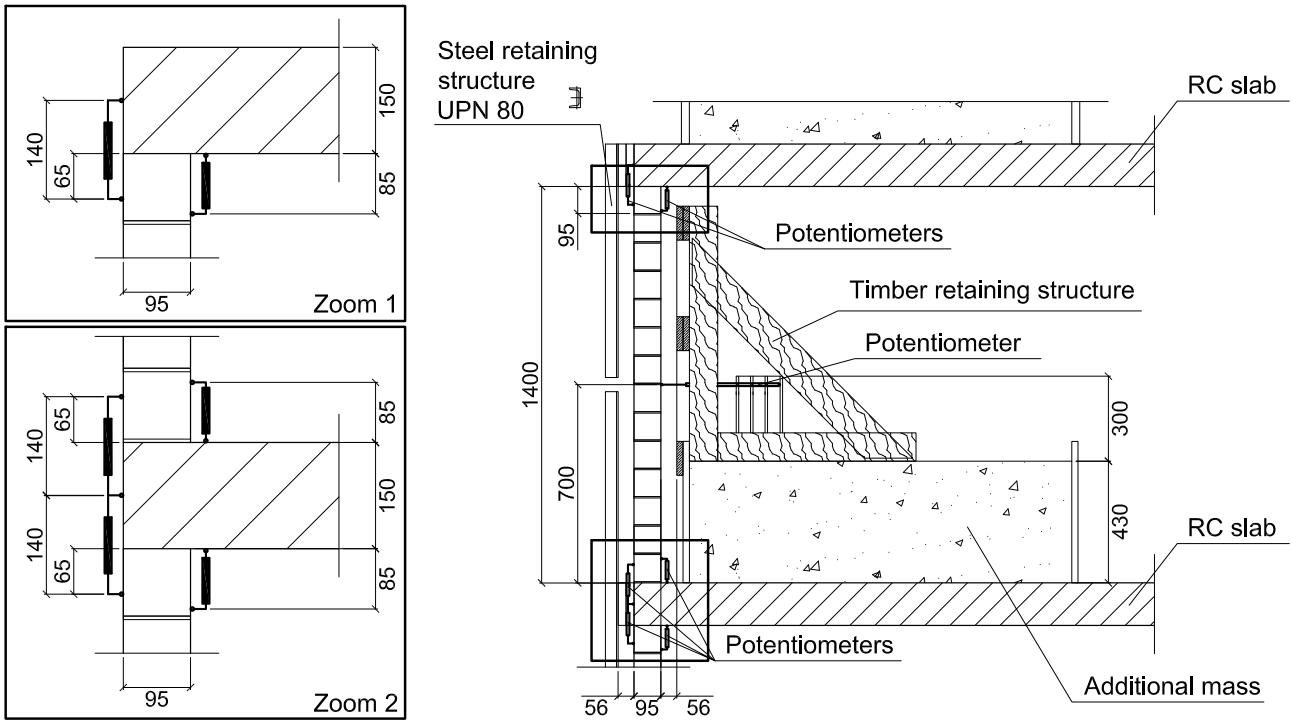

Figure 3.2. Vertical section of one of the out-of-plane loaded URM walls (dimensions in mm).

Each out-of-plane loaded wall of the second, third and fourth storey was instrumented with five potentiometers. One potentiometer measured the out-of-plane horizontal displacement at mid-height of the walls; the latter was fixed to a support on the additional mass and therefore directly connected to the RC slab. Two additional potentiometers were used to measure the internal and external vertical displacement of the top and bottom row of bricks and were connected to the RC slabs. An optical measurement system was employed to record the displacement response of the structure during shaking. This system [55] uses high definition cameras to record the 2D displacement of reflecting markers that are glued to the structure and was used to record the in-plane displacements of the URM walls and RC slabs of the West façade of the structure.

Figure 3.2 shows the retaining structures that were installed on the outer and inner side of the out-of-plane loaded URM walls. The purpose of these structures was to avoid the collapse of the walls onto the shake table. The retaining elements were installed at a clear distance of 56 mm from the walls (Figure 3.2), which corresponds to approximately 60% of the wall thickness, and therefore greater than the unstable point of static equilibrium for the out-of-plane mechanism.

3.1.2 Ground motion, testing sequence and data set

The input motion was the E-W component of the ground motion recorded at the Ulcinj-Hotel Albastros station during the April 15th, 1979 Montenegro Earthquake. The time axis of the record was divided by a factor of $\sqrt{2}$ to account for the fact that the test was carried out at half-scale. The record was selected for its broad frequency content. Nine dynamic tests were performed with increasing value of peak ground

acceleration (PGA), from 0.05 g to 0.9 g. Only the last two tests will be discussed in the following; these had PGAs of 0.7g and 0.9g respectively. A description of the in-plane damage and comparison to the predicted response is presented in Beyer et al. [13]. Additionally, the full data set collected during the experimental campaign is publically available at 10.5281/zenodo.11578.

3.1.3 Visual observations of out-of-plane response of URM walls

After each run, a survey of the structure was performed to investigate the progression of the level of damage to the structure. Up to run 8, some out-of-plane displacement occurred but no residual damage was observed in the out-of-plane loaded URM walls. During the last test (PGA = 0.9 g), significant out-of-plane displacements of the second to fourth storey walls of the North face were observed. The wall on the top storey clearly hit the inner support structure while the second and third storey walls did not touch the support structures. The mechanism of the top storey wall included the formation of bed joint cracks at the top and bottom and at mid-height of the wall, which was confirmed by an inspection after the test (Figure 3.3).

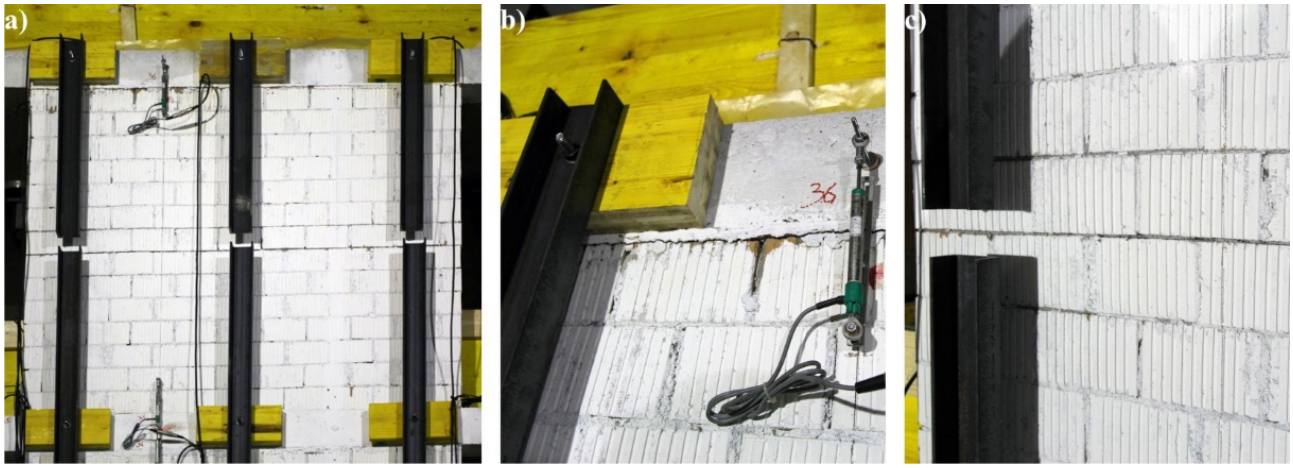

Figure 3.3. Damage in the 4th storey out-of-plane loaded wall on the North side of the structure: a) full wall view, b) detail of the top crack and c) detail of the mid-height crack.

The second and third storey walls did not hit the support structure but showed clear out-of-plane rocking displacements. For the second storey wall the third hinge seemed to have also formed at midheight while for the third storey wall it had formed at approximately three quarters of the storey height. Unlike the walls of the North face, the walls of the South face did not show any visible out-of-plane displacements.

3.1.4 Discussion of recorded data for out-of-plane response of URM walls

The seismic performance of the out-of-plane loaded URM walls and the influence of the flanking elements is documented in Figure 3.4. The figure presents the horizontal out-of-plane displacements of the 2nd, 3rd and 4th storey walls on the North and South end of the structure (Figure 3.4a and Figure 3.4b, respectively). The out-of-plane displacement is the horizontal displacement measured by the potentiometer at mid-height of the walls minus half the relative displacement between the top and bottom slab. The latter are obtained from the optical measurements of the slab displacements. Figure 3.4 shows the maximum and minimum values of the out-of-plane displacement for tests 6, 8, and 9, corresponding to PGA values of 0.6, 0.7 and 0.9 g respectively (test 7 represented an after-shock and had a PGA of 0.4 g). For the previous tests the out-of-plane displacements had been very limited. Positive values in Figure 3.4 represent displacements towards the South. Therefore, positive displacements represent inward displacements for the North walls and outward displacements for the South walls.

Figure 3.4 shows that the North walls experienced significantly higher out-of-plane displacement than South walls. The minimum and maximum displacements of the 4th storey walls during the last test were -20 mm and +63 mm for the North wall, but only -7 mm and +4 mm for the South wall. The North walls were flanked by URM walls while the South walls were flanked by the RC walls. These flanking elements had a

significant influence on the boundary conditions and therefore on the response of the out-of-plane loaded walls.

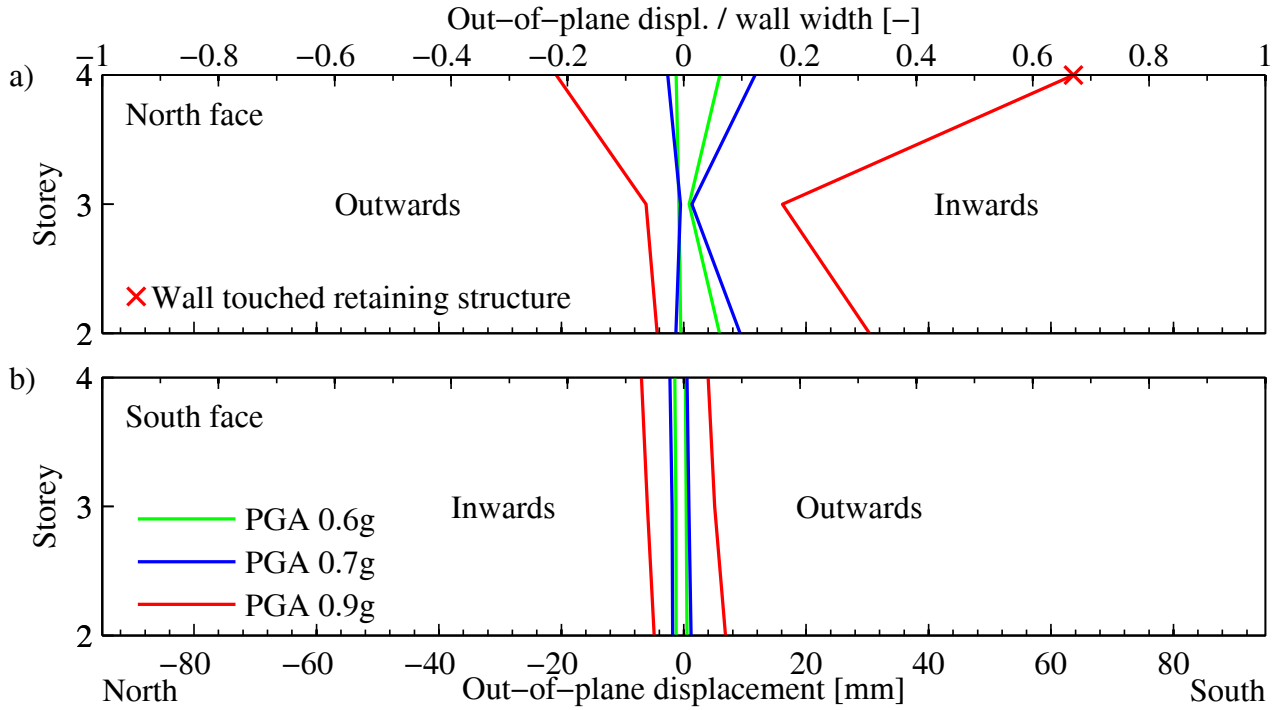

Figure 3.4. Out-of-plane horizontal displacement profiles: a) North walls, which are flanked by URM walls, and b) South walls, which are flanked by RC walls.

Figure 3.4 also shows that for the South walls the displacement profiles are fairly symmetrical and the displacement demands in the North and South direction are comparable. For the North walls, however, the out-of-plane displacements are significantly larger in the South direction than in the North direction. These results suggest that the loading direction plays a role when the flanking elements are URM walls, and out-of-plane rocking occurs, but not when the flanking elements are RC walls, which prevent nonlinear out-of-plane behaviour.

The observed behaviour can be explained with a schematic diagram depicting global in-plane behaviour of the structure (Figure 3.5). Due to the overturning moment, the axial force in the outer structural elements varied with the loading direction. When the structure was pushed from South to North, the axial load in the structural elements on the North side increased and the axial load decreased in the structural elements on the South side. The opposite happened when the seismic load was reversed. The loading direction had therefore an influence on the axial force to which the out-of-plane loaded walls, which were located at the perimeter of the building, were subjected.

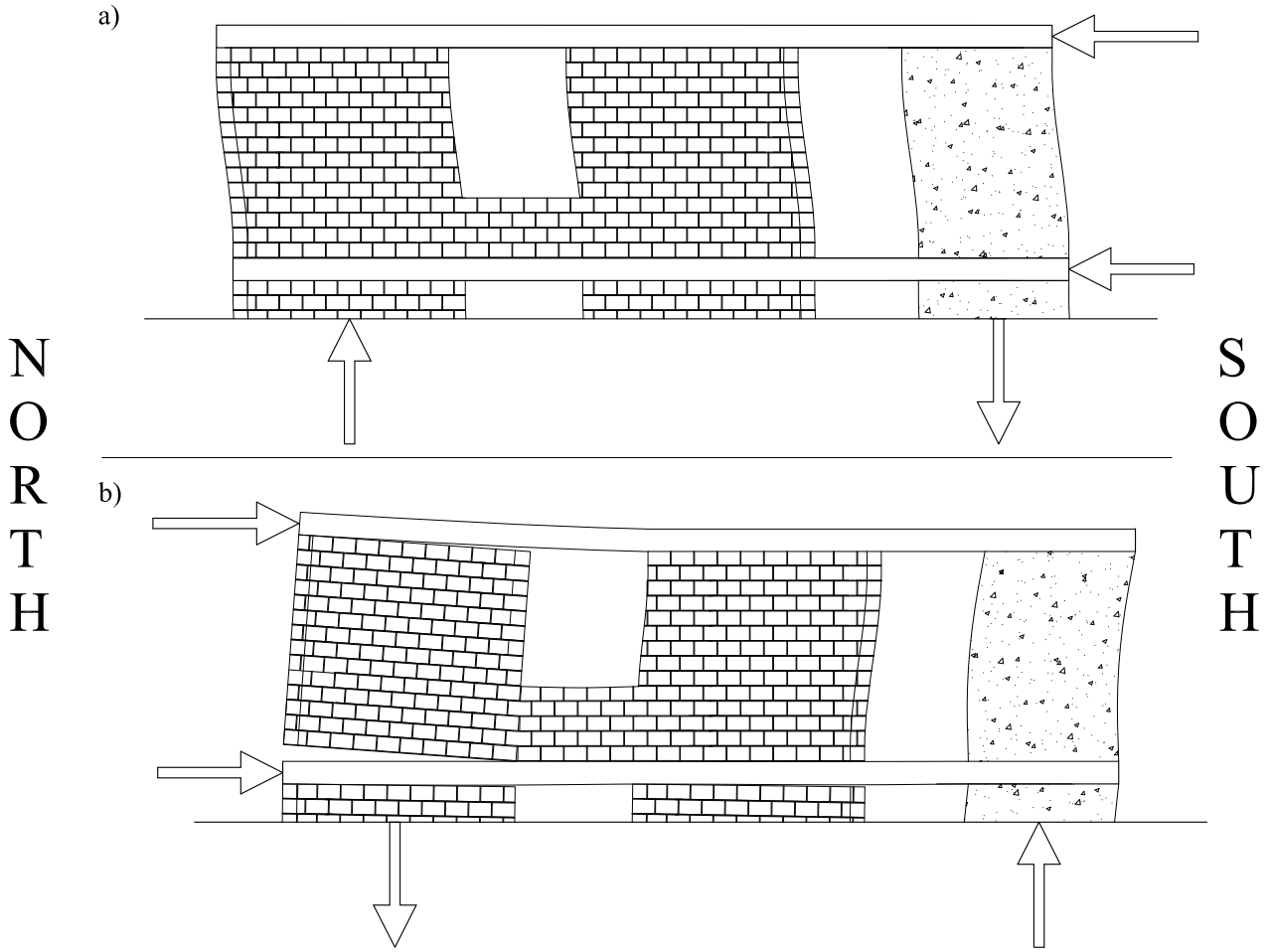

Figure 3.5. Schematic diagram of the effect of the loading direction: a) loading from South to North and b) loading from North to South.

Additionally, the kinematic boundary conditions are largely dependent on the flanking elements: on the North side the RC slab was simply supported on the in-plane loaded URM walls and could therefore uplift when the axial load was reduced and the in-plane URM walls rocked. At the instant when the slab uplifted, the vertical restraint to the North out-of-plane loaded wall reduced and rendered it vulnerable to out-of-plane excitation. Note that due to the elongation of the wall when rocking out-of-plane, the axial force in the out-of-plane loaded wall is not necessarily zero when the slab uplifts from the in-plane loaded wall. On the South side the RC walls restrained the RC slabs from uplifting and provided continuously a vertical restraint to the out-of-plane loaded wall.

These observations are supported by the data presented in Figure 3.6, which includes: i) the displacement time history of the fourth storey slab with respect to the foundation and with respect to the third storey slab, ii) the variation of the vertical distance between the two RC slabs framing the wall, where positive values correspond to an increase of distance between the two slabs (uplift) and iii) the out-of-plane mid-height horizontal displacements of the 4th storey URM wall on the North side, where positive values correspond again to displacements towards South.

The figure confirms a highly asymmetrical behaviour of the wall response as out-of-plane displacements in the South direction were significantly higher than in the North direction. Additionally, the peak out-of-plane displacement (at around 12 sec) occurs simultaneously to the peak uplift of the slab of 23 mm, confirming the interaction between slab uplift and vulnerability to out-of-plane deformations. The maximum value of out-of-plane mid-height displacement of 63 mm corresponds to the maximum displacement allowed by the retaining structure for a rocking mechanism with hinges at the extremities and at mid-height of the wall (the one experienced by the wall according to the horizontal cracks observed after the test, Figure 3.3). This

proves that the wall, during the last test, touched the internal retaining structure and would have collapsed out-of-plane had the retaining structure not been installed.

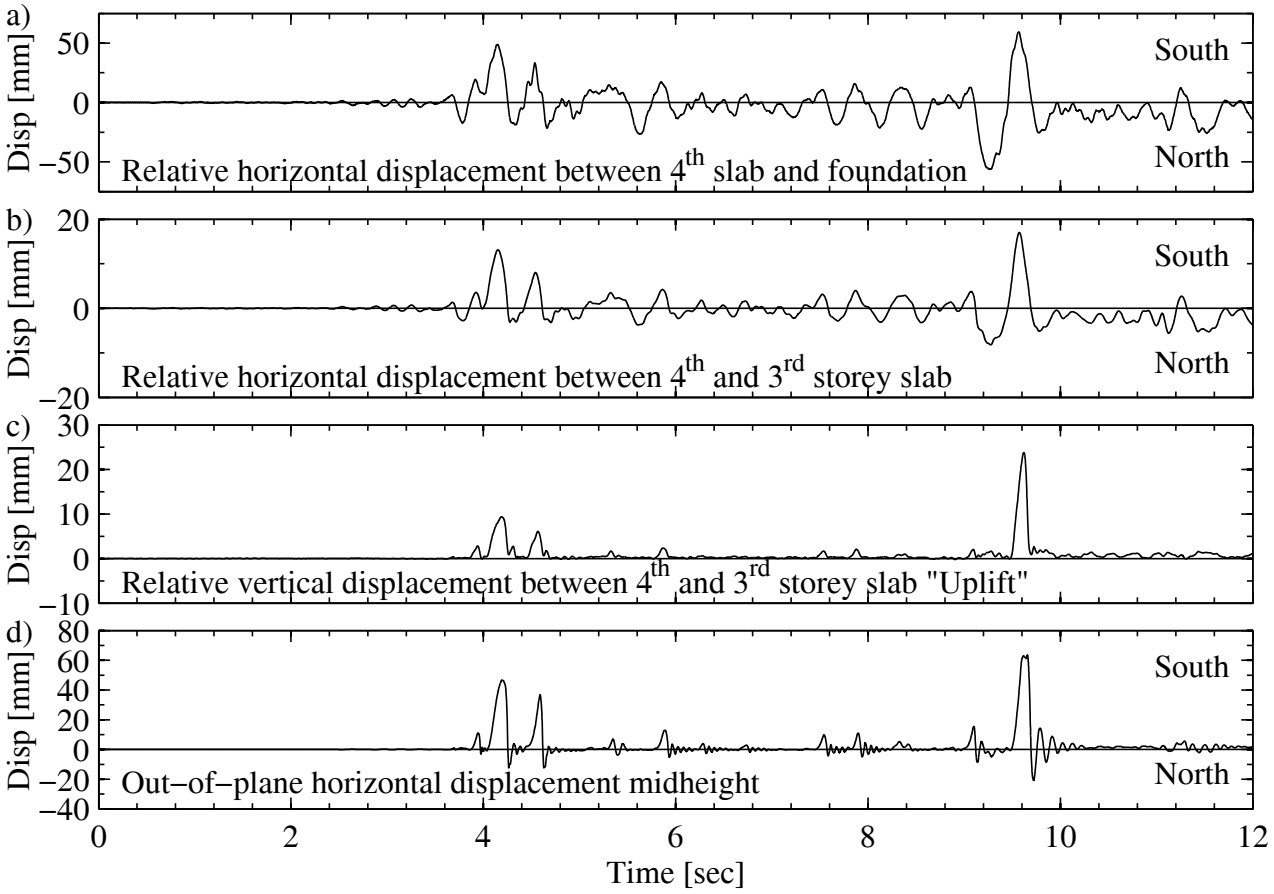

Figure 3.6. Time histories of a) horizontal displacement of the top storey slab with respect to shake table, b) horizontal displacement of the top storey slab with respect to the third storey slab, c) vertical uplift of the RC slab at the top of the wall with respect to the slab at the bottom of the wall and d) out-of-plane horizontal displacement at the mid-height of the 4th storey North side wall.

3.2 Discrete element modelling

The out-of-plane response of the North wall that failed will be analysed by means of a discrete element model using the commercial software UDEC [52]. The discrete or distinct element method (DEM), which is based on the work of Cundall [56] in the early 1970s, has been increasingly used over the years to analyse masonry structures. With DEM, the structure is modelled as an assemblage of discrete blocks, which can be either rigid or deformable. The blocks are separated by joint interfaces, along which the blocks can detach or slide without limit on relative displacement or rotation. Due to these features, DEM is particular suitable for analysing the dynamic behaviour of rocking masonry structures; past studies include investigation of the seismic behaviour of single blocks or block assemblages [57]–[59], masonry arches [57], [60], masonry facades [59], [61], free-standing columns [62], [63] and entire historical structures [64], [65].

This section describes the model geometry, the assigned material properties, the definition of the boundary conditions and the assumptions with regard to the assigned damping for the dynamic analyses.

3.2.1 Geometry and material properties

The 2D model represents a cross section of one of the out-of-plane loaded URM walls (Figure 3.7). The model consists of 14 equal-sized blocks for the brick rows and two blocks that represent the top and bottom

slab. The block of the top slab is subdivided into two blocks: The outer block, to which the boundary condi-conditions in terms of velocity histories are applied (see Section 3.2.2), and the smaller inner block, which is in contact with the top brick. The interfaces between the outer block and the inner block are assigned zero shear strength. Hence, when the outer block uplifts from the wall, the inner block slides downwards and lies on the top brick of the wall without applying an axial force to the wall (more precisely, the applied axial force at the top of the wall corresponds to the weight of the inner block, which is 0.096 kN/m). The interface between the inner block and the top brick is assigned the same interface properties as the interfaces between brick units. Due to the cohesive strength of the interface, the inner block prevents the sliding between top slab and wall, even if the wall uplifts. This top boundary condition was specified since sliding between wall and top slab was not observed in the test (Section 3.1.3). Most likely the mortar "fingers" reaching into the hollow core clay brick helped to prevent any sliding displacement.

The mortar joints are represented by interfaces of zero thickness. The height of the bricks was therefore increased from the actual 95 mm to 100 mm to include also the average thickness of a mortar joint. The bricks are 95 mm wide. The block corners are rounded off with a radius *r*, which is an input parameter to the model (Figure 3.7c). This parameter defines also the position of the two sets of springs from the outer wall edge that represent the axial and shear properties of the interface. Considerations with regard to its value and its influence on the dynamic response are presented in Section 3.3.4.

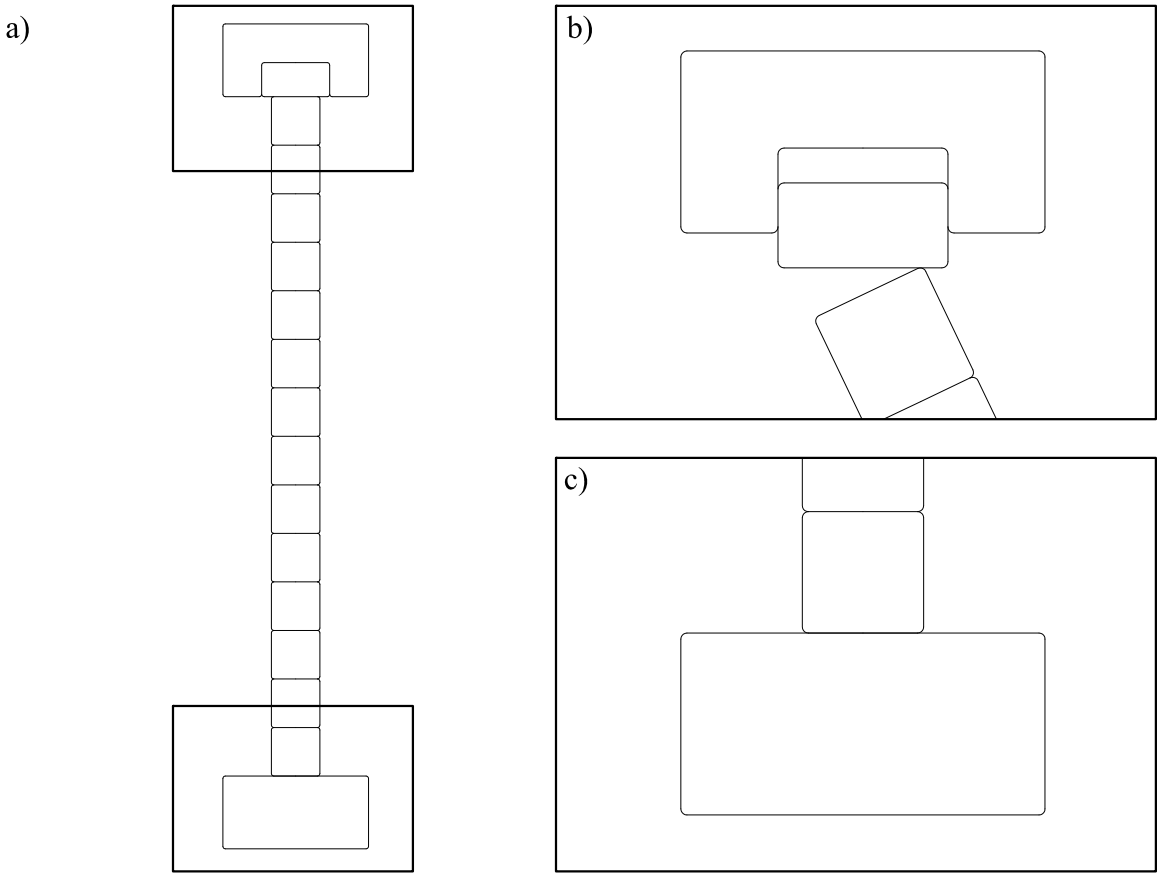

Figure 3.7. Geometry of the UDEC model (a). Detail of the top support when the top slab uplifts (deformation exaggerated) from the wall (b). Detail of brick with rounded corners (c).

In this paper, the blocks representing the masonry units are rigid and the deformability is entirely allocated to the interfaces that represent the mortar joints. This hypothesis is typically reasonable for low to moderate axial load ratios. The joints were modelled as interfaces to which a Mohr-Coulomb constitutive model was assigned. All interface properties were derived from standard material tests results (see

Table 3.1), which involved vertical compression tests on masonry units and shear triplet tests [13]. Mortar samples were taken regularly during the construction of the shake table test unit and the construction of the test units for material testing. Standard mortar tests showed that the mortar used for the construction of the material test units was stronger than the mortar used for the construction of the fourth storey walls. Also, material test properties had been computed with regard to the gross width of the wall (b = 95 mm) while the effective width of the interfaces in numerical model was only $b_{eff} = b-2r$ = 85 mm. To account for these differences, the interface properties of the numerical model were computed as follows: The cohesion assigned to brick interfaces in the numerical model was computed as the cohesion obtained from shear triplet tests times the ratio of the mortar tensile strength of the fourth storey walls ($f_{tm,Storey4}$) and the mortar strength of the triplets ($f_{tm,Triplet}$) and the ratio of nominal to effective wall width:

$$c_{UDEC} = c_{Triplet} \cdot \frac{f_{tm,Storey4}}{f_{tm,Triplet}} \cdot \frac{b}{b-2r} = 0.23 \cdot \frac{2.62}{3.23} \cdot \frac{95}{85} = 0.209\ MPa \tag{3.1}$$

The tensile strength assigned to brick interfaces in the numerical model was estimated from the cohesion c_{UDEC} and the friction coefficient μ_{UDEC}=$\mu_{Triplet}$ assuming a parabolic tension cut-off:

$$f_{t,UDEC} = \frac{c_{UDEC}}{2\mu_{UDEC}} = \frac{0.209}{2 \cdot 0.7} = 0.149\ MPa \tag{3.2}$$

The friction coefficient was obtained ($\alpha_{UDEC} = \alpha_{Triplet}$) directly from the triplet tests and corresponds to a friction angle $\alpha_{Triplet}$ of 35°. The elastic modulus $E_{m,Wallette}$ and the Poisson's ratio $\nu_{Wallette}$ of the masonry were obtained from compression tests on masonry wallettes. To account again (i) for the fact that the compression strength of the mortar used for the construction of the fourth storey wall ($f_{m,Storey4}$) was less than that of the mortar used for the construction of the wallettes ($f_{m,Wallette}$) and (ii) for the ratio of nominal to effective wall width, the normal stiffness of the brick interface was computed as:

$$K_{nn} = \frac{E_m}{h_{block}} \cdot \left(\frac{f_{m,Storey4}}{f_{m,Wallette}}\right)^{0.3} \cdot \frac{b}{b-2r} = \frac{4.50}{0.1} \cdot \left(\frac{7.04}{13.95}\right)^{0.3} \cdot \frac{95}{85} = 41.0\ \frac{GPa}{m} \tag{3.3}$$

This equation uses the following relationships between mortar strength f_m, brick strength f_b, masonry compressive strength f_k and the elastic modulus of the masonry E_m [28]:

$$E_m = 1000 \cdot f_k \tag{3.4}$$

$$f_k = K \cdot f_b^{0.7} \cdot f_m^{0.3} \tag{3.5}$$

The shear stiffness was computed as ($\nu_{UDEC} = \nu_{Triplet}$):

$$K_{tt} = \frac{K_{nn}}{2(1+\nu)} = \frac{41}{2(1+0.2)} = 17.1\,\frac{GPa}{m} \tag{3.6}$$

The interfaces between bricks and slabs were assigned the same stiffnesses as the interfaces between two bricks. This accounted for the fact that the masonry flexibility resulted mainly from the joints and not from the bricks, which would have justified a higher joint stiffness for the interfaces between wall and slabs.

The masonry wallettes had not been weighed and therefore the density of masonry was estimated as ρ_{mUDEC} = 1000 kg/m^3. The Mohr-Coulomb law implemented in UDEC obeyed an elastic-brittle relationship in tension, i.e., upon reaching the tensile strength capacity, the tensile strength drops immediately to zero. However, the cohesion was not reduced upon reaching the shear strength of the interface.

Table 3.1. Masonry properties from standard material tests [13], [54].

E-modulus of the masonry for vertical compression $E_{m,Wallettes}$ (GPa)	4.50
Poisson ratio $\nu_{Wallette}$ (-)	0.20
Cohesion $c_{Triplet}$ (MPa)	0.23
Friction angle $\alpha_{Triplet}$	35°
Masonry compressive strength $f_{cm,Wallette}$ (MPa)	5.66
Tensile strength of mortar for triplet test units $f_{tm,Triplet}$ (MPa)	3.23
Tensile strength of mortar used for the construction of the shake table test unit $f_{tm,Storey4}$ (MPa)	2.62
Compressive strength of mortar for wallettes test units $f_{m,Wallette}$ (MPa)	13.95
Compressive strength of mortar used for the construction of the shake table test unit $f_{m,Storey4}$ (MPa)	7.04

3.2.2 Definition of the boundary conditions

In UDEC, dynamic boundary conditions are defined as velocity histories applied at the rigid block centre. The wall model was loaded in three steps: First, the gravity load of the wall itself was applied as vertical acceleration of 9.81 m/s^2. Second, the axial force was applied as a constant downward velocity over a duration Δt of the top block. The applied displacements were computed to yield an axial force of 15.5 kN/m at the base of the wall. The axial force was obtained from a TREMURI [10] model of the test unit, which was validated by Mandirola [66] to assess the in-plane behaviour of the test unit. Third, the seismic loading of the wall was applied as horizontal and vertical velocity time histories at the outer top and the bottom block, which represent the slabs. These velocity time histories were derived from the displacement histories of the slabs, which were recorded by the optical measurement system [13]. The rotation of the top and bottom slab was set to zero since optical measurements showed that the rotations had been rather small (maximum value of 3.4x10^{-3}).

3.2.3 Modelling of the damping

Damping was added through stiffness proportional Rayleigh damping, with the primary objective of damping out higher frequency vibrations which can cause individual blocks to unrealistic vibrate apart in the computational model [59], [60]. This was done by heavily damping the natural frequency associated with rotational vibration of individual bricks, while minimising the damping at lower frequencies which govern mechanism displacements [60]. The damping matrix is therefore:

$$C = \beta \cdot K \tag{3.7}$$

where K is the stiffness matrix. The rocking frequency ω_r of a single block representing one of the brick rows was computed and a fraction of critical damping of ξ was assigned to this frequency, which can be approximated by [60]:

$$\omega_r^2 = \frac{3 \cdot E_{m,UDEC} \cdot b(b-2r)^2}{2 \cdot \rho_{m,UDEC} \cdot h_b^2 \cdot (b^2 + h_b^2)} \tag{3.8}$$

The β-parameter is therefore:

$$\beta = 2 \cdot \frac{\omega_r}{\xi} \tag{3.9}$$

The damping coefficient ξ could not be determined from experimental results. For this reason, Section 3.3.3 investigates the sensitivity of the dynamic response to the assumed value of ξ.

3.3 Validation of the numerical model against experimental results

To validate the numerical model, the 4th storey wall of the North face was modelled and the numerical results in terms of out-of-plane displacement at mid-height, top and base rotation and failure mechanism were compared to the experimental response. The final model included a block rounding r = 5 mm and a damping coefficient of ξ = 20%. First, the model was validated for this final parameter configuration. Then, the sensitivity of the results with respect to r and ξ was tested.

3.3.1 Validation of the chosen model

The model was validated for test 9, during which the wall hit the retaining structure at 9.6 sec, which will be considered in the following as the point of collapse. Figure 3.8a presents the comparison of the experimental and numerical time histories of out-of-plane displacements at mid-height of the wall; the out-of-plane displacement is again defined as the horizontal displacement at mid-height of the walls minus half the relative displacement between the top and bottom slab (Section 3.1.4). The numerical model is able to accurately predict the overall global behaviour of the wall even if it does not capture the small vibrations recorded in the shake table test between the two main peaks. The model also estimates the mechanism at collapse correctly (Figure 3.9).

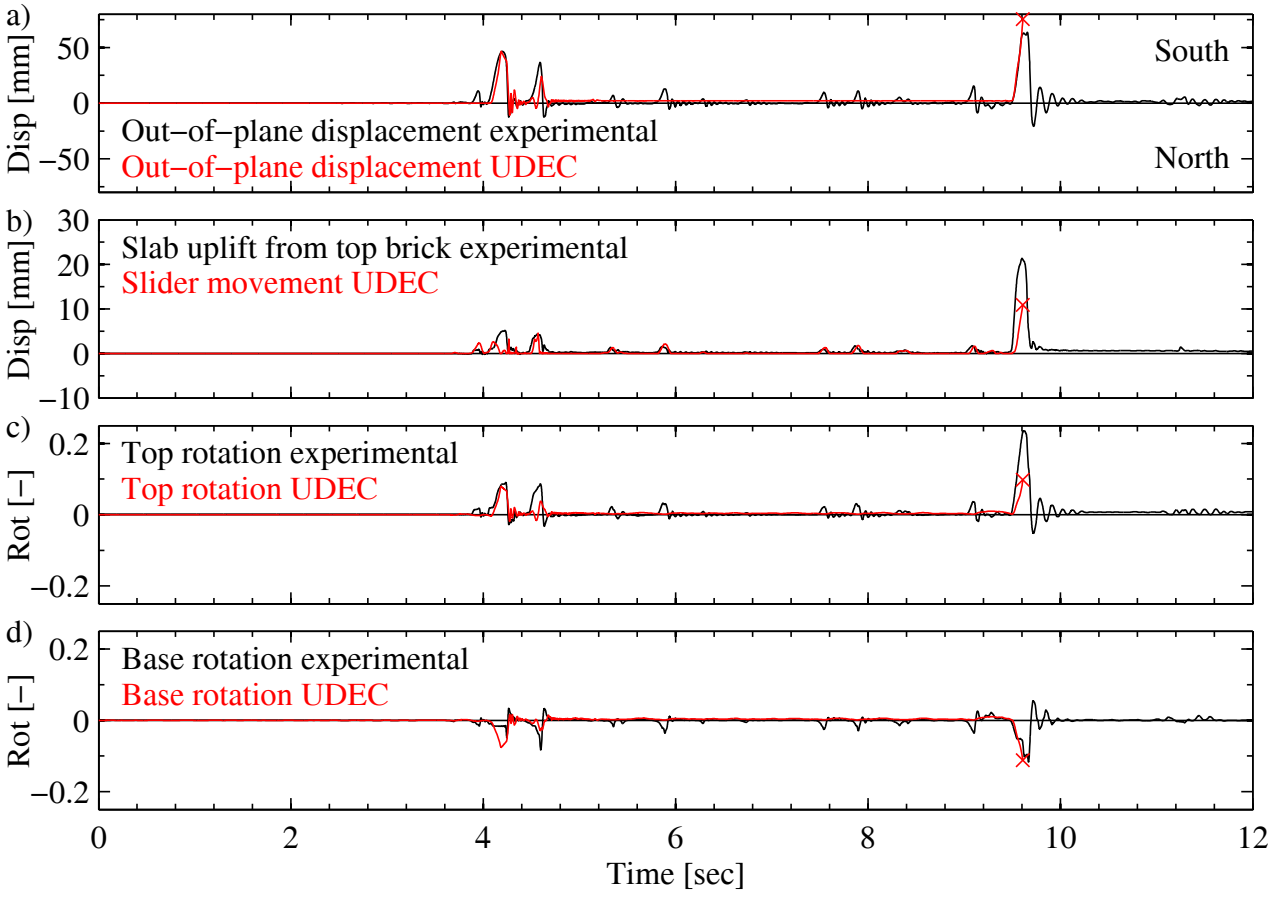

Figure 3.8. Comparison of numerical and experimental results for the final model of the 4th storey wall of the North face: Out-of-plane displacement at mid-height (a), uplift between slab and wall at the top (b), relative rotation between slab and wall at the top (c), relative rotation between slab and wall at the base (d).

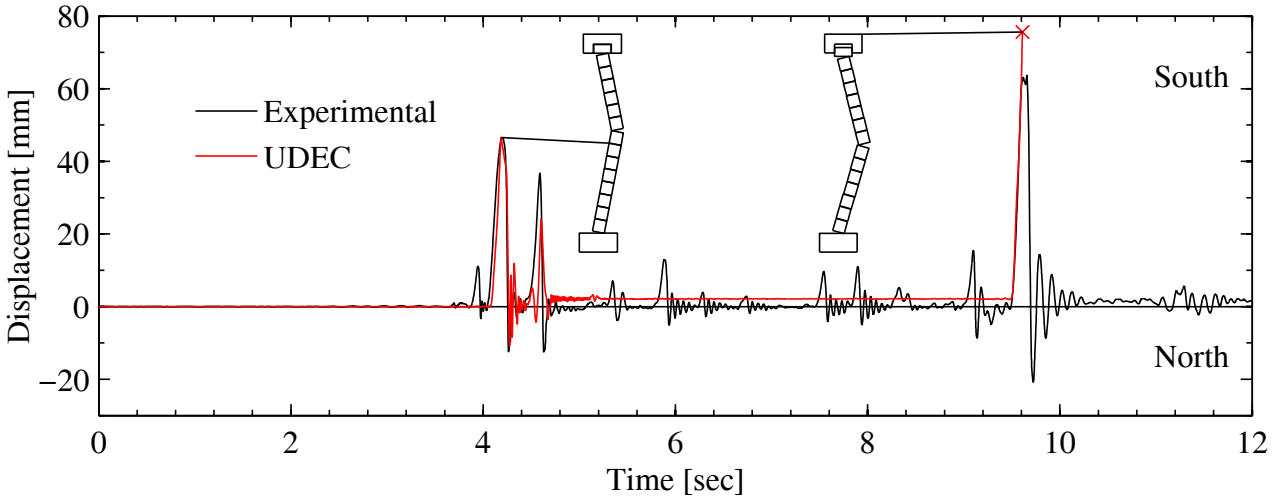

Figure 3.9. Comparison of experimental and numerical out-of-plane displacement with deformed shapes at 4.2 s and at failure at 9.6 s.

Figure 3.8b shows the comparison between the experimentally observed uplift of the slab from the top brick (computed as average displacement of the two LVDTs at the top of the wall, Figure 3.2) and the vertical movement of the sliding element with respect to the top element recorded during the numerical analyses. Before reaching collapse of the wall, at 9.6 sec, the vertical movement of the slider is less than 4 mm. It seems plausible that the "mortar fingers" that reached into the bricks accommodated this movement and modelling the top boundary condition with a slider (see Section 3.2.1) therefore justified. Note that the movement of the slider is much less than the increase in distance between the bottom and top slab, which reached a maximum value of 23.8 mm before collapse (Figure 3.8). The difference is explained by the elongation of the wall due to rocking.

Finally, Figure 3.8c and 8d compare the experimental and numerical values of the top and bottom rotation of the wall respectively; also for these parameters there is a good correlation between the two sets of results.

3.3.2 Effect of pre-damage

In the experiment, the building was subjected to nine runs and only the last one led to the out-of-plane collapse of the fourth storey wall. It remains, however, open in which regard the previous runs influenced the response during the ninth run. Although a visual inspection after run 8 had not revealed any significant damage (Section 3.1.3), it cannot be excluded that hairline cracks had been present. To investigate the effect of the pre-damage, the wall was analysed by subjecting it first to run 8 and then to run 9. At the end of run 8, the numerical model showed cracks at the top and bottom interfaces of the wall. Figure 3.10 shows that this pre-damage had only a minor influence on the out-of-plane displacement during run 9. The mechanism that formed at collapse was also unaffected by the pre-damage.

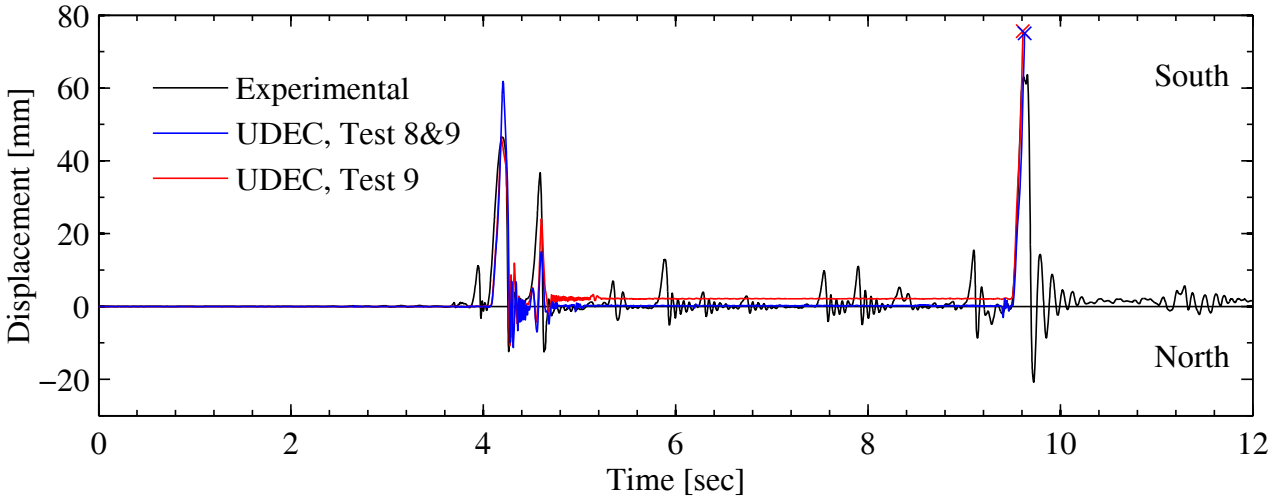

Figure 3.10. Mid-height displacement of the 4th storey wall of the North face: Comparison of numerical results when run 9 is applied to the undamaged wall and to the wall that had been pre-damaged by run 8.

3.3.3 Sensitivity to the chosen damping level

The choice of the damping level for discrete element analyses has been discussed by several authors (e.g. [57], [60], [62], [63]). The initial portion of the strong ground motion response of models was found to be rather insensitive to the damping level [62], [63] while continued strong shaking and the reduction in amplitude of the free vibration can be sensitive to the damping [63]. For rocking motions, the natural rocking period is not constant [67], and therefore it is impossible to specify a constant level of damping for a given mode. Specifying 0% damping at all frequencies can lead to a good approximation of the initial portion of the strong ground motion response [65], but can also lead to unrealistic vibration displacements at no-tension interfaces [59] and overestimation of the response to either continued strong shaking or large separated pulses in the ground motion [59]. This overestimation can be limited by specifying a small stiffness-proportional damping level that eliminates the high frequency rotational vibration of individual blocks [60]. To investigate the sensitivity of the results with regard to the assumed damping level, Figure 3.11 shows the out-of-plane displacement at mid-height for damping ratios between ξ = 0-100% at the rocking frequency ω_r (Eq. (3.8)). Since no mass proportional damping is specified, the damping level decreases with decreasing frequency. At the natural frequency of the wall (assuming a simply supported beam) the corresponding damping ratios vary therefore only between 0-1.0%.

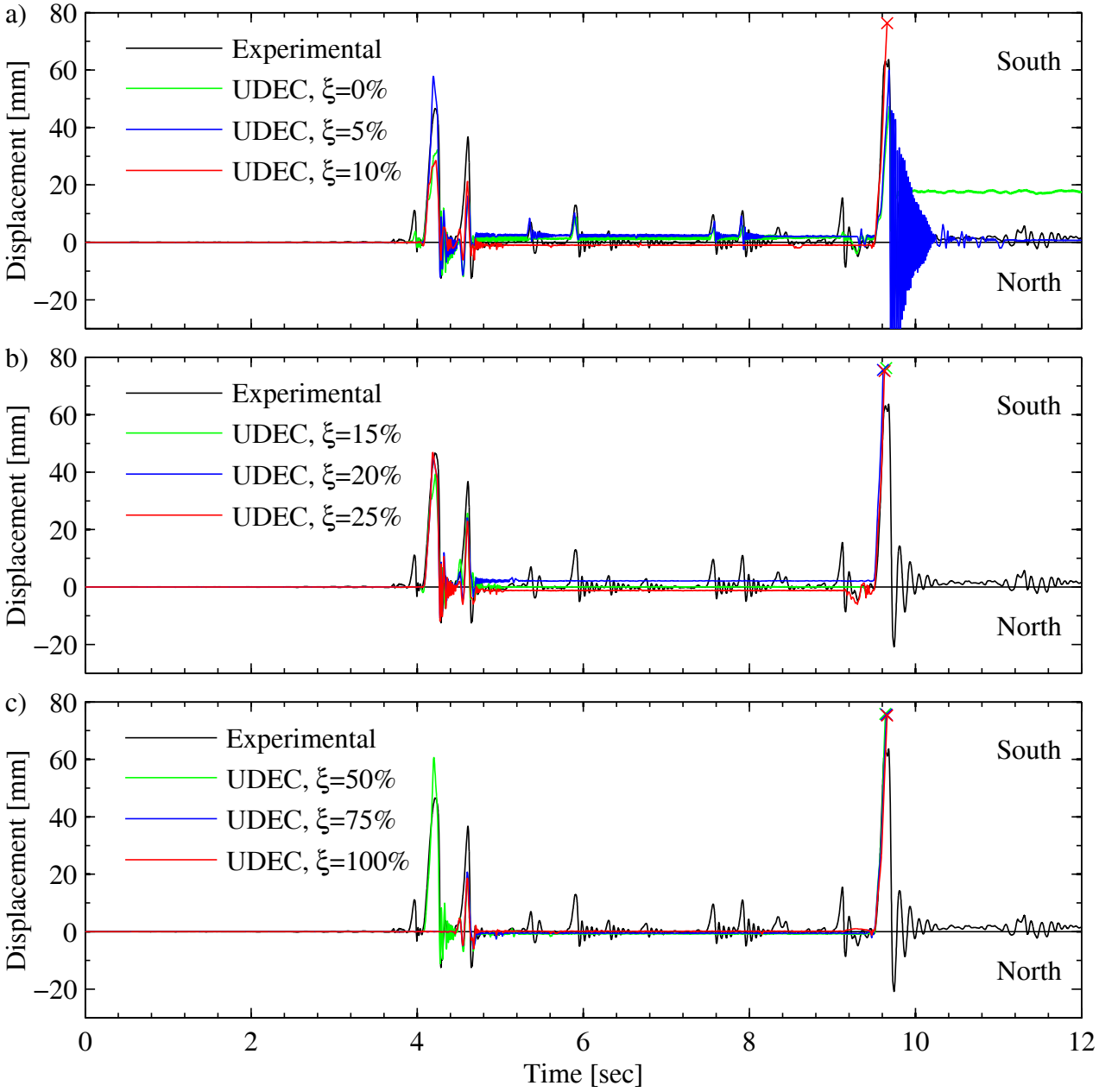

Figure 3.11. Mid-height displacement of the 4th storey wall of the North face, sensitivity to damping level: ξ=0-10% (a), ξ=15-25% (b) and ξ=50-100% (c).

The results fall into two groups: For the first group of analyses with ξ=0-10%, the displacement histories show a very high frequency content which is related to the rocking of the individual blocks and suggests that the rocking motion of the individual blocks is not sufficiently damped. For the second group of analyses with ξ=15-100% this high frequency content largely disappears. All analyses of this second group predict wall failure at 9.6 s. They differ with regard to the predicted mechanism (central hinge between rows 7 and 10) and the amplitude of the displacements prior to failure.

Of the six analyses of the second group, the one with ξ=20% predicts the experimentally recorded displacements best and also the mechanism is well predicted with a central hinge forming at the mid-height. For these reasons, $\xi = 20\%$ at $\omega_r = 2570$ Hz was chosen as the final damping ratio; this corresponds to a damping ratio of 0.20% at the natural frequency of the wall.

3.3.4 Sensitivity with regard to the assumed block rounding

The rounding of the blocks affects the location of the pivot points that characterise rocking and the elastic out-of-plane displacements before the springs that represent the interface are damaged and rocking starts. The position of the actual pivot point depends on the axial load ratio [68], the state of degradation of the mortar joints [68] and the depth of the groove that is often carved into the mortar joint.

Under gravity load and when subjected to out-of-plane bending, the compression zone depth of the investigated wall can be approximated by:

$$b_c = \frac{N}{0.85 f_{cm,UDEC}} = 15.5 \frac{kN}{m'} \cdot \frac{1}{0.85 \cdot 4.61 MPa} = 3.96\ mm \tag{3.10}$$

where N is the axial force under gravity loads and $f_{cm,UDEC}$ is the compressive strength of the masonry. If it is assumed that the pivot point is located at approximately half the compression zone depth, the rounding r should be set to b_c / 2 plus the depth of the groove (~2 mm), i.e., to ~4 mm. Figure 3.12 shows the numerical results for three block rounding values. Overall, the response is not very sensitive to this range of block rounding. For r = 5 mm, the first peak and the mechanism are best predicted. For these reasons, r was set to 5 mm.

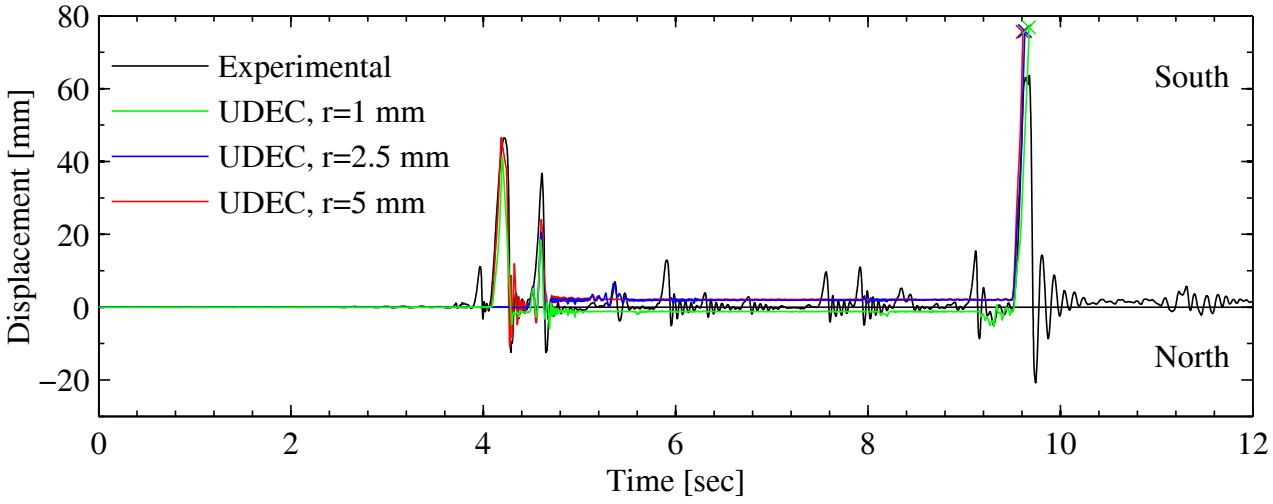

Figure 3.12. Mid-height displacement of the 4th storey wall of the North face: sensitivity to block rounding.

3.4 The influence of dynamic boundary conditions on the out-of-plane response of URM walls

This section investigates the influence of the dynamic boundary conditions on the out-of-plane behaviour of URM walls. The investigated parameters are the relative horizontal and relative vertical displacements between the bottom and top slab, as well as the effect of the sliding restraint at the top of the wall.

3.4.1 Effect of relative horizontal displacement between slabs

Figure 3.13 shows the numerical results of the 4th storey wall for different horizontal excitation at the top and the bottom. The result labelled "UDEC, α = 1.0" corresponds to the analysis presented in Section 3.3.1, where the vertical and horizontal velocities of the top and bottom slab are the slab displacements that were measured during the shake table test. Note that the maximum displacement relative to the foundation measured at top floor slab was 59.4 mm (Figure 3.6), while the maximum difference between the horizontal displacements measured at the 3rd and 4th floor slabs was 17 mm.

To investigate the effect of differential top and bottom slab movements, analyses with the following top and bottom horizontal input velocities were carried out:

$$v_t = \frac{v_4 + v_3}{2} + \alpha \frac{v_4 - v_3}{2} \tag{3.11}$$

$$v_b = \frac{v_4 + v_3}{2} - \alpha \frac{v_4 - v_3}{2} \tag{3.12}$$

where v_3 and v_4 are the horizontal velocities of the third and fourth storey slabs. A value of $\alpha = 1$ yields the real input motions and $\alpha = 0$ the average input motions (Figure 3.13). Figure 3.13 shows further analyses for α -values between 0 and 1. Although all sets of input motions apply the same average acceleration of $(v_3+v_4)/2$, the maximum out-of-plane displacements differ because different mechanisms are activated. However, all analyses except the one for $\alpha = 0$ lead to collapse at $t = 9.6$ s.

The results indicate that some relative displacement between the top and bottom of the wall was important because it created a mechanism needed to accommodate the relative displacements, which then affected rocking response. However, the magnitude of the relative displacement (α = 0.33 to 1.0) did not have a consistent effect on the results. Thus, while the presence of some relative displacement was important, the magnitude was less important, indicating that the effects of increasing magnitude (in the range tested) did not govern over the sensitivity of the rocking response.

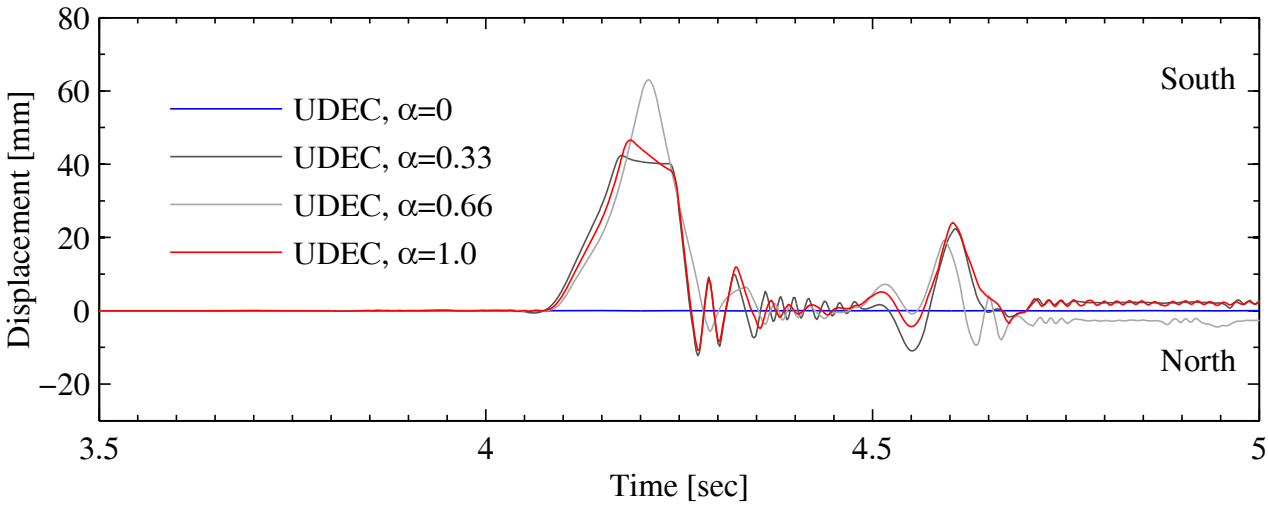

Figure 3.13. Mid-height displacement of the 4th storey wall of the North face: sensitivity to the difference in horizontal input motion at the top and bottom of the wall.

3.4.2 Effect of relative vertical displacement between slabs

The experimental results showed that the 4th storey wall developed its largest out-of-plane displacement when there was an uplift of the top slab due to rocking of the flanking wall (Section 3.1.4). At this instant, the vertical restraint at the top of the wall is weakened or completely absent and the wall is more vulnerable to deform and collapse out-of-plane. It was shown that the 4th storey North wall collapsed for a differential vertical displacement of the supports of 23 mm. Using the numerical model the 4th storey North wall, Test 9 was analysed for different levels of vertical excitation. The horizontal excitation applied to the top and the base of the wall was the same for all analyses while the vertical excitation were scaled to match values in a range of 0-100% of the original vertical excitation (Figure 3.14).

Only for the original input ("UDEC, 100% Uplift") and a slightly reduced vertical input ("UDEC, 80% Uplift") is it possible to observe the large displacement at 4.2 sec. Furthermore, only for values of 60-100% of vertical excitation was wall collapse at $t = 9.6$ sec observed. For the 40% case the gap between top slab and wall closes before the horizontal out-of-place displacement reaches the instability limit, which forces the wall to return to a stable configuration and induces strong oscillations. For zero or small vertical uplift (0-

20%), limited or no out-of-plane deformations are observed. Zero or 20% vertical uplift is representative of the boundary conditions of a wall flanked by RC walls, e.g. the 4th storey South wall, for which no significant out-of-plane displacement was observed (Figure 3.4b).

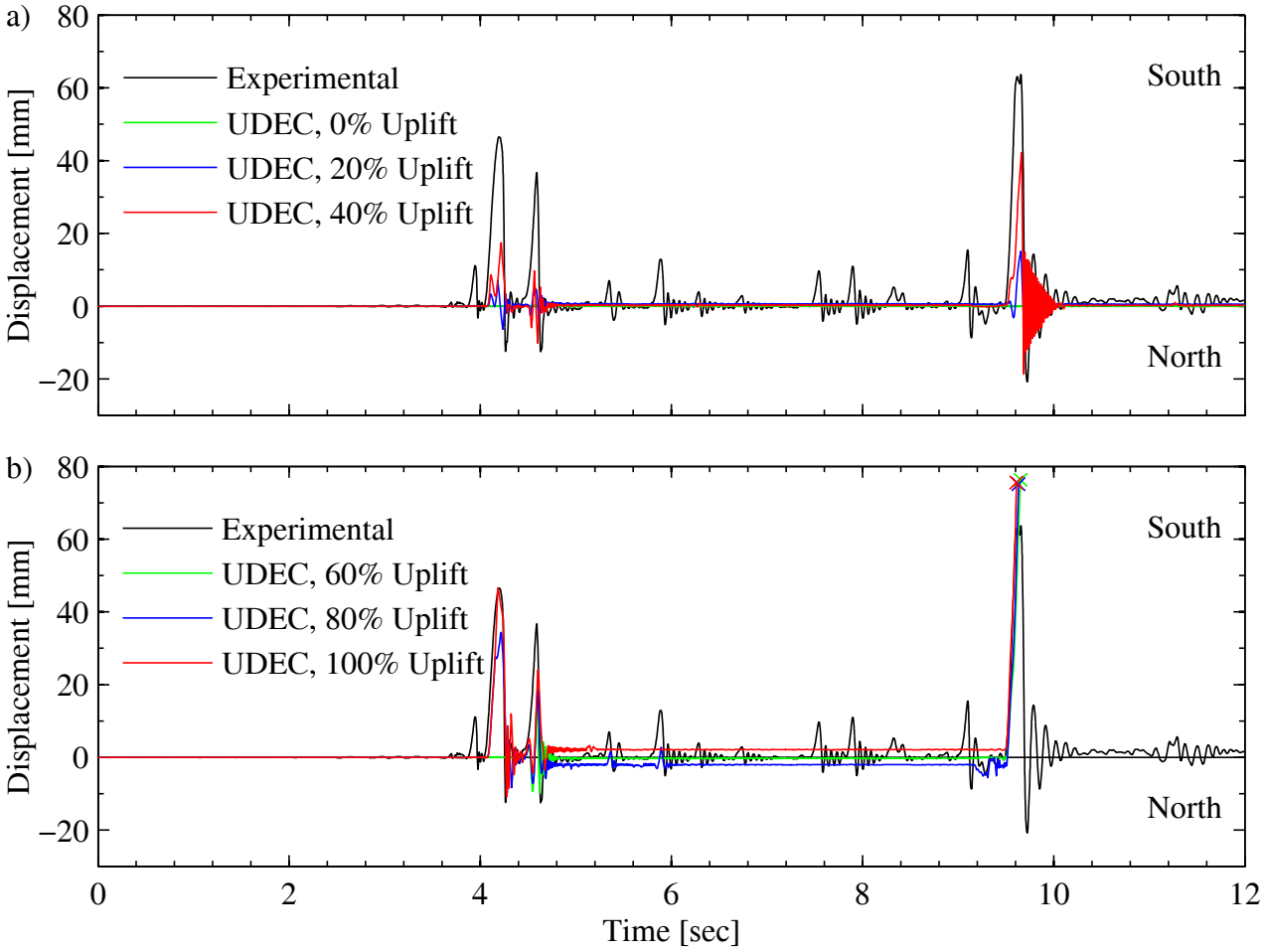

Figure 3.14. Mid-height displacement of the 4th storey wall of the North face, sensitivity to vertical uplift: 0-40% of vertical uplift (a) and 60-100% of vertical uplift.

3.4.3 Effect of sliding restraint at the top of the wall

In the UDEC model, the top slab was modelled as composed by two elements, a main outer element and a secondary inner element that could slide vertically with regard to the outer element (Section 3.2.1). This modelling solution provides a horizontal restraint to the top of the wall when the top slab uplifted from the wall and aimed to represent the restraining action of the mortar fingers reaching into the holes of the bricks. Figure 3.15 shows the numerical result if this horizontal restraint is not modelled ("UDEC without slider"): the wall collapses out-of-plane at the first peak displacement, which does not capture the response observed in the test. This is also confirmed by the mechanism, which is a simple rigid body overturning mechanism with a single hinge at the base. Modelling this horizontal restraint ("UDEC with slider") seems therefore essential for capturing the experimental response. Further, for buildings of this type where slab uplift could occur, it is important to prevent complete separation and loss of lateral restraint at the top of the wall.

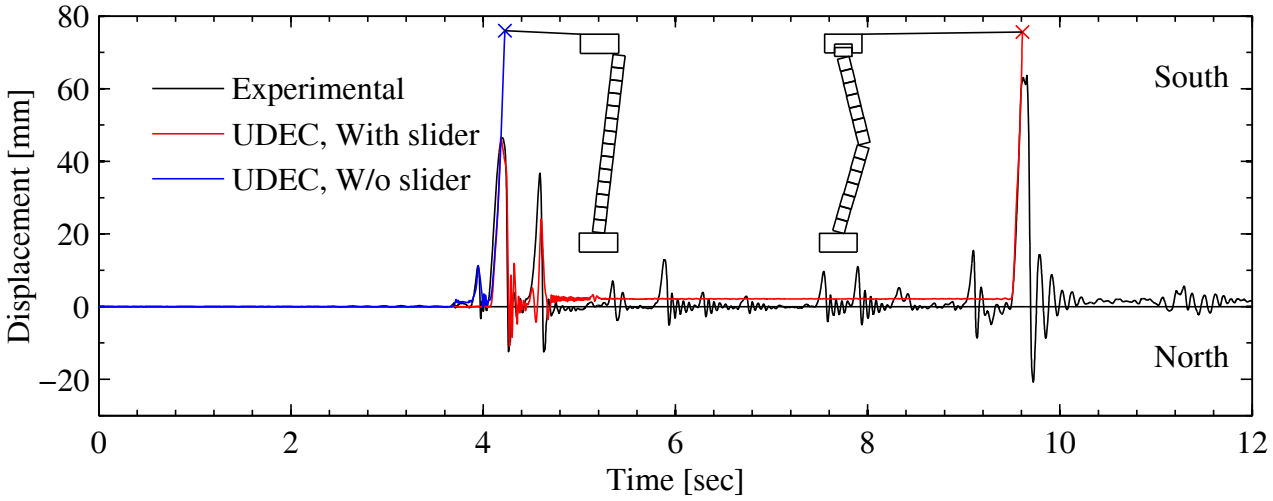

Figure 3.15. Mid-height displacement of the 4th storey wall of the North face: different top restraint modelling options.

3.5 Conclusions

The paper investigates experimentally and numerically the out-of-plane response of URM walls in buildings with stiff RC slabs. A discrete element model was set up and validated against the response of the 4th storey wall that failed out-of-plane. Three new findings are presented:

- The out-of-plane response is controlled by the vertical restraint that is provided by the top slab. The largest out-of-plane displacements were observed when the top slab uplifted from the wall. This uplift was caused by rocking of flanking walls that were orthogonal to the wall that was loaded out-of-plane. Numerical analyses show that with less than 60% of this uplift, the wall would not have collapsed out-of-plane. The uplift of the slab from the wall seems therefore a key parameter in the out-of-plane response of URM walls in buildings with stiff RC slabs.

- Although the slabs uplifts from the wall, it was still able to provide a horizontal restraint at the top of the wall. Numerical results show that if this horizontal restraint is omitted, a global overturning mechanism results without a hinge at mid-height. In the experiment and the model with horizontal top restraint, a mechanism with a hinge at the top and bottom and approximately mid-height formed.

- In the experiment, the motions naturally differed at the top and bottom of the walls due to the amplification of motions over the height of the structure and higher mode effects. The top slab of the wall that was analysed (4th storey slab) was therefore subjected to larger horizontal accelerations than the bottom slab (3rd storey slab). Eliminating these relative horizontal accelerations, while maintaining the experimentally observed vertical slab uplift, also eliminated the out-of-plane rocking response in the numerical model. This indicates that it was not only the absolute out-of-plane accelerations and the slab uplift that affected behaviour, but the relative horizontal acceleration of the top and bottom of the wall also played a role. Therefore, differential floor motion may also be relevant for stiff slabs, not just for flexible slabs.

4 OUT-OF-PLANE BEHAVIOUR OF URM WALLS – PARAMETRIC STUDY

When evaluating the seismic performance of unreinforced masonry (URM) buildings, the out-of-plane stability of URM walls is assessed through simplified approaches, which typically provide limits on the wall slenderness ratio h_w/t_w. This chapter uses the numerical model that was validated in the previous section to analyse a large range of wall configurations and input motions. The results are compared to the maximum slenderness ratios provided in different codes.

4.1 Wall thickness and slenderness limits in codes

The slenderness limitations h_w/t_w in the Swiss pre-code SIA 269/8 [34] are a function of the boundary conditions, the peak ground acceleration $\gamma_f Sa_{gd}$ and the minimum compliance factor α_{min}. The ratio of wall height h_w to wall thickness t_w is limited by

$$\frac{h_w}{t_w} \leq \frac{k \cdot g}{\alpha_{min}\gamma_f Sa_{gd}} \leq \sqrt{\frac{100g}{\gamma_f Sa_{gd}}} \tag{4.1}$$

The factor k represents the boundary conditions; in buildings with RC slabs the factor k is set to 2.0 [34]. The parameter g is the acceleration due to gravity.

The document SIA 2018 [69] provides slenderness limits for URM walls as a function of the seismic region, of the construction work class and of the position of the wall in the building (Table 4.1). Unlike the pre-code SIA 269/8, which only considers the peak ground acceleration as input, it therefore accounts indirectly for the amplification of the motion over the height of the building.

Table 4.1: SIA 2018 [69]: Limits on slenderness ratios of URM walls.

Seismic region / Construction work class	Z1 / CO I Z1 / CO II	Z2 / COI Z2 / CO II	Z3 / CO I Z3 / CO II Z1-3 / CO III
Upper storeys of a multistorey structure	≤ *18*	≤ *17*	≤ *17*
Bottom storey of a multistorey structure	≤ *20*	≤ *19*	≤ *18*
All the other cases	≤ *19*	≤ *18*	≤ *17*

EC8 – Part 1 [12] recommends minimum wall thicknesses of 240 mm for URM walls in regions of high seismicity while the minimum thickness is reduced to 170 mm for regions of low seismicity. The maximum slenderness ratios are set to 12 and 15 for regions of high and low seismicity respectively. The Italian code NTC08 [70], [71] requires for high seismic zones (Italian Zones 1-3) a minimum thickness of 240 mm and a maximum slenderness of 12, which corresponds to the EC8 requirements for high seismicity regions. For

structures in low seismic zones (Zone 4) the requirements are, however, stricter than in EC8: the minimum required thickness is 200 mm while the maximum slenderness is 20.

4.2 Computation of floor accelerations

The nonlinear time history analyses that are carried out in this chapter require the definition of the time histories of the floor accelerations at the bottom and at the top of the wall. To obtain these time histories, five ground motions are selected and a 2D model of a four storey reference structure is analysed using the software Tremuri [10]. From these analyses the acceleration time histories of the third and fourth floor are extracted and used as input definition for the parametric analyses of the out-of-plane loaded walls (Section 4.3).

4.2.1 Choice of records

Griffith et al. [72] used five real and one artificial accelerogram for their study on equivalent SDOF systems for out-of-plane loaded URM walls. They chose these records for their different ground motion characteristics, which are reflected in the different spectral shapes. Since the study follows up on the study by Griffith et al., the five real records of that study are used for the study presented here (Table 4.2, Figure 4.1); the artificial record was not used as it was not publically available. All five ground motions do not show a strong pulse, which would be representative of near-field effects.

Table 4.2: Ground motions used for the numerical study and their characteristic values

Label [72]	Earth-quake	Date	Magn itude	Station	PGA [m/s2]	Ground type	Compo nent	Record filename
ElCentro[1)]	Imperial Valley	18.5. 1940	6.9	ElCentro	3.13		NS	ELCENTRO.DAT
Taft[2)]	Kern County	1952	7.4	Taft Lincoln School	1.74	D	EW	TAF111.AT2
San Salvador[2)]	San Salvado r	1986	5.8	National Geografic al Inst	6.00	D	NS	NGI270.AT2
Gemona[3)]	Friuli	15.9. 1976	6.1	Gemona	6.36	B	EW	IV.GMN.HNE.D.19 760915.031518.C.A CC.ASC
Sturno[2)]	Irpinia	23.11. 1980	6.9	Sturno	3.51	B	NS	A-STU270.AT2

1) Source: Chopra [73]

2) Source: PEER NGA-database [74]

3) Source: Itaca 2.0 http://itaca.mi.ingv.it [75], [76]

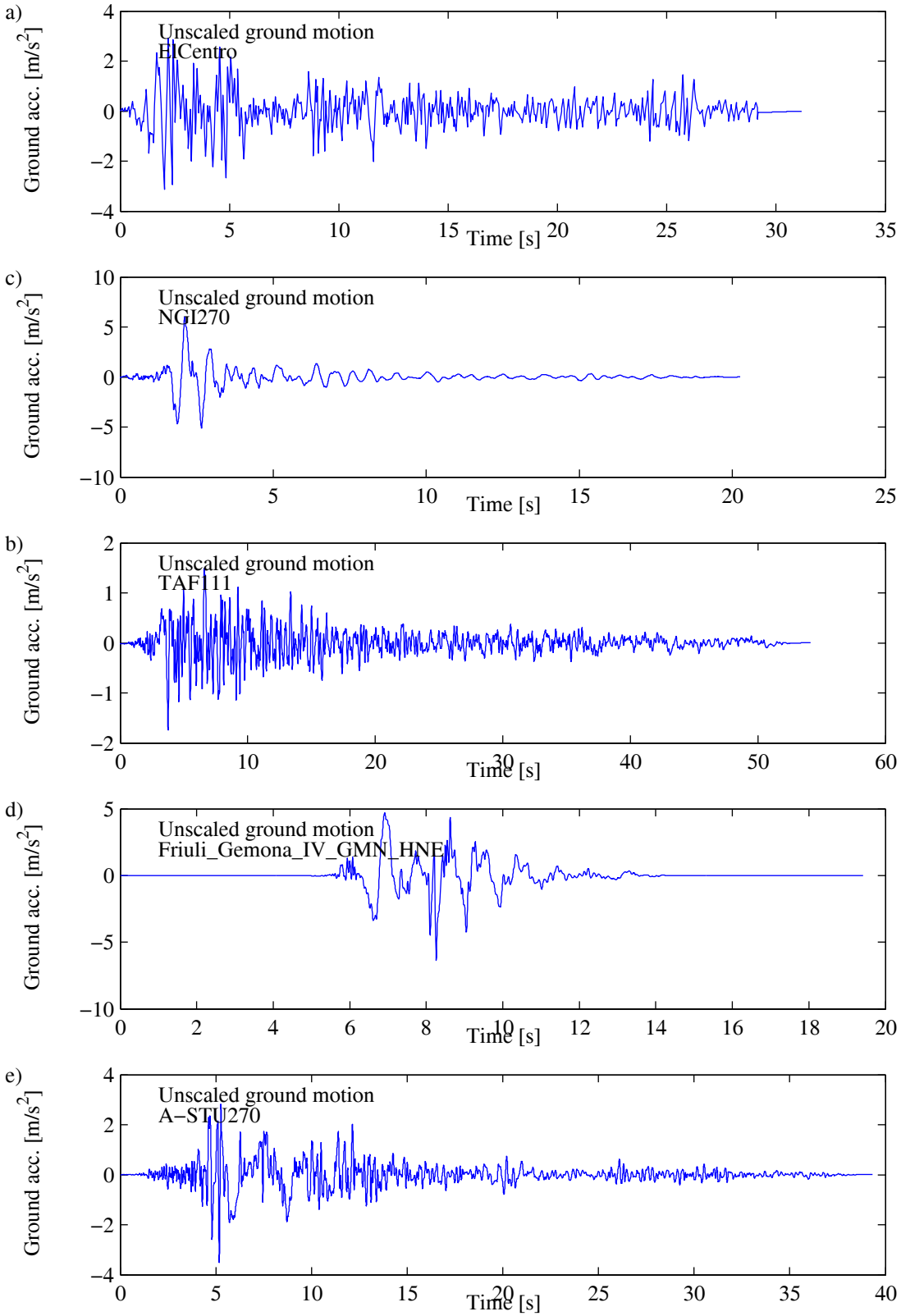

Figure 4.1: Acceleration time histories of five accelerograms that are used for the parametric study.

4.2.2 Model for computing acceleration at floor levels

Griffith et al. [72] used the ground motion records directly for the parametric study on the out-of-plane behaviour of URM walls. In modern URM buildings with RC slabs, the walls that will be most susceptible to out-of-plane failure are the walls of the top storeys. For this reason, in this study the input motion for the out-

of-plane study will be computed using a simple model of a four storey URM building and the third and fourth storey level response will be taken as input motions. The 2D model consists of two URM walls, each of a length of 3 m, which are coupled by 0.2 m thick RC slabs (Figure 4.2). The storey heights are 3 m and the clear distance between the walls 2 m. The structure is regular over the height and the storey masses M are tuned in such a way that the first effective period of the structure is 0.30 s, 0.45 s, and 0.60 s, respectively. The axial load at each storey due to gravity loads is computed as N=gM/2 assuming that the mass is largely concentrated in the slabs and half the weight of the slab is carried by walls orthogonal to the direction of excitation.

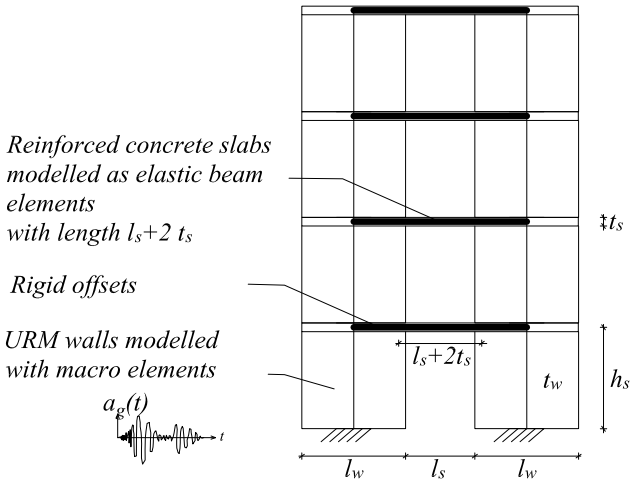

Geometry:
Storey height: h_s=3.0 m
Wall length: l_w=3.0 m
Clear span: l_s=2.0 m
Slab thickness: t_s=0.2 m
Wall thickness: t_w=0.3 m

Beam elements representing reinforced concrete slabs:
*$E_{c,eff}$=0.5*E_c=0.5*30 GPa=15 GPa*
*A_{slab}=6*t_w*t_s=0.36 m^2*
*I_{slab}=6*t_w*t_s^3 /12 =0.0012 m^4*

Macro elements representing URM walls:
f_m=6 MPa
*$E_{m,eff}$=0.3*1000*f_m=1.8 GPa*
*$G_{m,eff}$=0.25*$E_{m,eff}$=0.45 GPa*
μ=0.36
c=0.13 MPa

Figure 4.2: Tremuri model for computing storey responses

Inelasticity in the structural behaviour is known to affect the floor response spectra significantly (e.g. [77]). To derive the input motions at the 3rd and 4th storey level, the inelastic response of in-plane loaded walls should therefore be considered. To reach reasonable levels of inelasticity the following procedure was adopted: When designing standard buildings, a seismic hazard level corresponding to a return period of 475 years is considered and standard buildings are expected to reach for this return period the limit state "Significant Damage" [19]. URM walls failing in shear are expected to reach at this limit state an interstorey drift of 0.4%. The accelerogram is therefore scaled in such a way that the first storey drift corresponds to 0.4% (accepted variation: ±5%). For comparison, also the response of the elastic structure was computed. The ratio R of the maximum base shear of the elastic structure to the inelastic structure varies for the three structures with T=0.30 s, 0.45 s and 0.60 s subjected to five records between 1.3 and 3.8 with one outlier of 5.2 (Table 4.3). These values are values that could also be reached for more rigorous code designs, albeit they are somewhat higher than typical force-reduction factors used in seismic design. Figure 4.3 shows the acceleration response spectra that one obtains for the scaled ground motions.

For the analysis, the out-of-plane response of a fourth storey wall will be analysed. Such a wall is supported at the base by the third floor slab and at the top by the fourth floor slab. To gauge the influence of using an average accelertaion rather than defining the third and fourth floor accelerations at the bottom and top of the wall respectively, the average acceleration of the third and fourth storey is computed. This acceleration is in the following referred to as the 4th storey mid-height acceleration or short mid-height acceleration.

Table 4.3: Scaling factors and force reduction factors for the three systems with T=0.30 s, 0.45 s, 0.60 s subjected to the five records.

	T=0.30 s			T=0.45s			T=0.60 s		
Earthquake	PGA_{scaled} [m/s^2]	PGA_{scaled}/PGA_{orig} [-]	$R^{1)}$ [-]	PGA_{scaled} [m/s^2]	PGA_{scaled}/PGA_{orig} [-]	$R^{1)}$ [-]	PGA_{scaled} [m/s^2]	PGA_{scaled}/PGA_{orig} [-]	$R^{1)}$ [-]
ElCentro	3.35	1.07	1.98	2.64	0.84	3.08	2.37	0.76	3.57
Taft	3.84	2.20	3.04	2.21	1.26	3.78	2.37	1.36	3.06
San Salvador	2.51	0.42	1.44	1.80	0.30	1.90	1.57	0.26	2.43
Gemona	2.93	0.46	1.31	2.18	0.34	1.68	1.88	0.29	2.01
Sturno	3.97	1.13	5.22	2.27	0.65	2.00	1.57	0.45	1.42
Average	3.32	1.06	2.60	2.22	0.68	2.49	1.95	0.62	2.50

1) R=maximum base shear of elastic system / maximum base shear of inelastic system

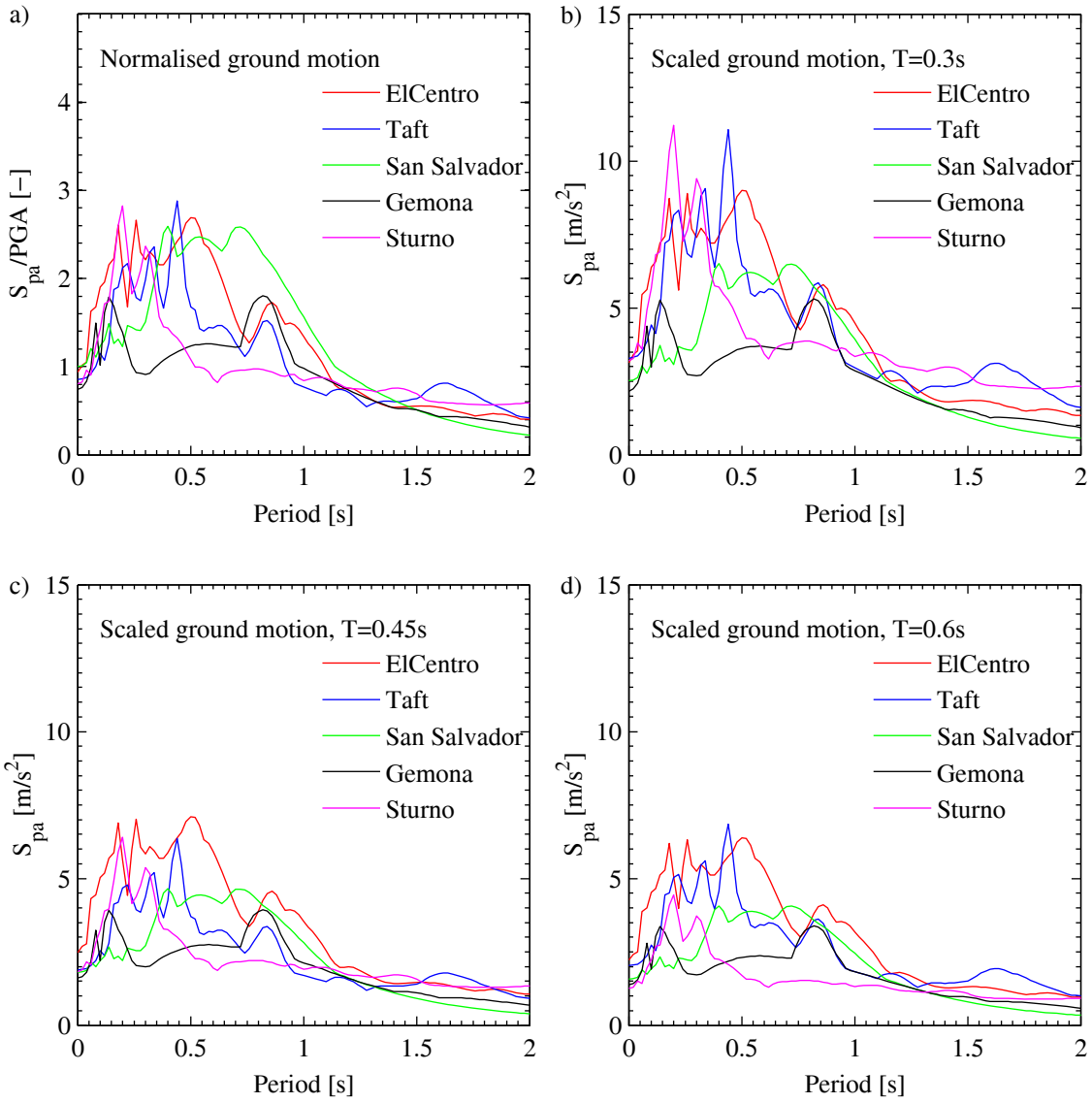

Figure 4.3: Ground motions, scaled and unscaled acceleration response spectra for 5% damping

4.2.3 Floor response spectra obtained from numerical analyses

Figure 4.4 and Figure 4.5 show the floor spectra for the inelastic and elastic model respectively. The floor spectra are computed using the average response of the third and fourth storey as input. For the elastic models, the maximum amplification of the acceleration occurs around the fundamental period of the structure. For the inelastic models, the maximum amplification occurs for longer periods since the fundamental period elongates as the structure undergoes inelastic deformations.

Figure 4.6 shows as example the floor spectra of the inelastic structure with a fundamental period of T=0.3 s. This plot shows next to the spectra for the average acceleration but also the spectra of the third and fourth storey. The difference between the spectra varies between records but is in general between 0-20%.

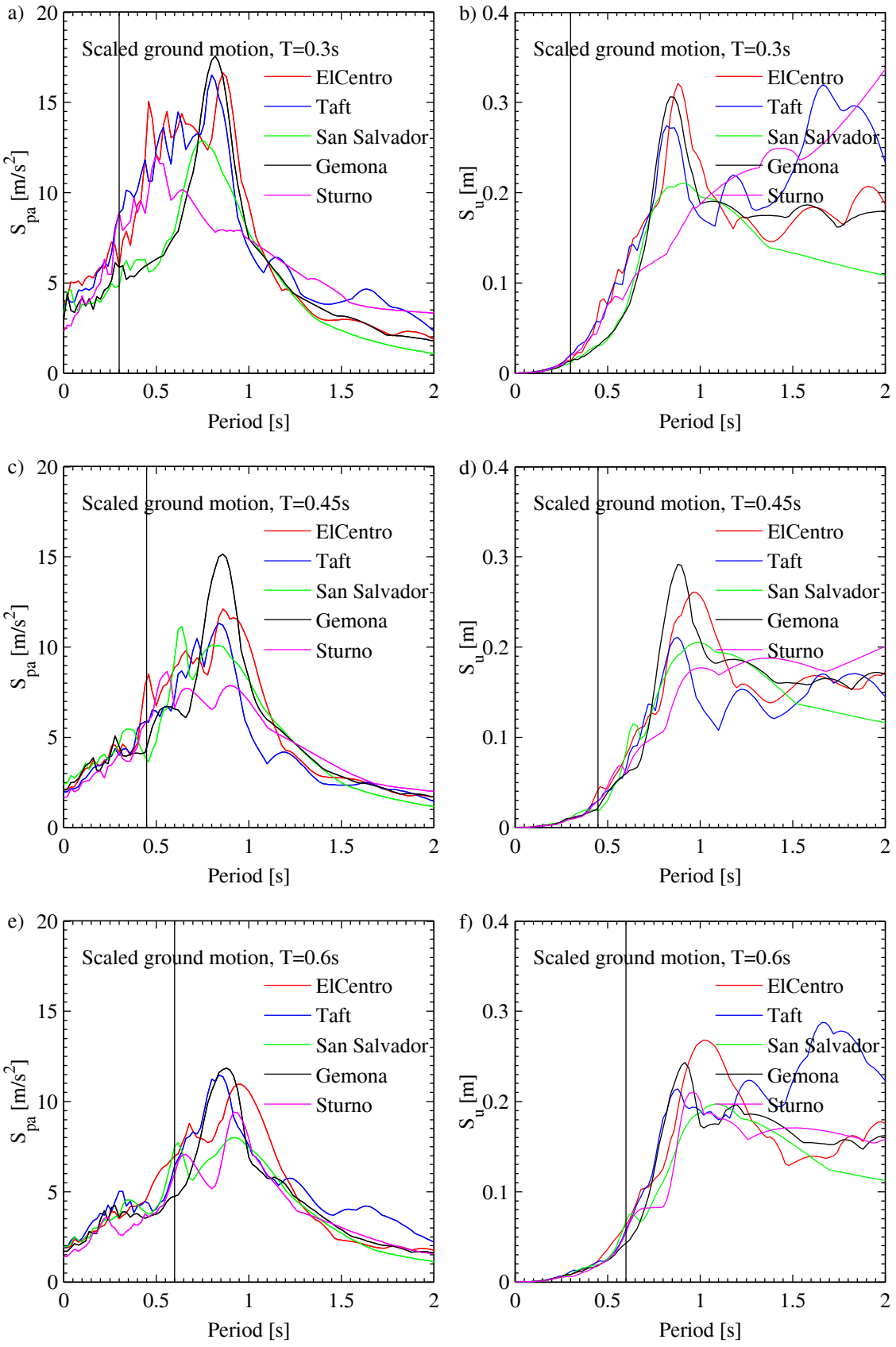

Figure 4.4: Inelastic model: Storey acceleration and displacement response spectra for midheight of fourth storey, 5% damping. The vertical line indicates the fundamental period of the elastic structure.

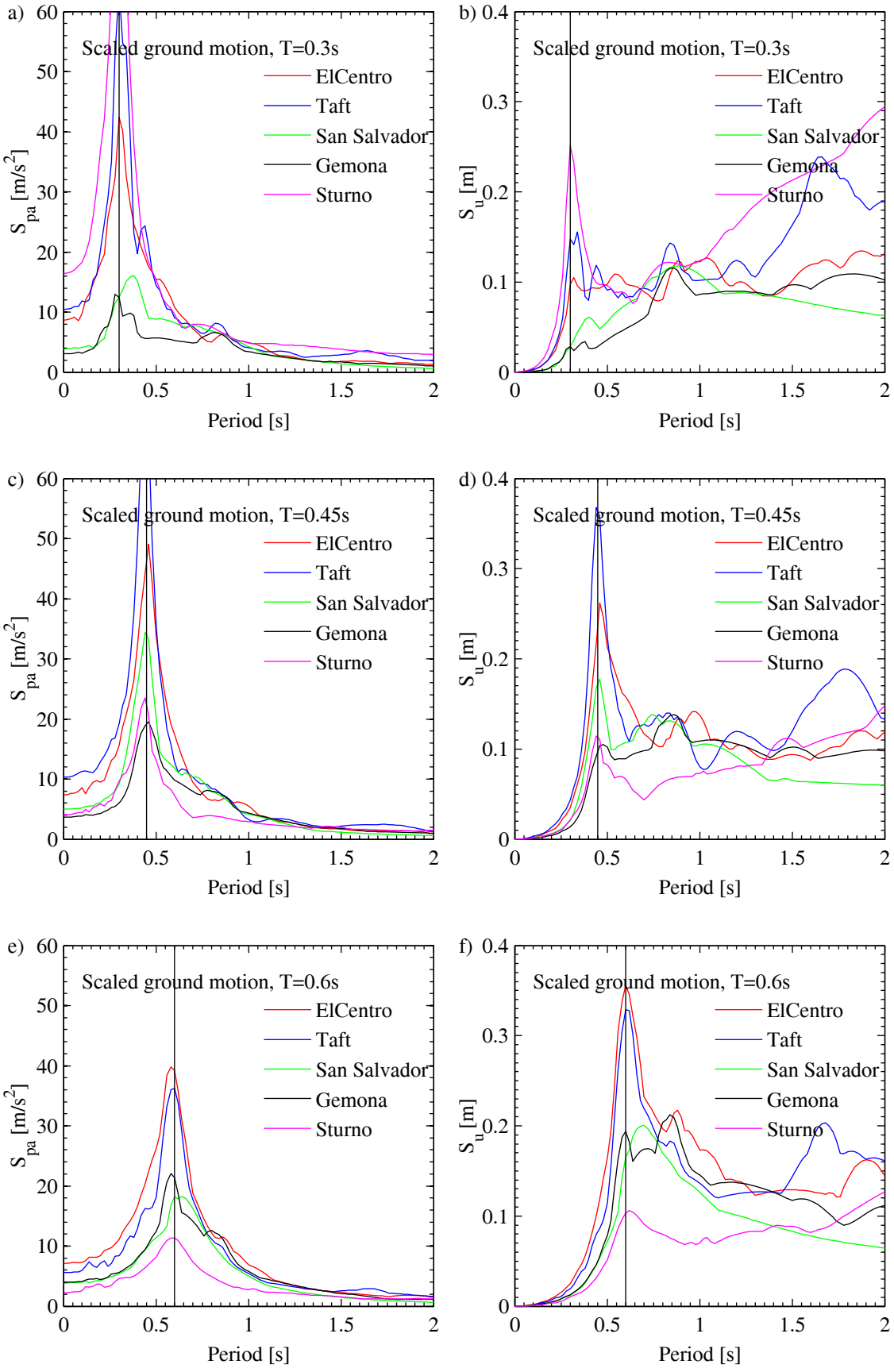

Figure 4.5: Elastic model: Storey acceleration and displacement response spectra for midheight of fourth storey, 5% damping. The vertical line indicates the fundamental period of the elastic structure.

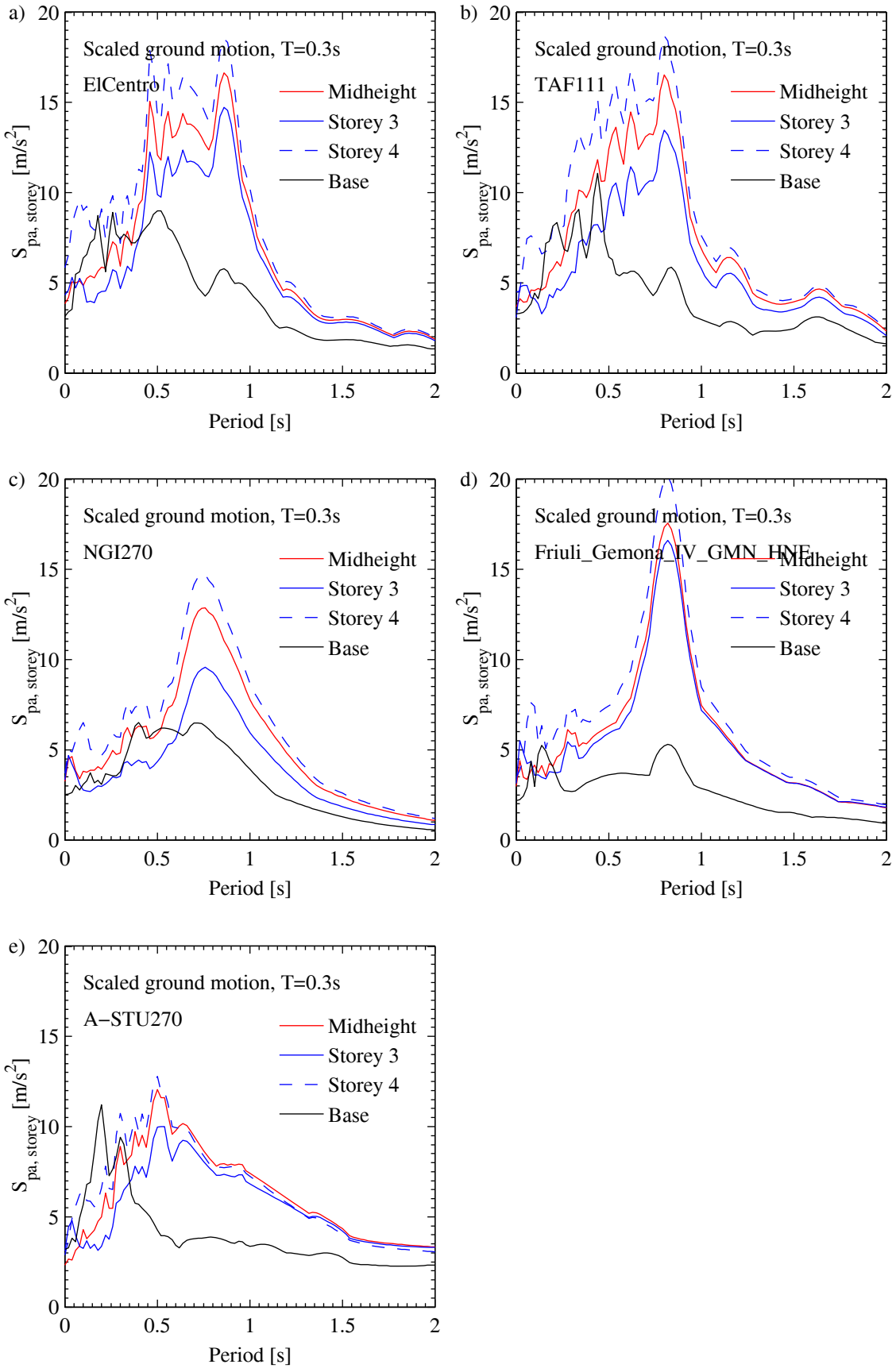

Figure 4.6: T=0.3 s: Comparison of response spectra at third and fourth storey and midheight of fourth storey, 5% damping

4.2.4 Comparison of floor response spectra obtained from numerical analyses to results from code approaches for estimating the floor response spectra

Both the SIA 261 [78] and the EC 8 [12] provide formulae for estimating the storey acceleration spectra. These spectra are provided for the design of non-structural elements but are applied here to estimate the out-of-plane demand on URM walls. In EC8, the spectral acceleration at level Z above the foundation within a structure is given as:

$$S_a = \alpha S \left[\frac{3\left(1+Z/H\right)}{1+\left(1-T_a/T_1\right)^2} - 0.5 \right] \geq \alpha S \tag{4.2}$$

where α is the peak ground acceleration; S is the coefficient accounting for the site class; H is the total height of the structure; T_1 is the vibration period of the first mode of the structure and T_a is the period of the non-structural element. The Swiss standard SIA 261 is in many ways based on the EC8 and therefore the equation is very similar:

$$S_a = \gamma_f \frac{a_g}{g} S \frac{1}{q_a} \left[\frac{3\left(1+Z/H\right)}{1+\left(1-T_a/T_1\right)^2} - 0.5 \right] \geq \gamma_f \frac{a_g}{g} S \frac{1}{q_a} \tag{4.3}$$

where γ_f is the importance factor; $a_g S/g$ is equivalent to αS in the equation of EC 8; q_a is the q-factor of the non-structural element. For γ_f =1 and q_a =1 the SIA 261 equation corresponds to the EC 8 equation and therefore only the latter will be discussed in the following.

Figure 4.7 and

Figure 4.8 show the comparison of the floor response spectra obtained for the inelastic and elastic model respectively with regard to the prediction by EC8. Since the code formula for S_a does not account for the lengthening of the structure's fundamental period due to inelastic response, it predicts the largest amplification always for the fundamental period of the elastic structure. As a result, for the inelastic structure, this amplification occurs for periods that are too short (

Figure 4.7). The maximum spectral accelerations are well predicted for the inelastic model but underestimated for the elastic model. Due to the lower bound spectral acceleration value, which is taken equal to the peak ground acceleration, the shake of the spectral displacements is not correctly captured. The latter are important as future codes might include displacement-based assessment methods for the out-of-plane response of URM walls.

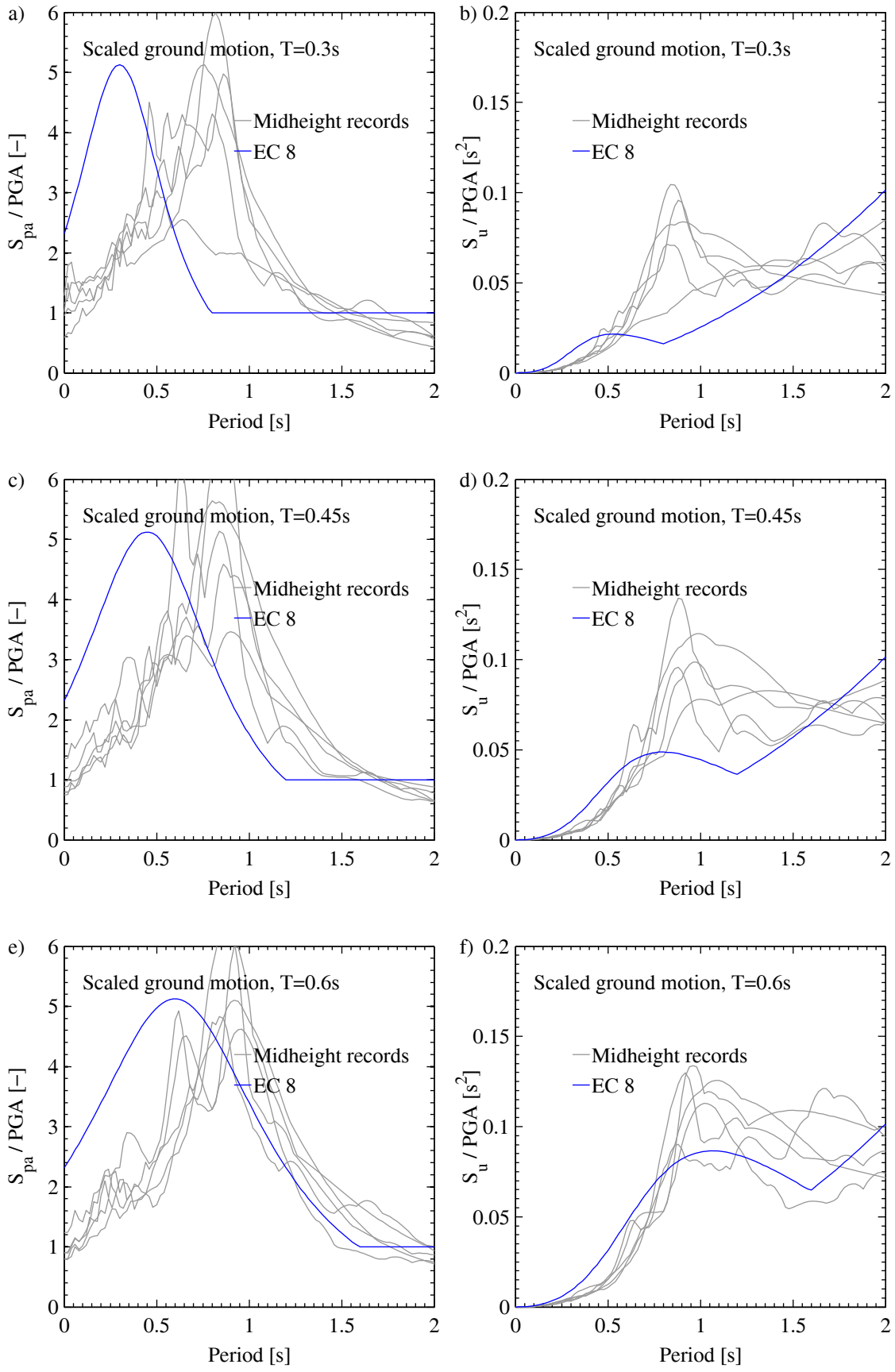

Figure 4.7: Inelastic models: Storey acceleration and displacement response spectra for midheight of fourth storey, 5% damping. Comparison to EC8 floor spectra.

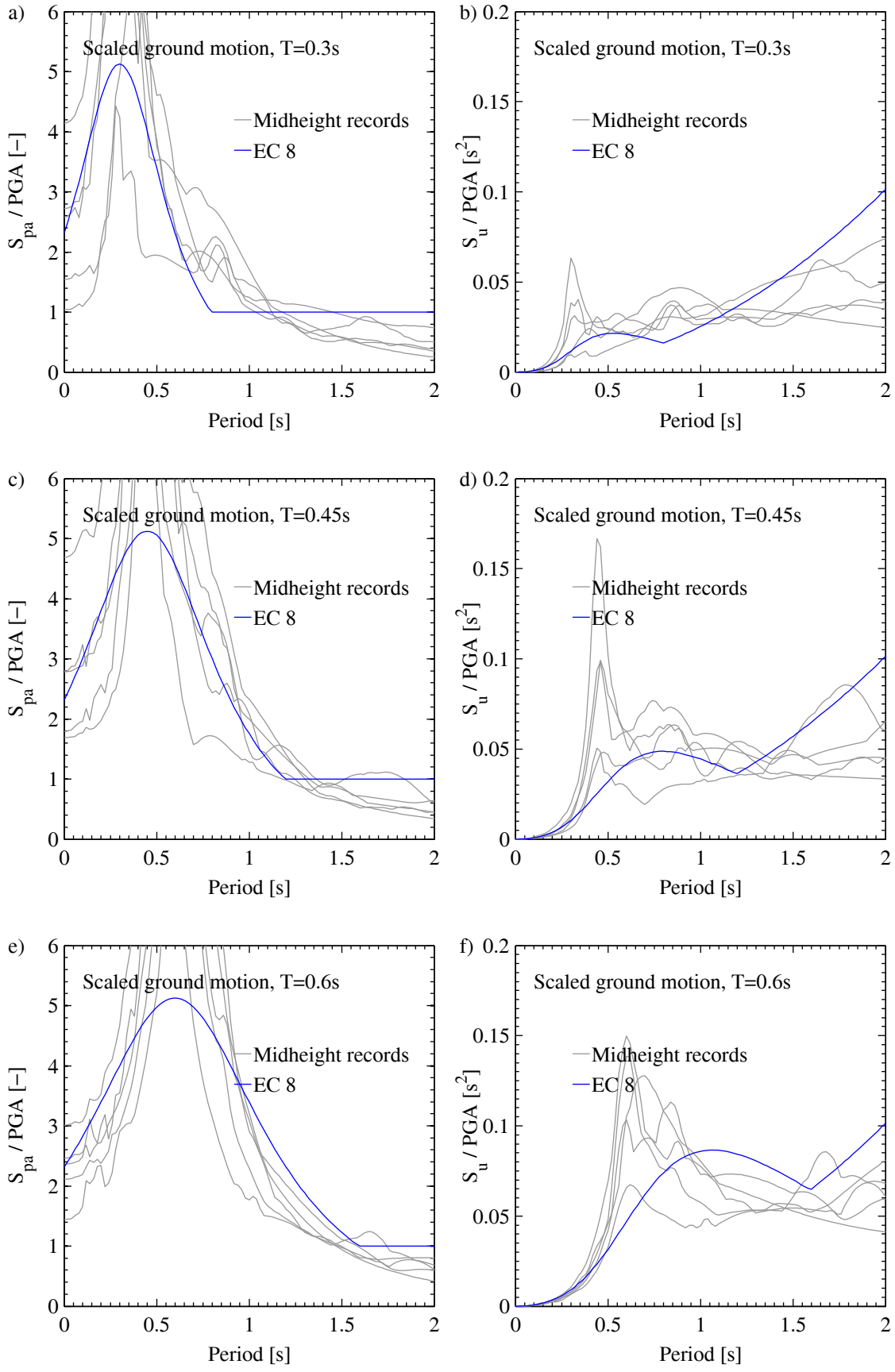

Figure 4.8: Elastic models: Storey acceleration and displacement response spectra for midheight of fourth storey, 5% damping. Comparison to EC8 floor spectra.

4.3 Parametric study

To assess the performance of the slenderness limits that codes propose for assessing the out-of-plane stability of URM walls (Section 4.1), a parametric study with in total 960 nonlinear analyses was conducted. The following sections describe the numerical model (Section 4.3.1), the parameters that are investigated (Section 4.3.2), the results of the parametric study (Section 4.3.3) and the comparison of these results to the slenderness criteria included in current codes (Section 4.3.4).

4.3.1 Numerical model used for the analysis

The out-of-plane response was analysed using the code UDEC [52]. The model is based on the numerical model of the previous chapter but instead of the half-scale model a full-scale model is now analysed. The wall is 2.8 m high while the wall thickness is one parameter that is varied within the scope of the parametric study (Figure 4.9). The wall is supported at the top and the bottom by a concrete slab. Unlike in the analyses presented in the previous chapter, the axial load P(t) that is applied at the top of the wall is maintained constant throughout the analysis. The wall is analysed for horizontal input velocities that are applied to the top and bottom slab. The vertical velocity of the bottom slab is set to zero. The vertical movement of the top slab is not restraint since the force boundary condition $P(t)=P_0$ is applied. The top slab is therefore always in contact with the wall and a "slider" as in Chapter 3 is not necessary. The assumed material properties are summarised in Table 4.4.

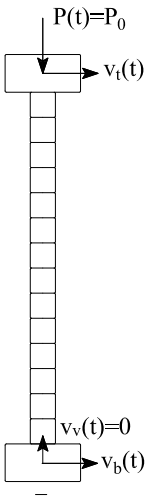

Figure 4.9: Parametric study: Numerical model for UDEC analyses

Table 4.4. Masonry properties for discrete element model used in the parametric study

E-modulus of the masonry for vertical compression (MPa)	5000
G-modulus of the masonry (MPa)	1875
Cohesion of mortar joints (MPa)	0.23
Friction angle of mortar joints	35°
Masonry compressive strength (MPa)	5.00
Tensile strength of mortar joints (MPa)	0.123
Density of masonry (kg/m^3)	1200

4.3.2 Investigated parameters

Six different parameters were investigated within the scope of this parametric study. These parameters are:

- The ground motion record
- The fundamental period of the structure
- The input velocities derived from the inelastic vs the elastic building models
- The difference in input velocities at the top and bottom of the wall (α=0 and α=1)
- The wall thickness
- The axial load ratio

In total 960 analyses were conducted. The following paragraphs outline how the different parameters were varied.

Ground motion record: Five different records were used for the analyses (Section 4.2.1). None of the records featured a velocity pulse that would be characteristic of a near-field effect. The records were scaled to reach for the inelastic building model a first storey drift of 0.4%. The acceleration response spectra of these scaled records are shown in Figure 4.3.

Fundamental period of the structure: The fundamental period influences the frequency content of the floor accelerations (Section 4.2.3). Also the peak ground acceleration that is required to reach a first storey drift of 0.4% (Table 4.3) reduces with increasing fundamental period. As outlined in Section 4.2.2 the storey masses were tuned such to obtain fundamental periods of 0.3 s, 0.45 s and 0.6 s for the four storey structure.

Inelastic vs elastic building model: As described in Section 4.2.3, the ground motion was scaled to reach 0.4% first storey drift for the inelastic building model. The same scaled ground motion was then applied to an elastic building model and the third and fourth floor acceleration determined. Whether a building behaves elastically or inelastically has an influence on the frequency content of the floor accelerations and on the amplification of the accelerations around the fundamental period. For an elastic behaviour of the building the floor accelerations are amplified more strongly but in a narrower band than for an inelastic behaviour of the building. For the inelastic building longer periods than for the elastic building are amplified due to the elongation of the fundamental period as a result of the inelastic deformations (Section 4.2.3).

Same vs different input velocities at the top and bottom: Many previous studies on the out-of-plane response of URM walls used simplified models that required that the top and bottom of the wall were subjected to the same acceleration time history. The advanced discrete element model that is used here allows to analyse also walls that are subjected to different motions at the top and bottom, which reflect the difference in motion of the third and fourth floor. The analyses of the previous chapter showed that different input motions at the top and bottom can lead to a larger out-of-plane response (Section 3.4.1). To investigate the influence of the different input motions at the top and bottom, the results are compared to the results obtained when the average velocities is applied at the top and bottom. For convenience the equations of Section 3.4.1 that define the input velocities at the top (v_t) and at the bottom (v_b) of the slab are repeated here:

$$v_t = \frac{v_4 + v_3}{2} + \alpha \frac{v_4 - v_3}{2} \tag{4.4}$$

$$v_b = \frac{v_4 + v_3}{2} - \alpha \frac{v_4 - v_3}{2} \tag{4.5}$$

where v_3 and v_4 are the horizontal velocities of the third and fourth floors as obtained from the Tremuri models. A value of $\alpha = 1$ yields the real input motions which are different at the top and the bottom of the wall and $\alpha = 0$ the average input motions.

Wall thickness: The wall thickness was varied between 12.5 cm, 15 cm, 17.5 cm and 25 cm. The wall height was for all models 2.8 m. Changing the wall thickness alters therefore also the wall slenderness h_w/t_w to values between 11.2 and 22.4.

Axial load ratio: The axial load per metre wall length that was applied at the top of the wall was varied between 0 and $0.4\%t_w f_c$ where f_c is the compressive strength of the masonry (f_c=5 MPa). This corresponds to the axial loads as indicated in Table 4.5. The axial load at the base results from the applied axial load, the weight of the wall and the weight of the top slab. The weight of the wall is 4.1 kN, 4.9 kN, 5.8 kN and 8.2

kN for the four wall thicknesses. The dimensions of the top slab are 0.5 x 0.1 m. The top slab is assigned the same density as the wall and therefore its weight is 0.6 kN.

Table 4.5: Axial loads at the base of the walls as function of the nominal axial load ratio ν and the wall thickness t_w. Values in brackets are actual axial load ratios at the wall base that include the applied axial load, the weight of the wall and the weight of the top slab.

	ν=0%	ν=1%	ν=2%	ν=4%
t_w=125 mm	4.7 kN (0.8%)	11.0 kN (1.8%)	17.2 kN (2.8%)	29.7 kN (4.8%)
t_w=150 mm	5.5 kN (0.7%)	13.0 kN (1.7%)	20.5 kN (2.7%)	35.5 kN (4.7%)
t_w=175 mm	6.4 kN (0.7%)	15.1 kN (1.7%)	23.9 kN (2.7%)	41.4 kN (4.7%)
t_w=250 mm	8.8 kN (0.7%)	21.3 kN (1.7%)	33.8 kN (2.7%)	58.8 kN (4.7%)

4.3.3 Results of parametric study

This section presents and discusses the results of the study with regard to the six parameters outlined in the previous section.

Wall thickness: Figure 4.10 shows the ratio of the maximum normalised out-of-plane displacement Δ_{max}/t_w for different wall thicknesses. These maximum normalised out-of-plane displacements are computed as the absolute displacement at midheight divided by the wall thickness. If a value equal or larger than one is attained, the wall is considered as having failed and the value of the normalised wall displacement is set to one. The normalised out-of-plane displacements are in general either very small or equal to one. Hence, the wall undergoes either very small out-of-plane displacements or collapses out-of-plane. When the input motion was derived from the inelastic building model and the average velocity was used as top and bottom input (α=0, Figure 4.10a), no wall failed. The largest number of walls failed when the input was derived from the elastic building model and different top and bottom velocities were defined as input (α=1, Figure 4.10d). This is also confirmed by Figure 4.11, which shows that for the latter case 40% of the 12.5 cm thick walls and 10% of the 25 cm thick walls failed. In Figure 4.11 all walls whose maximum normalised out-of-plane displacements were smaller than one were considered as walls that did not fail.

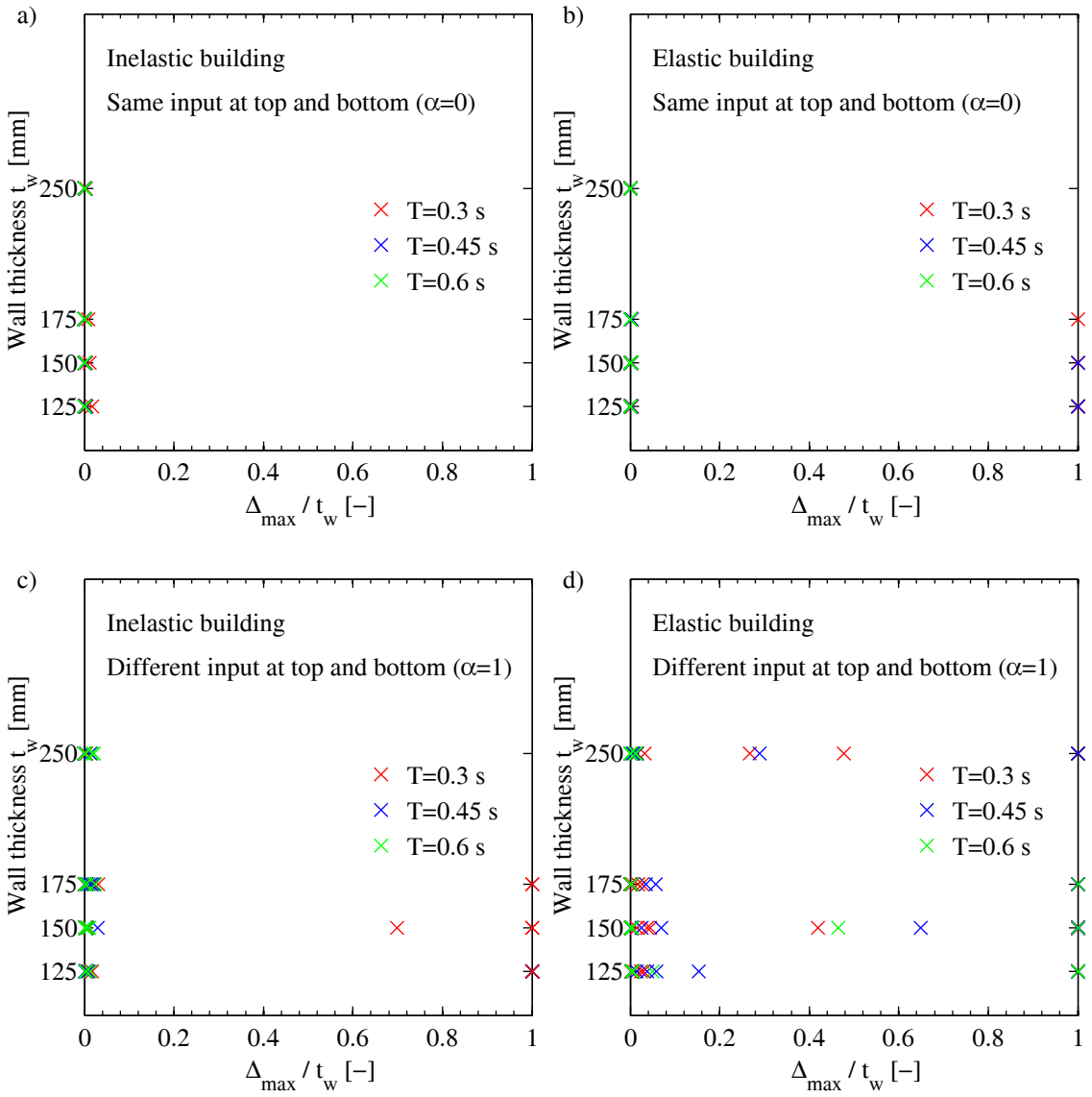

Figure 4.10: Parametric study: Ratio of maximum normalised out-of-plane displacement Δ_{max}/t_w for different wall thicknesses.

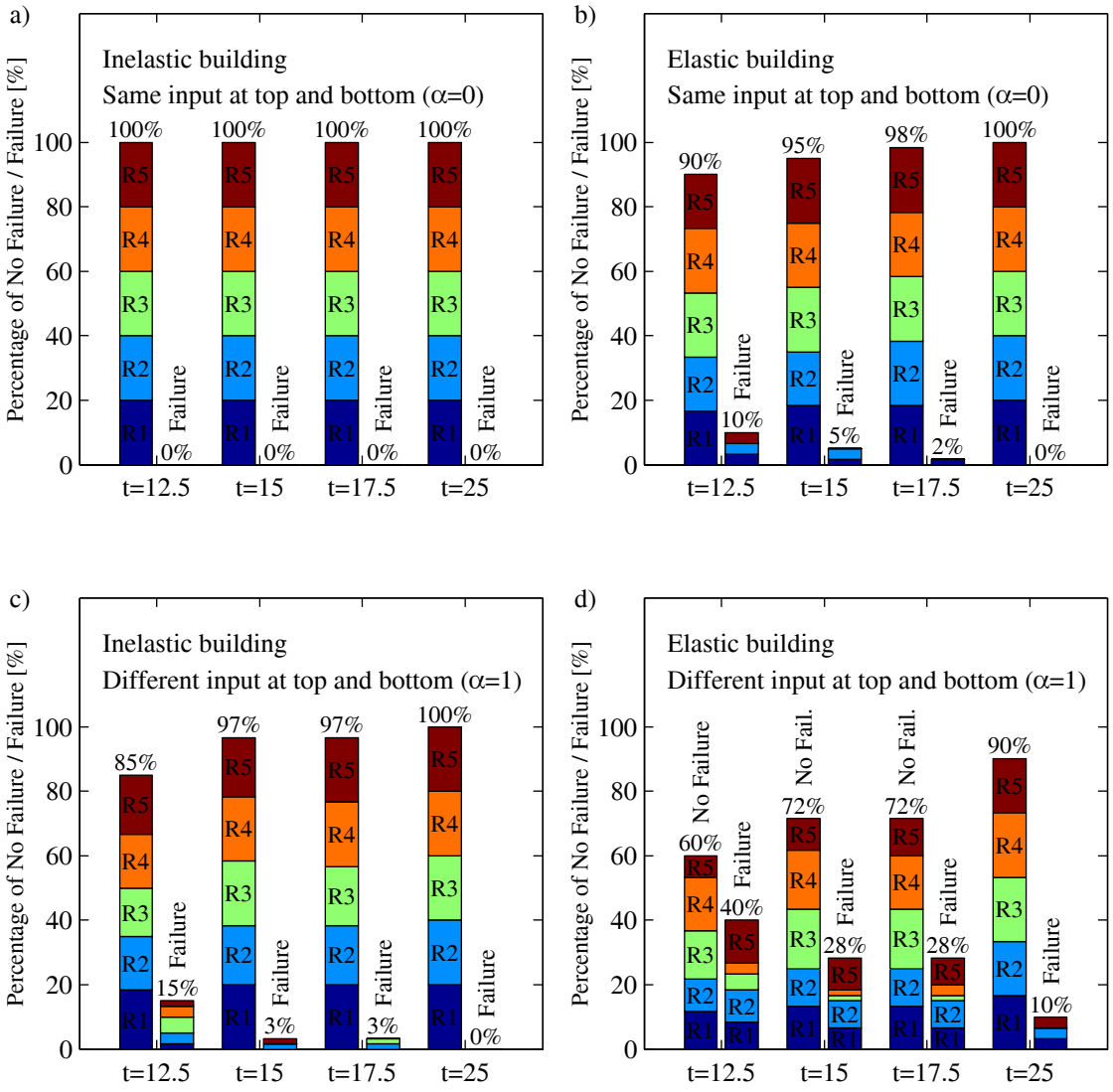

Figure 4.11: Parametric study: Percentage of walls that failed / did not fail for different building models (inelastic / elastic) and input definitions (α=0 and 1). The colours of the bars show the records: R1=Sturno, R2=ElCentro, R3=Gemona, R4=San Salvador, R5=Taft.

Axial load ratio: Two well-known trends are noticeable with regard to the axial load ratio (Figure 4.12 and Figure 4.13): First, the larger the axial load ratio, the less susceptible the wall is to out-of-plane failure. Second, the larger the axial load ratio, the more sudden the out-of-plane failure [11]. As a result, for an axial load ratio of 4% there are no walls that undergo a maximum normalised out-of-plane displacement between 0.1 and 1. The walls are subjected either to very small out-of-plane displacements less than $0.1t_w$ or the wall collapses out-of-plane (Δ_{max}/t_w=1).

Ground motion record: Figure 4.11 shows the distribution of the walls that failed / did not fail for the different records. For the inelastic building model too few walls failed as that clear trends could be identified. For the elastic building models, the Gemona and San Salvador records contribute to a lesser extent to wall failures than the other three records. For the buildings with a fundamental period of 0.3 s the floor accelerations are smallest for these records if periods shorter than 0.7 s are considered. Note that it is not possible to determine a rocking period of the out-of-plane loaded walls as the period elongates with rocking amplitude (e.g. [72]).

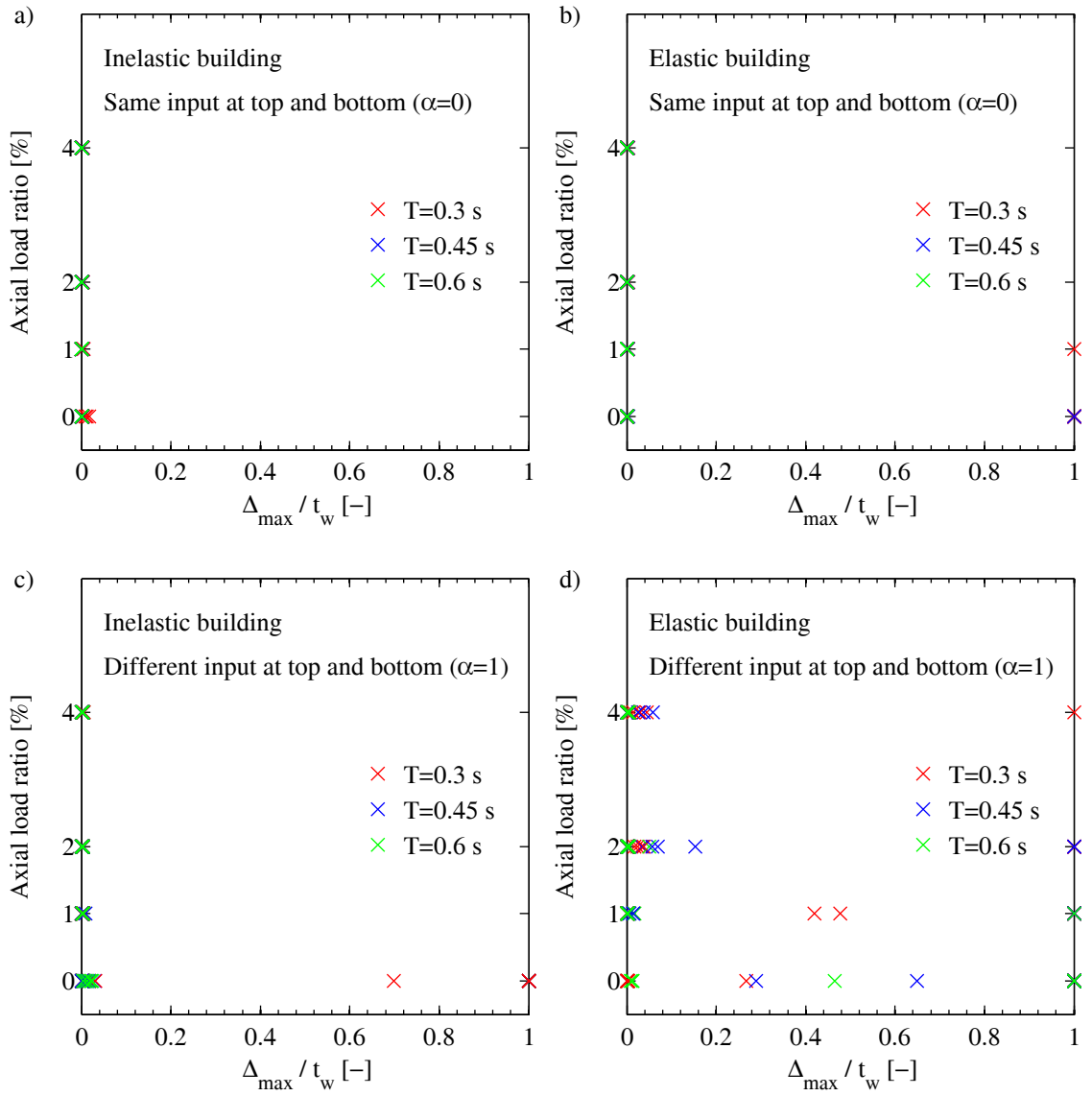

Figure 4.12: Parametric study: Ratio of maximum normalised out-of-plane displacement Δ_{max}/t_w for different axial load ratios.

The input velocities derived from the inelastic vs the elastic building models: Figure 4.11 and Figure 4.13 show the distribution of failure / no failure for the different input models. They clearly show that out-of-plane failure is more likely to occur in buildings that do not develop any significant inelastic deformations in their in-plane loaded walls. The analyses conducted here neglect of course any interaction of in-plane and out-of-plane resistance. Shear cracks due to in-plane loading can reduce the out-of-plane bending capacity of URM walls, if the walls are also supported along the vertical edges. Neglecting the interaction of in-plane and out-of-plane resistance is therefore a simplification. It is, however, justifiable since only vertically spanning walls are considered (vertical edges not restraint) and since in-plane damage of the top storey walls is typically unlikely.

The difference in input velocities at the top and bottom of the wall (α=0 and α=1): Figure 4.11 and Figure 4.13 confirm the findings from the analyses conducted in Section 3.4.1, which showed that the difference in horizontal excitation at the top and bottom increases the likelihood of out-of-plane failure when compared to analyses in which the wall is subjected to the same excitation at the top and bottom. In real buildings the out-of-plane loaded walls will be subjected to different excitations at its top and bottom since the floor motions of two floors are not the same. The differences are rather significant: For the inelastic building models the average ratio of wall failures increases from 0% (α=0) to 5.4% (α=1) and for the elastic building models

from 4.2 % (α=0) to 26.7% (α=1). This finding supports further the notion obtained from Section 3.4.1 that the different input motions at the top and bottom of the wall should be considered when assessing the out-of-plane vulnerability of URM walls.

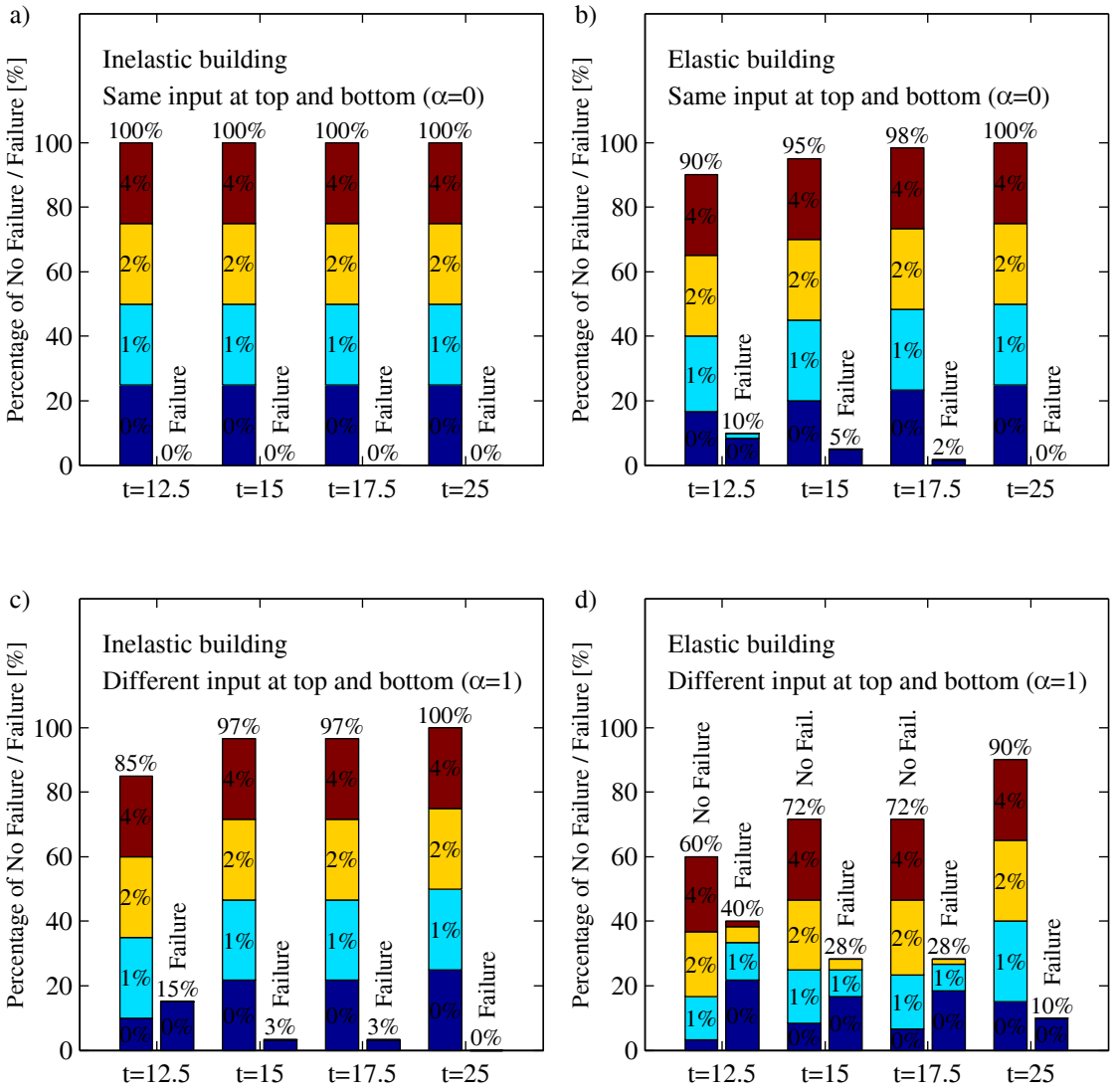

Figure 4.13: Parametric study: Percentage of walls that failed / did not fail for different building models (inelastic / elastic) and input definitions (α=0 and 1). The colours of the bars show the axial load ratio (0%, 1%, 2%, 4%).

Fundamental period of the building: Figure 4.14 shows for the input motions that were obtained from the elastic building with α=1.0 the influence of the fundamental period of the building on the distribution of wall failures. The building with the shortest period (T=0.3 s) leads overall to the largest number of out-of-plane failures. This trend is even stronger if walls with larger axial load ratios (Figure 4.14a) or larger wall thicknesses (Figure 4.14b) are considered. A larger axial load ratio or a larger wall thickness rigidifies the system and it is therefore more susceptible to input motions with a higher frequency content.

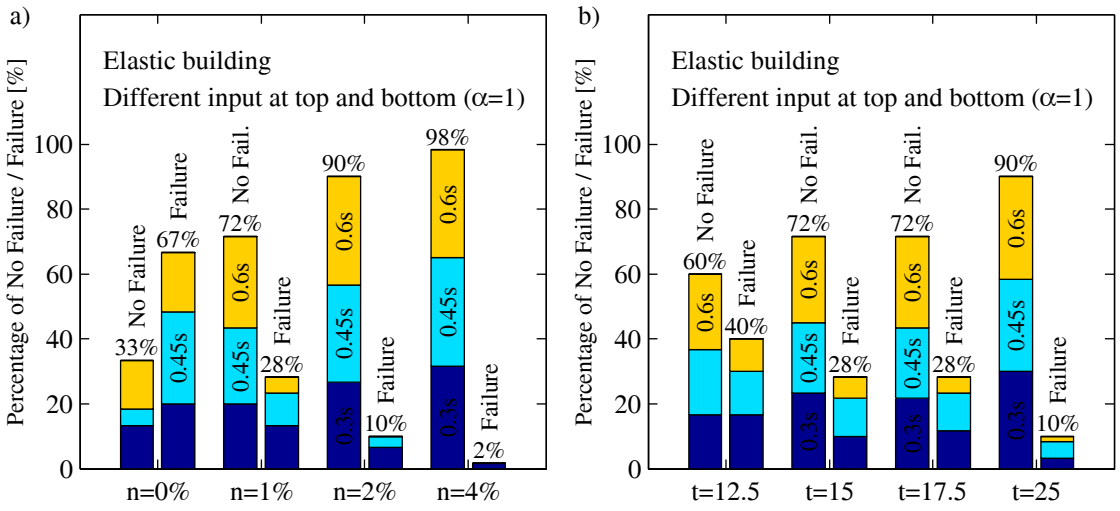

Figure 4.14: Parametric study: Percentage of walls that failed / did not fail for the elastic building models with different inputs at the top and bottom of the wall (α=1). The colours of the bars show the fundamental periods of the buildings (0.3 s, 0.45 s, 0.6 s). Plot (a) shows the distribution in function of the nominal axial load ratio and plot (b) the distribution in function of the wall thickness.

4.3.4 Comparison to slenderness limits in codes

This section compares the results obtained from the parametric study to the slenderness limits in codes. To do so, the results are plotted in graphs that show on the x-axis the peak ground acceleration PGA and on the y-axis the slenderness ratio of the out-of-plane loaded wall (Figure 4.15). As in the previous section, a separate graph is plotted for each input definition (inelastic vs elastic building model and α=0 vs α=1). Each building period and record leads to slightly different PGA values (Table 4.3). For this reason there are 15 different PGA-values for each input definition. The four wall thicknesses lead to four different slenderness ratios since the storey height is constant (h_w=2.8 m). Each graph contains therefore sixty data points. Each data point for a certain PGA-value and slenderness ratio represents four analyses for the four different axial load ratios. The marker is filled with white if none of these four walls failed and with black if all failed. The shades of grey reflect the percentage of walls that failed. As expected, the percentage of walls that failed tends to increase with increasing PGA-values and increasing slenderness ratios.

The slenderness ratios in codes were summarised in Section 4.1. Three of these codes (SIA 2018, EC8 and NTC) provide the slenderness ratio as values that depend on the seismicity (all codes). EC8 and NTC also prescribe minimum wall thicknesses. SIA 2018 accounts further for the building class and the position of the wall within the building (upper vs bottom storey). Assuming a wall in the upper storey of a building in a low seismicity region (Z3 for SIA 2018), which belongs to building class CO I, one obtains the following maximum slenderness ratios:

- SIA 2018: $(h_w/t_w)_{max} = 17$
- EC8: $(h_w/t_w)_{max} = \min(15, 2800/170=16.5) = 15$
- NTC: $(h_w/t_w)_{max} = \min(20, 2800/200=14) = 14$

These limits are shown by grey lines in Figure 4.15. The percentage of wall failures is summarised in Table 4.6. For the in-plane behaviour, a 5% fractile value is used [79] to which an additional safety factor is applied. If 5% wall failures is taken here as a first value, the slenderness ratio should lie between 11.2 and 16. The slenderness ratios proposed in EC8 and NTC would therefore satisfy this criterion while the SIA 2018 criterion would lead to walls that are too vulnerable for out-of-plane loading.

Table 4.6: Parametric study: Percentage of wall failures in function of wall slenderness ratios and input definition (inelastic vs elastic building model and α=0 vs α=1).

Percentage of wall failures	t_w=125 mm	t_w=150 mm	t_w=175 mm	t_w=250 mm
	h_w/t_w=22.4	h_w/t_w=18.7	h_w/t_w=16.0	h_w/t_w=11.2
I1: Inelastic building model, α=0	0.0%	0.0%	0.0%	0.0%
I2: Elastic building model, α=0	10.0%	5.0%	1.7%	0.0%
I3: Inelastic building model, α=1	15.0%	3.3%	3.3%	0.0%
I4: Elastic building model, α=1	40.0%	28.3%	28.3%	10.0%
Average I1-4	16.3%	9.2%	8.3%	2.5%

The slenderness limit in SIA 269/8, the new code for existing structures, depends explicitly on the PGA rather than on the seismic zone as in SIA 2018 (Equ. (4.)). In addition, a minimum thickness of $t_{w,min}$=150 mm is required. In Equ. (4.), the PGA corresponds to:

$$PGA = \gamma_f Sa_{gd} \tag{4.6}$$

Figure 4.15 shows the upper limit of the slenderness ratio and the limit obtained for α_{min}=1 and k=2 (RC slabs), which results in:

$$\frac{h_w}{t_w} \leq \frac{2 \cdot g}{PGA} \leq \sqrt{\frac{100g}{PGA}} \tag{4.7}$$

For α_{min}=0.25 and k=2 one obtains:

$$\frac{h_w}{t_w} \leq \frac{8 \cdot g}{PGA} \leq \sqrt{\frac{100g}{PGA}} \tag{4.8}$$

For α_{min}=1.0, almost all wall configurations would violate the slenderness criterion in SIA 269/8. For α_{min}=0.25, on the contrary, about two thirds of the wall configurations would pass the slenderness criterion. While the criterion seems to work rather well for Figure 4.15b and separates rather well wall configurations that fail from those that pass, this does not apply to Figure 4.15d. The difference between Figure 4.15b and d relates to the input motion at the top and bottom of the wall: Figure 4.15b represents analyses wherein the wall has been subjected to the same motion at the top and bottom while Figure 4.15d represents analyses where the input motions at the top and bottom differ, which represents the situation in real buildings. The current formulation in SIA 269/8 nor in any other code does not allow to account for the influence in difference between top and bottom excitation.

Based on the observations from the shake table test that was presented in Chapter 3, the analyses that were carried out here approximate only the boundary conditions in buildings with RC slabs: In a building with RC slabs the vertical movement of the slabs is typically controlled by the walls that are loaded in-plane. If these walls deform chiefly in shear, the vertical uplift is small and if the out-of-plane loaded wall starts to rock, the axial force in the out-of-plane loaded wall increases. If the in-plane loaded wall rocks, this will lead to an uplift of the slab and the axial load in the out-of-plane loaded wall tends to zero. However, the axial force is only zero for a relative short time interval. Approximating these kinematic boundary conditions with a force-boundary where the axial force is zero over the entire duration of the shaking, is therefore rather conservative. For this reason, also higher axial load ratios (1-4%) were investigated in the parametric study. For investigating the actual boundary conditions in buildings with RC slabs in more detail, a study that puts into relation the in-plane deformations of adjacent URM walls and the slab uplift is required.

Based on the findings represented in Figure 4.15 the following recommendations can be formulated:

- The peak ground acceleration is not the most suitable parameter to describe the demand on out-of-plane loaded walls. The floor acceleration would be a better parameter since it would allow to

distinguish between the floor accelerations in elastic and inelastic buildings; it is discussed in the following.

- The main limit functions that are proportional to $1/(\alpha_{min}PGA)$ seems to vary too strongly with the demand parameter PGA. The upper bound function, which varies with the square root of this factor seems more appropriate.
- As all other functions the slenderness limits in SIA 269/8 do not allow for the effect of different input motions at the top and bottom of the wall. This should be investigated further in the future.

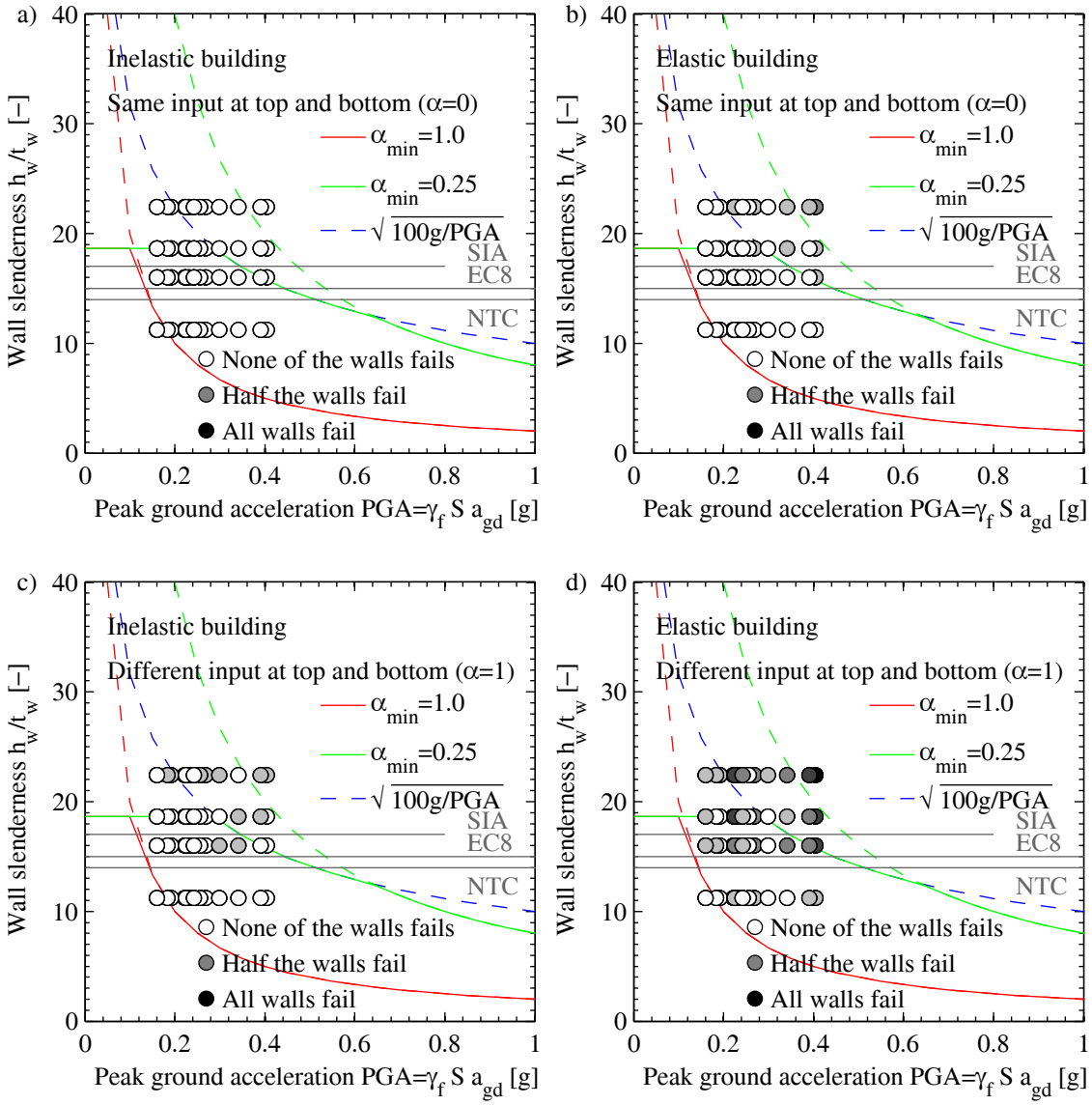

Figure 4.15: Parametric study: Comparison of results to slenderness limit in EC8, NTC and SIA D0237 (grey lines) and SIA 296/8 (red and blue line). Each circle represents the analyses with four different axial load ratios. The four plots show the results for different building models (inelastic / elastic) and input definitions (α=0 and 1).

As outlined above, the peak floor acceleration (PFA) would be a better parameter for describing the demand on the out-of-plane loaded walls than the peak ground acceleration (PGA). The graph shows that the following modified slenderness criterion seems to distinguish well between failures and passes for cases where the input definition at the top and bottom differs (i.e., as in reality). This applies for both the inelastic and the elastic building models:

$$\frac{h_w}{t_w} \leq \sqrt{\frac{100g}{PFA}} \tag{4.9}$$

For cases where the input motions at the top and bottom of the wall are equal, the criterion leads to conservative estimates of the wall slenderness that leads to failure. Before this criterion can be implemented in codes, further studies are required; these are outlined in Section 4.4.2.

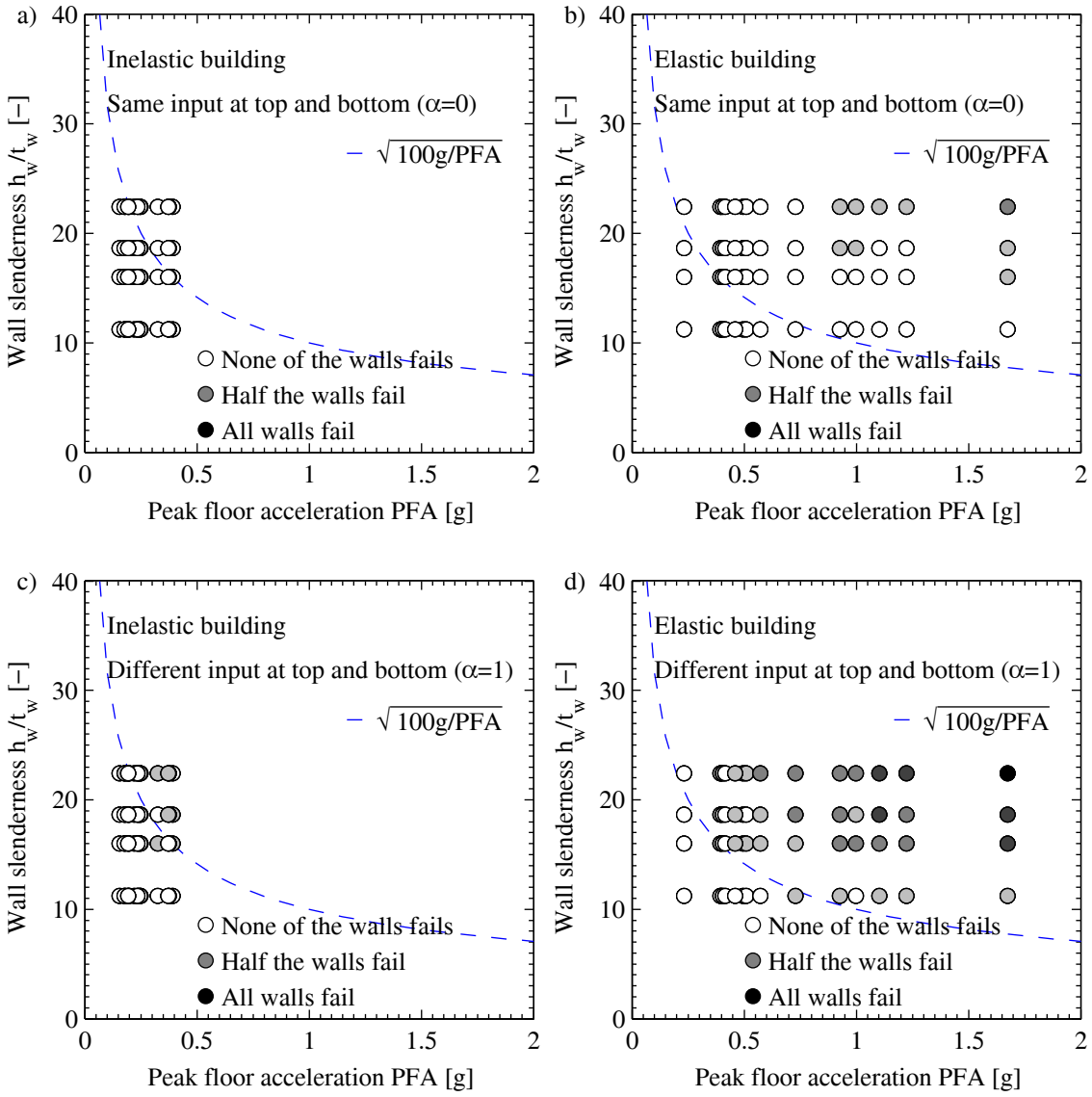

Figure 4.16: Parametric study: Comparison of results to a modified slenderness limit where the peak ground acceleration is replaced by the peak floor acceleration. Each circle represents the analyses with four different axial load ratios. The four plots show the results for different building models (inelastic / elastic) and input definitions (α=0 and 1).

4.4 Summary and recommendations

4.4.1 Summary

In this chapter the results of a parametric study on out-of-plane loaded URM walls were presented and discussed. The 2D model that was used in this study represented a vertically spanning wall of fourteen brick rows. The wall had a height of 2.8 m and the thickness was varied between 12.5 and 25 cm. The model was analysed using the discrete element software UDEC [52]. An axial force that remained constant throughout the analysis was applied at the top of the wall. The axial load ratio was varied between 0 and 4%. The walls were analysed for different horizontal input motions. These input motions were applied to the model at the top and bottom slab that framed the wall. The input motions corresponded to the floor motions that were derived from five different ground motion records and three different 4-storey building models with fundamental periods of 0.3 s, 0.45 s and 0.6 s respectively. These models were analysed using the software Tremuri [10]; both elastic and inelastic behaviour of the in-plane loaded walls was considered. The out-of-plane loaded walls that were analysed corresponded to walls of the fourth storey, i.e., to walls that were at their base supported by the third floor slab while the boundary condition at the top was provided by the fourth storey slab. The models were analysed for two sets of input motions: First, the average of the third and fourth floor motion was applied to the top and bottom slab, i.e., the top and bottom slab were subjected to the same motion. Second, the bottom slab was subjected to the third floor motion and the top slab to the fourth floor motion, i.e., the top and bottom slabs were subjected to different motions.

The results of this parametric study confirmed the influence of a number of well-known parameters on the out-of-plane stability of URM walls when subjected to seismic loading (Section 4.3.3). The most important ones are summarised here:

- The larger the wall thickness (i.e., the smaller the wall slenderness), the less vulnerable the wall to out-of-plane excitation.
- The larger the applied axial load, the less vulnerable the wall to out-of-plane excitation. The analyses confirmed further the experimental observation by Dazio [11] that for an increase in axial load the transition from a stable behaviour to an out-of-plane failure is more sudden.

Further, the vulnerability of the walls to out-of-plane failure also depends on the characteristics of the demand:

- The response of buildings with shorter fundamental periods tend to lead to floor motions that are more demanding on out-of-plane loaded walls than buildings with longer fundamental periods.
- The floor motions of buildings whose in-plane loaded walls respond inelastically are less demanding on out-of-plane loaded walls than the floor motions of buildings whose in-plane loaded walls respond elastically. This is because elastic building response leads to a stronger amplification of accelerations around the fundamental period of the building. Further, inelastic deformations lead to a lengthening of the fundamental period of the building.
- The parametric study also supported the observation which was first observed from the small numerical study in the previous chapter (Section 3.4.1): Considering the fact that walls will be subjected to different input motions at the top and bottom leads to a considerably larger out-of-plane vulnerability of URM walls than subjecting top and bottom to the same average motion. The latter is the standard procedure in existing studies (e.g. [68]).

The results of the parametric study were also compared to slenderness limits in codes in general and in particular to the new criterion included in SIA 269/8 [34]. With regard to the latter the comparison showed the following:

- The slenderness criterion obtained for α_{min}=0.25 separates rather well between failures and passes if the walls are subjected to the same input motion at the top and bottom but it is unconservative if different input motions at the top and bottom of the wall are considered.
- Using the peak ground acceleration as indicator for the demand does not account for the amplification of the motion at floor levels due to the building response. It further does not allow to account for the fundamental period of the building nor the effect of inelastic behaviour of the building on the amplification of floor accelerations.
- The main limit functions that are proportional to $1/(\alpha_{min}PGA)$ seems to vary too strongly with the

demand parameter PGA. The upper bound function, which varies with the square root of this factor seems more appropriate.

4.4.2 Recommendations

Based on the results obtained so far, the following recommendations for future revisions of SIA 269/8 can be formulated:

- The peak floor acceleration rather than the peak ground acceleration should be taken as measure for the demand.
- Empirical relations should be developed and included that estimate the peak floor accelerations PFA as a function of the fundamental period of the building and the level of inelastic deformations the structure is expected to undergo. Such relationships would not just be useful for the out-of-plane assessment of URM walls but for the seismic assessment of accelerations sensitive non-structural components.
- The slenderness criterion should take a form similar to Equ. (4.9), i.e., the slenderness limit should be proportional to the square root of $1/(\alpha_{min}\text{PFA})$.

The results should be supported by further studies. In addition to a model for estimating the peak floor acceleration, the following aspects require further investigation:

- *Same vs different input velocities at the top and bottom*: The effect of the difference in input definition at the top and bottom of the wall should be studied. At the moment, the difference has only been observed from analysis but cannot be explained by a mechanical approach.
- *Uplift of slab due to rocking of adjacent walls:* A model for the boundary conditions of the walls when uplift of the slab is considered should be developed. This would allow to describe better the boundary conditions in URM buildings with RC slabs. In this case, the axial load is only zero for a short instant in time and it is therefore expected that the vulnerability decreases with regard to the analysis for a zero axial load ratio.
- *Boundary conditions of walls that are connected to orthogonal walls:* In this study a 2D model was analysed, which represented a vertically spanning wall, i.e., a wall whose vertical edges are not supported. In residential buildings, the walls are often connected to orthogonal walls, what reduces the vulnerability to out-of-plane excitation. The impact of such boundary conditions can only be analysed if 3D models are used. Such models would further allow to study the effect of window and door openings on the out-of-plane stability.
- *Near-field effects:* In regions of low to moderate seismicity such as Switzerland, the seismic hazard is largely controlled by relatively close events, i.e., small epicentral distances. Such events can lead to ground motions that are characterised by a strong velocity pulse. The out-of-plane response of URM walls when the building is subjected to such near-field ground motions should be studied and compared to the response to ground motions without velocity pulse, which were used in this study.
- *Effect of other ground motion components*: This study considered only the ground motion component orthogonal to the wall plane. In reality, there are two further components, i.e., the horizontal in-plane component and the vertical component. The vertical component will vary the axial load and is therefore expected to have a significant influence on the out-of-plane response. The in-plane component will only have an effect if the walls are also supported at their vertical edges; it can only be considered if 3D models rather than 2D models are used.
- *Sensitivity of results to mechanical properties of masonry:* The sensitivity of the out-of-plane behaviour to mechanical properties of the masonry should be investigated. A small preliminary study showed that, for example, the tensile strength of the bed joint plays a significant role.
- *Comparison to other assessment methods:* Nonlinear static assessment methods have been developed by Priestley [80] and Doherty et al. [68] and implemented in modified forms in the Italian code [70], [71]. These methods are significantly more elaborate than the slenderness criteria but are still simple enough to be applied as a standard procedure in seismic assessment. The results of these nonlinear static assessment methods should be benchmarked against the results obtained by means of the discrete element model.

5 REFERENCES

[1] C. Graubner, "Nachhaltigkeit von Ein- und Zweifamilienhäusern aus Mauerwerk (Sustainability of one- and two family houses in URM)," Darmstadt, Germany, 2013.

[2] SIA, *SIA 160: Einwirkungen auf Tragwerke (Actions on structures)*. Zürich, Switzerland: Swiss Society of Engineers and Architects (SIA), 1989.

[3] SIA, *SIA 261: Einwirkungen auf Tragwerke (Actions on structures)*. Zürich, Switzerland: Swiss Society of Engineers and Architects (SIA), 2003.

[4] G. M. Calvi, "A displacement-based approach for vulnerability evaluation of classes of buildings," *J. Earthq. Eng.*, vol. 3, no. 3, pp. 411–438, Jul. 1999.

[5] K. Lang, "Seismic vulnerability of existing buildings," Swiss Federal Institute of Technology Zurich (ETHZ), 2002.

[6] M. J. N. Priestley, G. M. Calvi, and M. J. Kowalsky, *Displacement-based seismic design of structures*. Pavia, Italy: IUSS Press, 2007.

[7] K. Pfyl-Lang, F. Braune, and P. Lestuzzi, "SIA D0237: Beurteilung von Mauerwerksgebäuden bezüglich Erdbeben (SIA D 0237: Evaluation de la sécurité parasismique des bâtiments en maçonnerie)," Zürich, Switzerland, 2011.

[8] G. Magenes, "A method for pushover analysis in seismic assessment of masonry buildings," in *Proceedings of the 12 World Conference on Earthquake Engineering*, 2000, pp. 1–8.

[9] Y. Belmouden and P. Lestuzzi, "An equivalent frame model for seismic analysis of masonry and reinforced concrete buildings," *Construction and Building Materials*, vol. 23, no. 1. pp. 40–53, 2009.

[10] S. Lagomarsino, A. Penna, A. Galasco, and S. Cattari, "TREMURI program: An equivalent frame model for the nonlinear seismic analysis of masonry buildings," *Eng. Struct.*, vol. 56, pp. 1787–1799, Nov. 2013.

[11] A. Dazio, "The effect of the boundary conditions on the out-of-plane behaviour of unreinforced masonry walls," in *Proceedings of the 14th World Conference on Earthquake Engineering*, 2009.

[12] CEN, "Eurocode 8: Design of structures for earthquake resistance, Part 1: General rules, seismic actions and rules for buildings," Brussels, Belgium, 2004.

[13] K. Beyer, M. Tondelli, S. Petry, and S. Peloso, "Dynamic testing of a four-storey building with reinforced concrete and unreinforced masonry walls: Prediction, test results and data set," *Bull. Earthq. Eng.*, vol. in press, 2015.

[14] S. Lagomarsino, A. Penna, A. Galasco, and S. Cattari, "3muri." S.T.A. Data Srl, Torino, Italy, 2014.

[15] S. Petry and K. Beyer, “Influence of boundary conditions and size effect on the drift capacity of URM walls,” *Eng. Struct.*, vol. 65, pp. 76–88, Apr. 2014.

[16] S. Petry, “Force-displacement response of unreinforced masonry walls for seismic design,” École Polytechnique Fédérale de Lausanne (EPFL), 2015.

[17] S. Petry and K. Beyer, “Cyclic test data of six unreinforced masonry walls with different boundary conditions,” *Earthq. Spectra*, Jul. 2014.

[18] S. Petry and K. Beyer, “Scaling unreinforced masonry for reduced-scale seismic testing,” *Bull. Earthq. Eng.*, vol. 12, no. 6, pp. 2557–2581, Mar. 2014.

[19] CEN, “Eurocode 8: Design of structures for earthquake resistance, Part 3: Assessmemt and retrofitting of buildings,” Brussels, Belgium, 2005.

[20] P. E. Mergos and K. Beyer, “Loading protocols for European regions of low to moderate seismicity,” *Bull. Earthq. Eng.*, vol. 12, no. 6, pp. 2507–2530, Mar. 2014.

[21] P. B. Lourenço, “Two aspects related to the analysis of masonry structures: Size effect and parameter sensitivity,” Delft, Netherlands, 1997.

[22] S. Petry and K. Beyer, “Force-displacement response of in-plane loaded URM walls with dominating flexural mode,” *Submitt. to Earthq. Eng. Struct. Dyn.*, 2014.

[23] S. Petry and K. Beyer, “Limit states of modern unreinforced clay brick masonry walls subjected to in-plane loading,” *Bull. Earthq. Eng.*, 2014.

[24] A. Benedetti and E. Steli, “Analytical models for shear-displacement curves of unreinforced and FRP reinforced masonry panels,” *Constr. Build. Mater.*, vol. 22, no. 3, pp. 175–185, Mar. 2008.

[25] A. Penna, S. Lagomarsino, and A. Galasco, “A nonlinear macroelement model for the seismic analysis of masonry buildings,” *Earthq. Eng. Struct. Dyn.*, vol. 43, no. 2, pp. 159–179, 2014.

[26] A. Paparo, “Seismic behaviour and design of mixed RC-URM wall structures,” École Polytechnique Fédérale de Lausanne (EPFL), 2015.

[27] A. Paparo and K. Beyer, “Quasi-static cyclic tests of two mixed reinforced concrete–unreinforced masonry wall structures,” *Eng. Struct.*, vol. 71, pp. 201–211, Jul. 2014.

[28] CEN, “Eurocode 6: Design of masonry structures, Part 1-1: Common rules for reinforced and unreinforced masonry structures,” Brussels, Belgium, 2005.

[29] A. Paparo and K. Beyer, “Modelling the seismic response of modern URM buildings retrofitted by adding RC walls,” *J. Earthq. Eng.*, 2014.

[30] V. Cervenka, “ATENA – Computer program for nonlinear finite element analysis of reinforced concrete structures,” Prague, Czech Republic, 2007.

[31] A. Paparo and K. Beyer, “A displacement-based design approach for mixed RC-URM wall structures,” *Earthquakes Struct.*, 2014.

[32] P. Lestuzzi and M. Badoux, *Evaluation parasismique des constructions existantes*. Lausanne, Switzerland: Presses polytechniques et universitaires romandes, 2013.

[33] M. Eddamanhoury, "Comportement sismique de bâtimens en maçonnerie non armée avec dalles en béton armé (Seismic behaviour of unreinforced masonry buildings with reinforced concrete slabs)," Ecole Polytechnique Fédérale de Lausanne (EPFL), 2014.

[34] SIA, *prSN 505 269/8: Erhaltung von Tragwerken (Existing structures – Earthquakes)*. Zürich, Switzerland: Schweizerischer Ingenieur- und Architektenverein (SIA), 2014.

[35] S. Frumento, G. Magenes, P. Morandi, and G. M. Calvi, "Interpretation of experimental shear tests on clay brick masonry walls and evaluation of q-factors for seismic design," Pavia, Italy, 2009.

[36] S. A. Freeman, "The capacity spectrum method as a tool for seismic design," in *Proceedings of the 11th European Conference on on Earthquake Engineering*, 1998.

[37] C. Michel, P. Lestuzzi, and C. Lacave, "Simplified non-linear seismic displacement demand prediction for low period structures," *Bull. Earthq. Eng.*, vol. 12, pp. 1563–1581, 2014.

[38] M. Tomaževič, *Earthquake-Resistant Design of Masonry Structures*. London, United Kingdom: Imperial College Press, 1999.

[39] SIA, *SIA 266: Masonry*. Zürich, Switzerland: Swiss Society of Engineers and Architects (SIA), 2005.

[40] R. Flanagan and Bennet RM, "Bidirectional behavior of structural clay tile infilled frames," *J. Struct. Eng.*, vol. 125, no. 3, pp. 236–244, 1999.

[41] G. M. Calvi and D. Bolognini, "Seismic response of reinforced concrete frames infilled with weakly reinforced masonry panels," *J. Earthq. Eng.*, vol. 5, no. January 2015, pp. 153–185, 2001.

[42] M. F. P. Pereira, M. F. N. Pereira, J. E. D. Ferreira, and P. B. Lourenço, "Behavior of masonry infill panels in RC frames subjected to in plane and out of plane loads," *AMCM2011 - Proc. 7th Int. Conf. Anal. Model. New Concepts Concr. Mason. Struct.*, 2011.

[43] F. da Porto, G. Guidi, M. D. Benetta, and N. Verlato, "Combined in-plane/out-of-plane experimental behaviour of reinforced and strengthened infill masonry walls," 2013.

[44] P. Morandi, S. Hak, and G. Magenes, "In-plane experimental response of strong masonry infills," in *Proceedings of the 9th International Masonry Conference*, 2014, pp. 1–12.

[45] M. Mistler, A. Anthoine, and C. Butenweg, "In-plane and out-of-plane homogenisation of masonry," *Comput. Struct.*, vol. 85, no. 17–18, pp. 1321–1330, Sep. 2007.

[46] S. Kadysiewski and K. M. Mosalam, "Modeling of unreinforced masonry infill walls considering in-plane and out-of-plane interaction," Berkeley, California, 2009.

[47] ABK, "Methodology for mitigation of seismic hazards in existing unreinforced masonry buildings: wall testing, out of plane," El Segundo, 1981.

[48] M. Griffith, N. Lam, J. Wilson, and K. Doherty, "Experimental investigation of unreinforced brick masonry walls in flexure," *J. Struct. Eng.*, vol. 130, no. March, pp. 423–432, 2004.

[49] C. S. Meisl, K. J. Elwood, and C. E. Ventura, "Shake table tests on the out-of-plane response of unreinforced masonry wallsThis article is one of a selection of papers published in this Special Issue on Masonry.," *Can. J. Civ. Eng.*, vol. 34, pp. 1381–1392, 2007.

[50] C. C. Simsir, M. A. Aschheim, and D. P. Abrams, “Out-of-plane dynamic response of unreinforced masonry bearing walls attached to flexible diaphragms,” *Proc. 13th World Conf. Earthq. Eng. - WCEE*, no. 2045, 2004.

[51] O. Penner and K. Elwood, “Shake table study on the out-of-plane dynamic stability of unreinforced masonry walls,” in *Proceedings of the 12th Canadian Masonry Symposium*, 2013.

[52] Itasca, “UDEC—Universal Distinct Element Code, version 6.0. , 2014.” Itasca Consulting Group Inc, Minneapolis, Minnesota, 2014.

[53] H. Krawinkler, “Possibilities and limitations of scale-model testing in earthquake engineering,” in *Proceedings of the 2nd U.S. National Conference on Earthquake Engineering*, 1979, pp. 283–292.

[54] S. Petry and K. Beyer, “Scaling unreinforced masonry for reduced-scale seismic testing,” *Bull. Earthq. Eng.*, vol. 12, no. 6, pp. 2557–2581, Mar. 2014.

[55] F. Lunghi, A. Pavese, S. Peloso, I. Lanese, and D. Silvestri, “Computer vision system for monitoring in dnamic structural testing. Role of seismic testing facilities in performance-based earthquake engineering,” in *SERIES Workshop, Geotechnical, Geological and Earthquake Engineering*, Netherlands: Springer, 2012.

[56] P. Cundall, “Computer model for simulating progressive large scale movements in blocky rock systems,” in *Proceedings of the Symposium of International Society of Rock Mechanics*, 1971, p. Paper No. II–8.

[57] L. De Lorenzis, M. DeJong, and J. Ochsendorf, “Failure of masonry arches under impulse base motion,” *Earthq. Eng. Struct. Dyn.*, vol. 36, pp. 2119–2136, 2007.

[58] T. Winkler, K. Meguro, and F. Yamazaki, “Response of rigid body assemblies to dynamic excitation,” *Earthq. Eng. Struct. Dyn.*, vol. 24, pp. 1389–1408, 1995.

[59] G. de Felice, “Out-of-plane seismic capacity of masonry depending on wall section morphology,” *Int. J. Archit. Herit.*, vol. 5, no. 4–5, pp. 466–482, 2011.

[60] M. DeJong, “Seismic assessment strategies for masonry structures,” Cambridge, MA, 2009.

[61] O. Al Shawa, G. de Felice, A. Mauro, and L. Sorrentino, “Out-of-plane seismic behaviour of rocking masonry walls,” *Earthq. Eng. Struct. Dyn.*, vol. 41, pp. 949–968, 2012.

[62] I. N. Psycharis, D. Y. Papastamatiou, and a. P. Alexandris, “Parametric investigation of the stability of classic al columns under harmonic and earthquake excitations,” *Earthq. Eng. Struct. Dyn.*, vol. 29, no. 8, pp. 1093–1109, 2000.

[63] C. Papantonopoulos, I. N. Psycharis, D. Y. Papastamatiou, J. V. Lemos, and H. P. Mouzakis, “Numerical prediction of the earthquake response of classical columns using the distinct element method,” *Earthq. Eng. Struct. Dyn.*, vol. 31, no. 9, pp. 1699–1717, 2002.

[64] J. Azevedo, G. Sincraian, and J. V. Lemos, “Seismic behavior of blocky masonry structures,” *Earthquake Spectra*, vol. 16. pp. 337–365, 2000.

[65] I. N. Psycharis, J. V. Lemos, D. Y. Papastamatiou, C. Zambas, and C. Papantonopoulos, “Numerical study of the seismic behaviour of a part of the Parthenon Pronaos,” *Earthq. Eng. Struct. Dyn.*, vol. 32, no. 13, pp. 2063–2084, 2003.

[66] M. Mandirola, "Non-linear macroelement mdoelling of experimental tests on masonry specimens with rigid diaphragms," 2014.

[67] G. Housner, "The behavior of inverted pendulum structures during earthquakes," *Bull. Seismol. Soc. Am.*, vol. 53, no. 2, pp. 403–417, 1963.

[68] K. Doherty, M. Griffith, N. Lam, and J. Wilson, "Displacement-based seismic analysis for out-of-plane bending of unreinforced masonry walls," *Earthq. Eng. Struct. Dyn.*, vol. 31, no. 4, pp. 833–850, Apr. 2002.

[69] SIA, *SIA 2018: Überprüfung bestehender Gebäude bezüglich Erdbeben (Seismic assessment of existing buildings)*. Zürich, Switzerland: Swiss Society of Engineers and Architects (SIA), 2004.

[70] NTC, "Decreto Ministeriale 14/1/2008: Norme tecniche per le costruzioni. Ministry of Infrastructures and Transportations, G.U.S.O. n.30 on 4/2/2008;," Italy, 2008.

[71] MIT, "Ministry of Infrastructures and Transportation, Circ. C.S.Ll.Pp. No. 617 of 2/2/2009: Istruzioni per l'applicazione delle nuove norme tecniche per le costruzioni di cui al Decreto Ministeriale 14 Gennaio 2008. G.U. S.O. n. 27 of 26/2/2009, No. 47; 2008 [i," Italy.

[72] M. C. Griffith, G. Magenes, G. Melis, and L. Picchi, "Evaluation of out-of-plane stability of unreinforced masonry walls subjected to seismic excitation," *J. Earthq. Eng.*, vol. 7, no. SP 1, pp. 141–169, 2003.

[73] A. K. Chopra, *Dynamics of Structures*, Third Edit. Upper Saddle River, New Jersey: Prentice H, 2007.

[74] PEER, "PEER NGA database." Pacific Earthquake Engineering Research Center, Berkeley, California, 2014.

[75] L. Luzi, S. Hailemikael, D. Bindi, F. Pacor, F. Mele, and F. Sabetta, "ITACA (ITalian ACcelerometric Archive): A web portal for the dissemination of Italian strong-motion data," *Seismol. Res. Lett.*, vol. 79, no. 5, pp. 716–722, 2008.

[76] F. Pacor, R. Paolucci, L. Luzi, L. Sabetta, A. Spinelli, A. Gorini, M. Nicoletti, S. Marcucci, L. Filippi, and M. Dolce, "Overview of the Italian strong motion database ITACA 1.0," *Bull. Earthq. Eng.*, vol. 9, no. 6, pp. 1723–1739, 2011.

[77] A. Menon and G. Magenes, "Definition of seismic input for out-of-plane response of masonry walls: I. Parametric study," *J. Earthq. Eng.*, vol. 15, no. 2, pp. 165–194, 2011.

[78] 2014, *SIA 261: Einwirkungen auf Tragwerke (Actions on structures)*. Zürich, Switzerland: Swiss Society of Engineers and Architects (SIA).

[79] SIA, "prSIA 296/8: Existing structures – Earthquakes," Zürich, Switzerland, 2014.

[80] M. J. N. Priestley, "Seismic behaviour of unreinforced masonry walls," *Bull. New Zeal. Soc. Earthq. Eng.*, vol. 18, no. 2, pp. 191–205, 1985.

6 SUMMARY OF PROJECT RESULTS

This chapter summarises the data sets and documents that were published by the EESD laboratory on the seismic behaviour of modern URM structures with RC walls and on mixed structures with RC and URM walls. The chapter also comprises the PhD theses and Master theses that were completed on these topics.

6.1 Data sets

The results of the experimental campaigns that are presented in Chapter 1 have been curated in such a way that they can be used by others. They are publically available through the webpage http://eesd.epfl.ch/data_sets.

6.2 Peer-reviewed journal publications

All publications can be downloaded from the webpage http://eesd.epfl.ch/publications.

Under review:

- Tondelli M, Beyer K, DeJong M. (2015) Influence of boundary conditions on the out-of-plane response of brick masonry walls in buildings with RC slabs, submitted *to Earthquake Engineering and Structural Dynamics*.
- Paparo A, Beyer K. (2014) Development of a displacement-based design approach for mixed RC-URM wall structures, submitted to *Earthquakes and Structures*.
- Paparo A, Beyer K. (2014) Modelling the seismic response of URM buildings retrofitted by adding RC walls, submitted to *Journal of Earthquake Engineering*.
- Petry S, Beyer K. (2014) Force-displacement response of in-plane loaded URM walls with a dominating flexural mode, submitted to *Earthquake Engineering and Structural Dynamics*.

Published:

- Beyer K, Tondelli M, Petry S, Peloso S. (2014) Dynamic testing of a four-storey building with reinforced concrete and unreinforced masonry walls: Prediction, test results and data set, *Bulletin of Earthquake Engineering*, http://dx.doi.org/10.1007/s10518-015-9752-z .
- Petry S, Beyer K. (2014) Limit states of URM piers subjected to seismic in-plane loading, invited publication, *Bulletin of Earthquake Engineering*, Invited paper for special issue VEESD. http://dx.doi.org/10.1007/s10518-014-9695-9
- Petry S, Beyer K. (2014) Cyclic test data of six unreinforced masonry piers with different boundary conditions, *Earthquake Spectra*, published online. http://dx.doi.org/10.1193/101513EQS269
- Paparo A, Beyer K. (2014) Quasi-static cyclic tests of two mixed reinforced concrete– unreinforced masonry wall structures, *Engineering Structures* 71:201-2011. http://dx.doi.org/10.1016/j.engstruct.2014.04.002
- Petry S, Beyer K. (2014) Scaling unreinforced masonry for reduced-scale testing, *Bulletin of Earthquake Engineering*, 12(6): 2557-2581. http://dx.doi.org/10.1007/s10518-014-9605-1

- Petry S, Beyer K. (2014) Influence of boundary conditions and size effect on the drift capacity of URM walls, *Engineering Structures* 65:76-88. http://dx.doi.org/10.1016/j.engstruct.2014.01.048

6.3 PhD theses

- Sarah Petry, "Displacement-based design and assessment of URM buildings," EPFL, 2015.
- Alessandro Paparo, "Seismic behaviour of mixed RC-URM wall structures," EPFL, 2015.

6.4 Master projects

- Mohamed Eddamanhoury, "Comportement sismique de bâtimens en maçonnerie non armée avec dalles en béton armé (Seismic behaviour of unreinforced masonry buildings with reinforced concrete slabs)," EPFL, 2014.
- Benaboud Haroun, "Effective slab width in URM buildings with RC slabs," EPFL, 2013. SGEB-Prize for best EPFL-Master project in earthquake engineering.
- Salvatore Marino, "Force-deformation characteristics for composite spandrels," visiting Master student from the University of Bologna, Italy. Supervisor at alma mater: Prof. D. Diotallevi, Dr. L. Landi, 2013.
- Raphaël Bonvin, "Seismic assessment of an existing URM building in the canton Valais," EPFL, 2012.
- Sujith Mangalathu, "Analysis of masonry spandrels with shallow arches," visiting Master student from Roseschool, Istituto Universitario di Studi Superiori (IUSS) Pavia, Italy, 2012.
- Suleidy Perez, "Seismic design and analysis of mixed reinforced concrete–unreinforced masonry wall structures," EPFL, 2011. SGEB-Prize for best EPFL-Master project in earthquake engineering.